ISTC 1862P- 00

Final
Project Technical Report
of ISTC 1862P-00

Study of the process of mixing, temperature, and small signal gain in the active medium of supersonic COIL with advanced nozzle bank and DC discharge method of $O_2(^1D)$ production in a vortex tube

(From 1 October 2000 to 30 June 2001 for 9 months)

Valeri Dmitrievich Nikolaev
(Project Manager)
Lebedev Physical Institute RAS, Samara Branch

July 2001

This work was supported financially by United States Air Force / The European Office of Aerospace Research and Development and performed under the contract to the International Science and Technology Center (ISTC), Moscow.

REPORT DOCUMENTATION PAGE

Form Approved OMB No. 0704-0188

1. REPORT DATE *(DD-MM-YYYY)*	2. REPORT TYPE	3. DATES COVERED *(From – To)*
24-07-2001	Final Report	01/10/2000 - 23-Aug-01

4. TITLE AND SUBTITLE

The study of the mixing process, gas temperature, and small signal gain in the active medium of supersonic COIL with advanced nozzle bank and DC discharge method of production of O2 singlet delta in the vortex tube

5a. CONTRACT NUMBER
ISTC Registration No: 1862

5b. GRANT NUMBER

5c. PROGRAM ELEMENT NUMBER

6. AUTHOR(S)

Dr. Valeri Nikolaev

5d. PROJECT NUMBER

5d. TASK NUMBER

5e. WORK UNIT NUMBER

7. PERFORMING ORGANIZATION NAME(S) AND ADDRESS(ES)

P. N. Lebedev Physical Institute,
Nova-Sadovaya Str. 221
Samara 443011
Russia

8. PERFORMING ORGANIZATION REPORT NUMBER

N/A

9. SPONSORING/MONITORING AGENCY NAME(S) AND ADDRESS(ES)

EOARD
PSC 802 BOX 14
FPO 09499-0014

10. SPONSOR/MONITOR'S ACRONYM(S)

11. SPONSOR/MONITOR'S REPORT NUMBER(S)
ISTC 00-7016

12. DISTRIBUTION/AVAILABILITY STATEMENT

Approved for public release; distribution is unlimited.

13. SUPPLEMENTARY NOTES

14. ABSTRACT

This report results from a contract tasking P. N. Lebedev Physical Institute, as follows:

The objective of this project is to develop the optimal ejector nozzle bank for chemical oxygen iodine laser and to diagnose the gain and gasdynamic characteristics of the laser active medium employing the usual standard methods, laser induced fluorescence (LIF) and tunable one-mode semiconductor probe laser.

15. SUBJECT TERMS
EOARD, Electrotechnology & Fluidics, Lasers & Masers

16. SECURITY CLASSIFICATION OF:			17. LIMITATION OF ABSTRACT	18, NUMBER OF PAGES	19a. NAME OF RESPONSIBLE PERSON
a. REPORT	b. ABSTRACT	c. THIS PAGE			Alexander J. Glass, Ph.D.
UNCLAS	UNCLAS	UNCLAS	UL	80	19b. TELEPHONE NUMBER *(Include area code)* **+44 20 7514-4953**

Standard Form 298 (Rev. 8/98)
Prescribed by ANSI Std. Z39-18

ISTC 1862P- 00

Study of the process of mixing, temperature, and small signal gain in the active medium of supersonic COIL with advanced nozzle bank and DC discharge method of $O_2(^1\Delta)$ production in a vortex tube

(From 1 October 2000 to 30 June 2001 for 9 months)

Valeri Dmitrievich Nikolaev
(Project Manager)
Lebedev Physical Institute RAS, Samara Branch *)

The objective of this project is to develop the optimal ejector nozzle bank for chemical oxygen iodine laser and to diagnose the gain and gasdynamic characteristics of the laser active medium employing the usual standard methods, laser induced fluorescence (LIF) and tunable one-mode semiconductor probe laser. Several ejector nozzle bank designs have been developed, manufactured and tested. The mixing efficiencies of the gas jets, small signal gain distributions and Pitot pressure distributions have been comprised for these nozzle banks. The maximal COIL chemical efficiency has reached in the direct lasing experiments equal to 25%. The one-dimensional gasdynamic simulation has been developed for calculation of completely mixed gas stream parameters downstream of the ejector nozzle banks. The temperature dependence of pressure broadening of the atomic iodine line $^2?_{1/2}$-$^2?_{3/2}$ in the range T=220°? ÷340°? has been measured.

The other objective to investigate of the vortex-stabilized discharge characteristics in pure oxygen and singlet delta oxygen content in the downstream afterglow region for power load up to 3 kJ/g, measurement of iodine atoms concentration when methyl iodide is mixed into the discharge or downstream afterglow regions.

Keywords: chemical oxygen iodine laser, singlet oxygen, ejector, recovery pressure, mixing sonic-supersonic gas jets, vortex tube, electrical discharge.

*) 443011, Samara, Novosadovaya str., 221, Russia
Phone: (8462)356-654; fax: (8462)355-600
E-mail: laser@fian.smr.ru

The work has been performed by the following institutes and collaborators.

1. Participated institutes: The project was performed by one Institution.
Lebedev Physical Institute RAS, Samara Branch (LPI SB)
221, Novosadovaya st., Samara, Russia, 443011
Telephone: (8264) 343-918
Fax: (8264) 355-600;
E-mail: laser@fian.samara.ru

2. Foreign Collaborators: This is a partner project

CONTENT

Introduction

Objectives of the Project

The objective of this contract is study and optimization of COIL operation with advanced Verti-JSOG and new advanced nozzle banks. The another objective is study the singlet oxygen production in vortex-stabilized discharge in the flow of pure oxygen and mixtures oxygen with rare gases and to study iodine atoms production by means of iodine containing molecules dissociation with the help of this type of discharge.

Scope of Work and Technical Approach

The fulfillment of the project was in conjunction with the following items:

A-1. **Development of spectroscopy technique of active medium flow Mach number determination inside the resonator cavity, measuring the sonic velocity out of Doppler broadening of gain contour and flow velocity out of measurements of gain contour splitting.** To achieve this goal the probe laser beam should be at an angle to the gas flow vector.

A-2. **Development of one-dimensional mathematical model of mixing chamber with three types of jets at its inlet.** A simple mathematical model provides the possibility of qualitative study of the dependence of flow characteristics at the mixing chamber outlet on the gases' parameters at its inlet.

A-3. **Modification of the existing discharge system considering previous experimental results with intention to further increase discharge power load.** The modified discharge chamber has been designed and manufactured, with water cooled electrodes insulated from the discharge chamber body. This permits to reach higher discharge power load, to improve performance stability and reproducibility of results. The existing power supply has been be improved also.

A-4. **Study of the vortex-stabilized discharge characteristics in pure oxygen and singlet delta oxygen content in the downstream afterglow region for power load up to 3 kJ/g.** The intention was to study vortex-stabilized discharge behavior in pure oxygen for increased power load up to 3 kJ/g (approximately), and to determine the highest singlet oxygen content in the afterglow region vs discharge power, gas pressure, gas flow and electrode configuration.

A-5. **Improvement of design of the nozzle bank considering up to date understanding of the existent phenomena.** 8 different nozzle banks have been developed and there performances have been compared.

A-6 **To perform 'cold' gas dynamic tests of new design of the nozzle bank using the special resonator cavity without the mirror tunnels.** The special cavity without mirror tunnels has been designed and "clean" gas dynamic tests of new nozzle banks have been performed (without former found influence of gas flow from these tunnels on the mixed flow parameters). These investigations has allowed to determine the influence of gases' input parameters and details of design on the parameters of the completely mixed flow.

A-7 **Study of efficiency and mixing rate of iodine using laser induced fluorescence (LIF).** The goal of this study was to determine the distance from the new nozzle bank where all the components are fully mixed and where resonator optical axis should be placed. LIF pictures for all nozzle banks gave information about influence of the different nozzles' features on mixing efficiency.

A-8 **Measurement of small signal gain distribution within the resonator cavity cross section employing tunable single mode semiconductor laser, temporarily provided by the Partner.** The aim of this study was to measure small signal gain of the active medium, its variations along and across the flow. This measurements provided information about stored energy dissipation or loss of iodine atoms, which is important for understanding the processes taking place in the laser active medium.

A-9 **Study of the singlet delta oxygen content in the downstream afterglow region using mixtures of oxygen with rare gases.** The intention was to determine the upper limits and optimal conditions of singlet oxygen production at increased pressure (which is advantageous for further use in a supersonic flow system).

A-10 **Laser experiments with the new nozzle bank.** The experiments with laser operation and output power optimization summed up the results of nozzle bank design improvement and determine prospects of the new method of active medium production.

A-11 **Experiments with chlorine pre-diluted with helium in the ratio of Cl_2:He=1:1 to increase conductivity of the oxygen nozzles, singlet oxygen yield, small signal gain and output power.** The goal was to increase laser chemical efficiency with the existing nozzle bank as well as with the new one. This objective has been reached.

A-12 **Measurement of iodine atoms concentration when methyl iodide is mixed into the discharge or downstream afterglow regions.** The intention was to measure iodine atoms production rate produced by dissociation when methyl iodide is mixed into discharge or in the downstream afterglow region.
Excited atomic iodine concentration has been determined by absolute measurements of 1.315 μm line intensity. Absorption coefficient due to atomic iodine has been measured with the help of the tunable single mode semiconductor laser device, temporarily provided by the Partner.

The investigations were in part basic and in part applied.

The planned experimental and theoretical investigations were aimed to a great extent for further understanding of physical processes taking place during mixing of gaseous components and laser active medium preparation. The information was obtained about typical spatial mixing scale of iodine vapor with other flow components, about typical lengths downstream of nozzle bank where molecular iodine dissociation starts and finishes, about small signal gain value and its evolution along the flow, which is important for optimal placement of resonator optical axis and output coupling. Also, the information was obtained about the influence of the nozzle bank design and gas jets initial parameters on the full pressure after the straight shock wave, which is close to the recovery pressure at the diffuser outlet. The mathematical model of mixing chamber was developed to predict gas dynamic properties of fully mixed flow. The experiments with vortex-stabilized discharge provided knowledge about the main regular trends of discharge methods of excited oxygen metastablities generation. This helped to understand better the processes in weakly ionized gas discharge plasma. The information was obtained about the influence of power load, pressure, flow rate, gas mixture, electrode configuration in vortex-stabilized glow discharge on singlet oxygen production. For the first time the information was obtained about atomic iodine production by means of iodine-containing organic additives dissociation in vortex-stabilized glow discharge.

The knowledge obtained during investigation is to a large extent of a general physics nature. These results are necessary for the Executor and Partner for deep understanding of the active medium kinetics and for design of future laser systems, their supersonic diffusers and pump systems with smaller overall size and weight and lower power consumption.

Development of the highly efficient COIL, based on jet SOG with moderate pressure, with unique active medium characteristics became possible due to 15 years accumulation of results of thorough experimental and theoretical investigations of singlet oxygen generators, chemical oxygen-iodine laser and various methods of its active medium preparation, including electric discharge implementation, in Samara branch of LPI. The following factors and method developed in Samara branch of LPI prove the ability to carry out this project:

- Acknowledged by international scientific community high scientific and technical quality of investigations performed in Samara branch of LPI in this field;
- Facilities to develop (and adapt) COIL experimental setups and vortex-flow electric discharge tube with proper characteristics;
- High scientific and technical qualifications of personnel;
- Implementation of a number of refined methods of gas medium diagnostics and laser operation parameters in COIL:

– photometry method of [? $_2$ ($^1\Delta$)], [? $_2$($^1\Sigma$)], [H_2O] measurement;
– photometry method of [J_2] measurement;
– photometry method of [Cl_2] measurement with sensitivity < 0.1 torr;

- spectroscopy methods of measurements of small signal gain, static temperature and speed of a sonic in active medium using tunable single mode semiconductor laser;
- developed methods of measurement of gas dynamic characteristics;

- Methods of design of jet SOG and COIL, proved in experiments;
- Computer assisted data acquisition and processing system;
- Methods of vortex-flow tubes design proved in experiment;
- Experience in experiments with powerful gas discharge in gas flow;
- Method of ? $_2(^1\Delta)$ content absolute measurement with the help of spectrophotometer, calibrated against the black body radiation.

RESULTS

Specification:

P1-the pressure in reaction zone of JSOG, (accuracy 1 torr)
P2- the plenum pressure (in front of nozzle bank), ((accuracy 1 torr)
P3-the wall static pressure at the distance 64 mm from nozzle bank, (accuracy 0.5 torr)
P4 -the initial full pressure of the secondary buffer gas, (accuracy 1 torr)
P5- the Pitot (recovered) pressure, (accuracy 1 torr)
P5' –calculated Pitot pressure
P6 -the initial full pressure of the primary buffer gas (accuracy 10 torr)
P* - the full (stagnation) pressure of gas flow in the cavity (calculated)
M- Mach number of the gas flow
W_L(MHz)-pressure broadening width of the gain line
W_G(MHz)- the Doppler width of the gain line
g, SSG(%/cm)- small signal gain
$\Delta N(cm^{-3})$- inversion population
T (K)- static gas temperature
T*(K)- stagnation gas temperature
P_s (torr)static pressure calculated from W_L
$T=(W_G/14.49)^2$ – gain medium temperature calculated from Gaussian of Voight gain line
U(m/c)- gain medium absolute velocity
U_p (m/s)– transverse pulsation velocity
C_N, C_O, C_c - specific heat capacities of N2, O2, Cl2 gases
G_1-primary molar flow of N2, mmole/s
G_2 - secondary molar flow rate of N2, mmole/s
G_0 - chlorine molar flow rate, mmole/s
G_{I2}- iodine molar flow rate, mmole/s
Ut - chlorine utilization in the JSOG
Z - the distance between the probe beam position and the nozzle bank outlet
Y- the distance between the probe beam position and the center line of the gas stream

1. GAIN MEASUREMENTS OF ACTIVE MEDIUM PRODUCED BY EJECTOR NOZZLE BANK

1.1. THE GAIN SPECTRUM OF COIL ACTIVE MEDIUM.

The Chemical oxygen-iodine laser operates on the strongest $I(^2P_{1/2,F=3})\rightarrow I(^2P_{3/2,F=4})$ hyperfine component of the spin orbit transition of atomic iodine at the wavelength λ=1.315μm. The broadening of the gain line in the uniform laminar gas stream is due to pressure broadening and Doppler broadening that results in Voigt gain line shape. The small signal gain (SSG) on this transition is equal to:

$$g(X)=\frac{7}{12}\Delta N\frac{Al^2}{8p}V(X) \qquad (1)$$

$$V(X)=\sqrt{\frac{\ln(2)}{p}}\frac{W_L}{pW_G}\int_{-\infty}^{\infty}\frac{\exp\left(-Z^2 4\ln 2/W_G^2\right)}{(X-Z)^2+\left(\frac{W_L}{2}\right)^2}dZ$$

where ΔN is the total inverted population on the transition $^2P_{1/2}\rightarrow{}^2P_{3/2}$, A=5.1s^{-1}, X = ν-ν$_0$ is the frequency shift relative the centerline frequency ν$_0$ and V(X) is a Voigt line shape function, normalized to unity, W_L is the pressure broadening term (FWHM), W_D is the Doppler width (FWHM). The inverted population is determined by the total concentration of iodine atoms N_I, the singlet oxygen yield $Y=[O_2(^1\Delta)]/([O_2(^1\Delta)]+[O_2(^3\Sigma)])$ and the static temperature T of the active medium:

$$\Delta N=\frac{(Y-Y_{th})(K_{eq}+0.5)}{(K_{eq}-1)Y+1}N_I \qquad (2)$$

where K_{eq}=0.75exp(401/T) is the equilibrium constant for the process
$O_2(^1\Delta)+I(^2P_{3/2})\leftrightarrow O_2(^3\Sigma)+I(^2P_{1/2})$, and $Y_{th}=(2K_{eq}+1)^{-1}$ is the threshold fraction of $O_2(^1\Delta)$ at which the inverted population vanishes.

The pressure broadening term (FWHM) $W_L=P\Sigma a_i x_i f_i(300/T)$ scales linearly with the total pressure *P*, the parameters α_i are the pressure broadening coefficients at room temperature, x_i molar fraction of "i" gas component. With the assumption that the functional form for the temperature dependence for all gas components can be expressed as $(300/T)^\gamma$ the pressure broadening term (FWHM) width is given by:

$$W_L=P(300/T)^\gamma\Sigma a_i x_i. \qquad (3)$$

With these assumptions it has been found that γ=0.87±0.13 for the temperature interval 220°K-340°K [See Part 4]. In contrast to low pressure COIL the pressure broadening is a very essential for high pressure, low temperature COIL gain medium generated by the ejector nozzle bank. The Doppler width, (FMHM) is given by:

$$W_D(MHz)=14.49\,T^{1/2} \qquad (4)$$

where T is measured in °K.

As a result of the Doppler effect the measured central frequency of the SSG spectrum for a beam directed at an angle φ with respect to the normal of the gas flow velocity is shifted by

$$\Delta\nu=\sin(\varphi)U/\lambda. \qquad (5),$$

1.2. EXPERIMENTAL SET-UP

The special set-up was designed for measurements of COIL parameters with probe laser. The gas flow part of COIL consists of the Jet SOG, nozzle bank, mixing chamber, chamber with the optical wedges. JSOG produced the high pressure $O_2(^1\Delta)$ flow. This JSOG was earlier used as energy source of 1.4 kW COIL with slit nozzle[1]. The designed of nozzle banks will be described later. The outlet cross section of each nozzle bank was 15x50 mm^2. The COIL active length was equal to 50 mm. The nozzle bank was connected to mixing chamber. Mixing chamber has initial cross section 16x50 mm^2. The walls of the chamber were turned on 2° relatively to the flow direction.

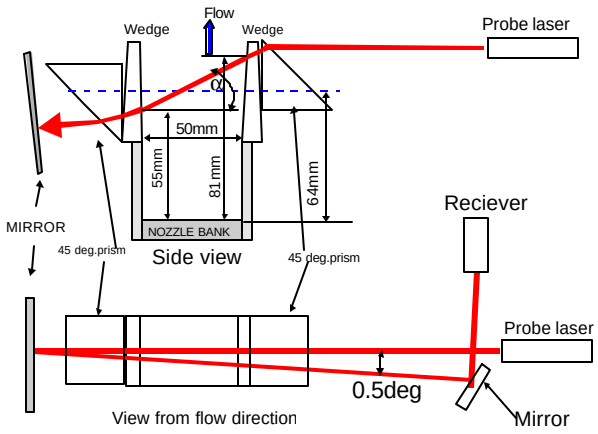

Fig.1.1. Oblique beam direction.

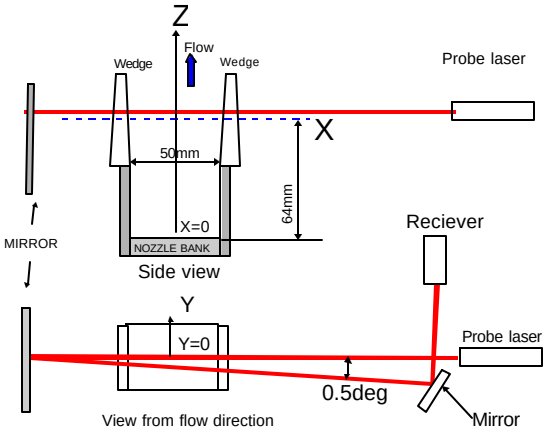

Fig.1.2. Normal beam direction

The positions of pressure gauges are shown in fig.1.3

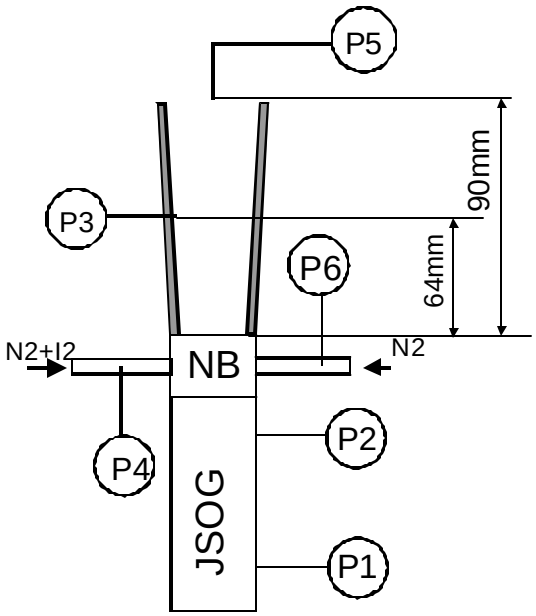

Fig.1.3. The set-up of pressure gauges.

A diode laser probe (Physical Sciences Inc.) was tuned to the resonant frequency of the iodine transition $I(^2P_{1/2},F=3) \rightarrow I(^2P_{3/2},F=4)$ to measure gain. The line shape of the probe laser is close to Lorenzian with FWHM $\Delta\nu_p \approx$ 8MHz, and the laser frequency was varied ±1500MHz relative to line center. Two different optical schemes were used in these experiments. In the first, the probe laser beam was deflected by a prism from normal incidence and entered the active medium at an angle of –27.5°. The probe beam entered and exited the medium at 81mm and 55mm, respectively, from the nozzle exit plane. The path of probe beam was located in the middle plane of the mixing chamber. After reflection from a planar mirror, the probe laser beam returned through the active medium at an angle of $\varphi \approx +27.5°$. The intensity of the probe laser was measured by a photodetector. The photodetector and probe laser locations differed slightly due to the 0.5° angle between the primary and reflected beams. The round trip gain spectrum measured with this configuration consisted of two peaks, each Doppler shifted on $\Delta\nu$ from line center due to the flow velocity of the gas, $g(X) = [g_1(X-\Delta\nu)] + [g_2(X+\Delta\nu)]$. The quantities $g_1(X-\Delta\nu)$ and $g_2(X+\Delta\nu)$ are the SSG for primary and reflected beams respectively. It is assumed that in the general case the Voigt line shape function and the peak of the SSG may be different for the primary and reflected beams but constant along each path.

In the second experimental configuration the probe beam entered the cavity normal to the gas flow velocity, (φ=0). This configuration allowed the determination of a map of the SSG and spectral parameters of the active medium over the limits of the window aperture. The error of the probe beam alignment was estimated to be ~1°. The angle alignment error for the normal incidence beam causes additional spectral broadening g(X) due to the Doppler effect. Numerical simulation of this effect indicates that the ±1° error increases W_G by 1 MHz .

Scanning the SSG spectrum was achieved during 5 seconds when all gas flows were stationary. The probe laser hardware and software provided for real time acquisition of the SSG spectrum and calculation of $g(X)=[g_1(X-\Delta\nu)+g_2(X+\Delta\nu)]$ for the first optical scheme or $g(X)=1/2[g_1(X)+g_2(X)]$ for the second optical scheme. It is possible to separate the Gaussian and Lorenzian spectral components if $g_1(X)$ and $g_2(X)$ are assumed to be Voigt functions. In fact, $g_1(X-\Delta\nu)$ and $g_2(X+\Delta\nu)$ were calculated individually for first optical scheme and $[g_1(X)+g_2(X)]$ was calculated for the second scheme. Since the probe laser has a Lorenzian line shape with $\Delta\nu_p$ =8MHz, the observed spectrum is a convolution of the probe and the gain spectrum. Therefore, the observed width of the Lorenzian line shape is $W_L+\Delta\nu_p$. Further mathematical processing of these functions allows the determination of the peak SSG $g_1(0)$, $g_2(0)$ as well as $\Delta\nu$, W_L, and W_G.

The orifice for measuring P_3 was located in the center of the mixing chamber wall of 64 mm, downstream from the nozzle exit plane. In hot experiments the Pitot tube of 5 mm in diameter with 1 mm receiving hole was placed in the center of the mixing chamber of 90 mm, downstream from nozzle exit plane. The molar flow rates of primary nitrogen G_1, secondary nitrogen G_2 and iodine molar flow rate G_{I2} were measured with accuracy 5%. The BHP temperature t° was measured by a diode sensor with accuracy 0.5°C

1.3. CALCULATION OF GAS FLOW PARAMETERS FROM SPECTROSCOPIC DATA

A typical SSG spectrum for the case φ=27.5° is presented in fig.1.4 As a result of the Doppler effect, the SSG spectrum consists of two Voigt functions shifted with respect to each other by the value 2Δν. The right peak in fig.2 correspondents to the forward trip of the probe beam and the left to the return trip. The SSG spectral line shape factors and peaks differ slightly for the forward and reverse probe laser beam trips due to pressure losses along the feed manifolds that result in inhomogeneous injection of the iodine and primary nitrogen flow into the mixing chamber. During mathematical resolution of spectrum the peak gain and broadening parameters W_{L1},W_{L2}, W_{D1},W_{D2} have been obtained for both resolved Voigt functions. The average values $W_D=(W_{D1}+W_{D2})/2$ and $W_L=(W_{L1}+W_{L2})/2$ have been used in further analysis. During spectrum resolution it was also possible to install the constraining relations $W_L=W_{L1}=W_{L2}$ and $W_D=W_{D1}=W_{D2}$ to obtain two Voigt function with identical broadening parameters. The values of W_L and W_D calculated by both methods differ less that 1% for all data presented here. In the case of second optical scheme the broadening parameters and peak gain have been determined by usual routine [2].

The gas flow parameters were calculated in the next manner. The average peak SSG of the active medium from these measurements is defined by $g=(g_1(0)+g_2(0))/2$. The absolute gas velocity is calculated by:

$$U = \frac{\Delta n \times l}{\sin(j)} \qquad (6),$$

The uncertainty in the angle (±1°) of the probe beam alignment results in 3,3% error of velocity determination .
The gas temperature T(°K) is calculated by

$$T = \left(\frac{W_D}{14.49}\right)^2 \qquad (7)$$

where W_D(MHz) is the average Doppler width for both resolved Voigt functions.
The Mach number of the stream is estimated by

$$? = U\sqrt{\frac{m}{kRT}} = 14.49\frac{\Delta n \cdot l}{W_D \sin(j)}\sqrt{\frac{m}{kR}}, \qquad (8)$$

where R=8.31J/mole/K is the universal gas constant, k=1.4 is the specific heat ratio, μ is the molecular weight. The stagnation gas temperature is defined by

$$T^*=T(1+0.2M^2)^{3.5} \qquad (9)$$

Under assumption of total mixing of all three flows the total heat power of the flow is defined by

$$Q=CGT^*, \qquad (10)$$

where C is the molar heat capacity, $G=G_0+G_1+G_2+G_{I2}$ is the total molar flow rate.

Using spectroscopic data it is possible to calculate the static pressure P_s in the supersonic core and compare it with measured static wall pressure P_1 in the boundary layer. Since the composition of the active medium consists primarily of nitrogen and oxygen P_s in the center of the mixing chamber is estimated by:

$$P_s = \frac{W_L}{5.5x_{N2} + 5x_{O2}}\left(\frac{T}{300}\right)^{0.87} \qquad (11)$$

where 5.5MHz/torr and 5MHz/torr are parameters of the collisional broadening at 300K° by N_2 and O_2 respectively [4], x_{N2}, x_{O2} are the mole fractions of nitrogen and oxygen, W_L is the average pressure broadening parameter for both Viogt functions.

The stagnation pressure of flow is calculated by

$$P^*=P_s(1+0.2M^2)^{3.5} \qquad (12)$$

and the expected total pressure downstream normal shock wave or Pitot pressure is estimated by

$$P_5' = P_s \frac{166.7 M^7}{\left(7M^2 - 1\right)^{2.5}} \quad (13)$$

The density of inversion population is equal to

$$DN = \frac{8p}{A_{34} l^2} \int_{-\infty}^{\infty} SSG(n)dn \quad (14)$$

It is necessary to remark that the probe beam interacts only with gain zones of the gas stream. Hence the gas flow parameters calculated from (6-14) will be valid only for gas zones containing iodine atoms.

The example of gain line profile is shown in Fig.1.4.

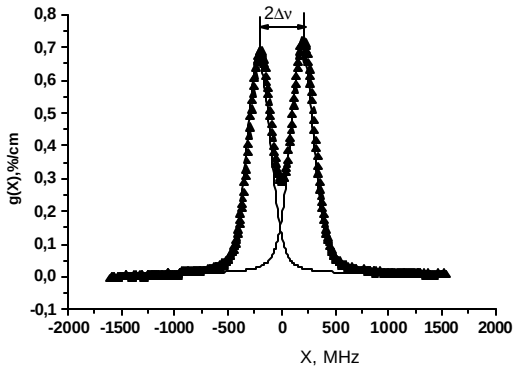

Fig.1.4

SSG spectrum for the probe laser beam. Triangles is experimental spectrum g(X), solid curve Voigt functions $g_1(X)$ and $g_2(X)$ resolved from g(X).

1.4. GAIN AND SOME GASDYNAMIC PARAMETERS OF THE GAIN STREAM, GENERATED BY NB-1.

The sketch of nozzle bank NB-1 is shown in Fig. 1. 5

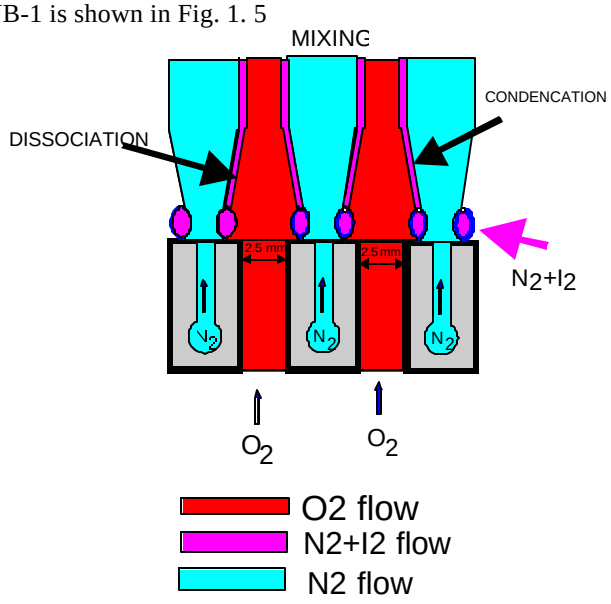

Fig.1.5 The sketch of NB-1.

Brief description. It consists of 7 slits (2.5x15 mm) for $O_2(^1\Delta)$, the distance between centers of slits was D= 6.5 mm, 8 rows with 7 cylindrical holes ∅1 mm for the primary N2, 14 tubes with 15 holes ∅0.5mm in each tube for N2+I2. The N2+I2 flowed into tubes from both sides for more uniform injection of iodine. The N2+I2 flow is injected parallel to $O_2(^1\Delta)$ flow. The primary nitrogen also flowed into injector from both sides for uniform injection in Y direction. Previous tests demonstrated that the best results have been reached at lower secondary nitrogen flow rate (11 mmole/s than 40 mmole/s which was used in earlier experiments described in AIAA Paper 2427 –2000) and this value was used in all our experiments.

1.4.1 Variation of primary nitrogen molar flow rate MNP.

G_1	**Variable**
G_2	11 mmole/s
G_0	39.2 mmole/s
He dilution of chlorine	0:1
G_{I2}	0.8 mmole/s
T(BHP)	-16C
oblique probe beam direction, y=0	

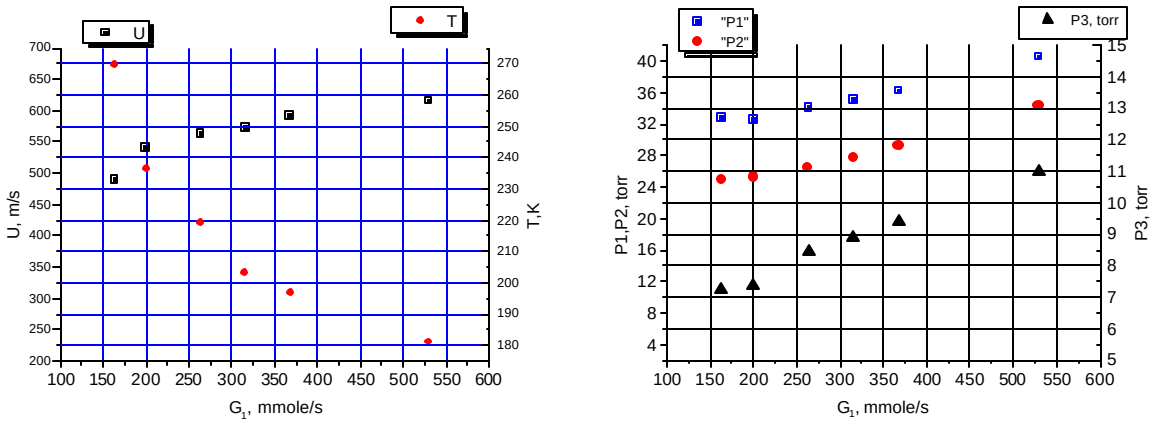

a ***b***

Fig.1.6 The dependencies of pressures, maximum gas temperature T_m and gas velocity on primary nitrogen molar flow rate.

The rise of G_I results in increase of pressure in cavity, plenum pressure and pressure in JSOG. It indicates that choking effect takes place. The rise of G_I results in increasing of Pitot pressure also but reduction of SSG (Fig. 1.7a). In spite of decreasing of gas temperature and W_G , the increase of pressure broadening W_L and reduction of the inversion population (Fig.1.7b) leads to the decrease of SSG. The decrease of ΔN may be due to reduction of N_I or $O_2(^1\Delta)$ fraction Y with the rise of MNP. The degrades Y should accompany by the rise heat release and gas temperature what is in conflict with experiments. Probably the water vapor condensation on the BHP aerosol took place during gas jets mixing and then iodine atoms and molecules attached to these small ice particles. The heterogeneous water vapor condensation on the small salt centers is more probable process in real conditions than homogeneous condensation. This process may occur at less value of the water vapor supersaturation.

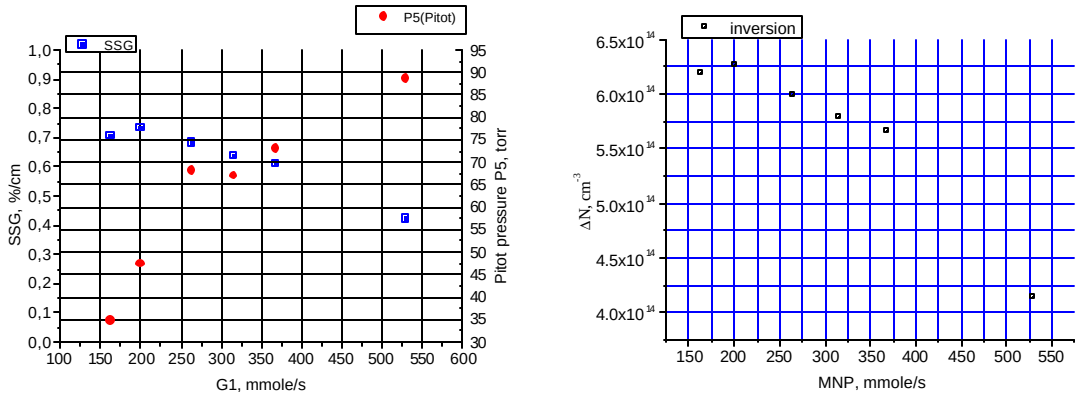

a b

Fig 1.7 The dependence of SSG, Pitot pressure P5 and inversion population on G_1.

1.4.2 Variation of BHP temperature.

G_1 (nitrogen)	270 mmole/s
G_2 (nitrogen)	11 mmole/s
G_0	39.2 mmole/s
He dilution of chlorine	0:1
G_{I2}	0.8 mmole/s
T(BHP)	**variable**
oblique probe beam direction, y=0	

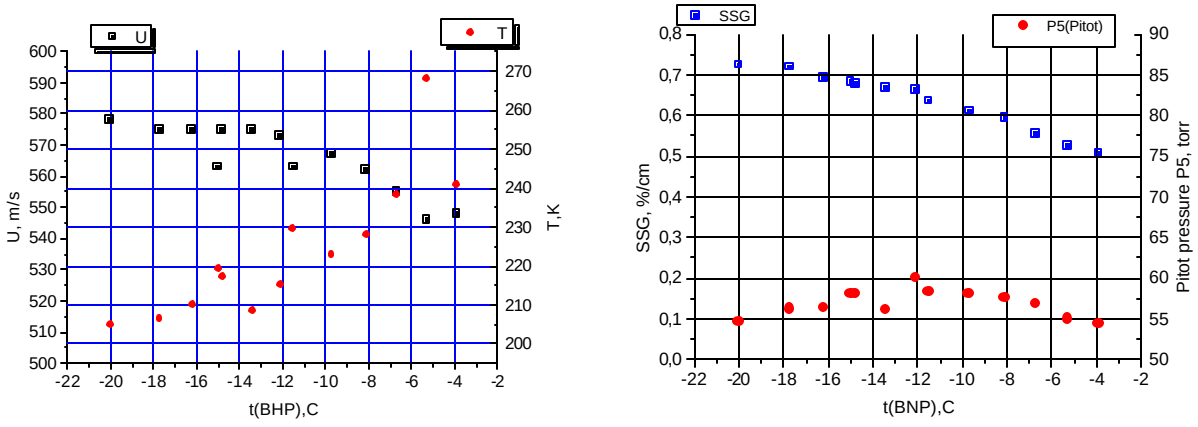

a b

Fig. 1.8 Dependence of SSG, Pitot pressure P5, gas velocity U and gas temperature T on BHP temperature.

The rise of BHP temperature results in increase of water vapor fraction in gas flow and worsening of the I2 dissociation. The quenching of I* and $O_2(^1\Delta)$ leads to the raise of gas temperature T.

1.4.3 The dependence of SSG and T on iodine molar flow rate.

G_1 (nitrogen)	250 and 500mmole/s
G_2 (nitrogen)	11 mmole/s
G_0	39.2 mmole/s
He dilution of chlorine	0:1
G_{I2}	**variable**
T(BHP)	-16C
oblique probe beam direction, y=0	

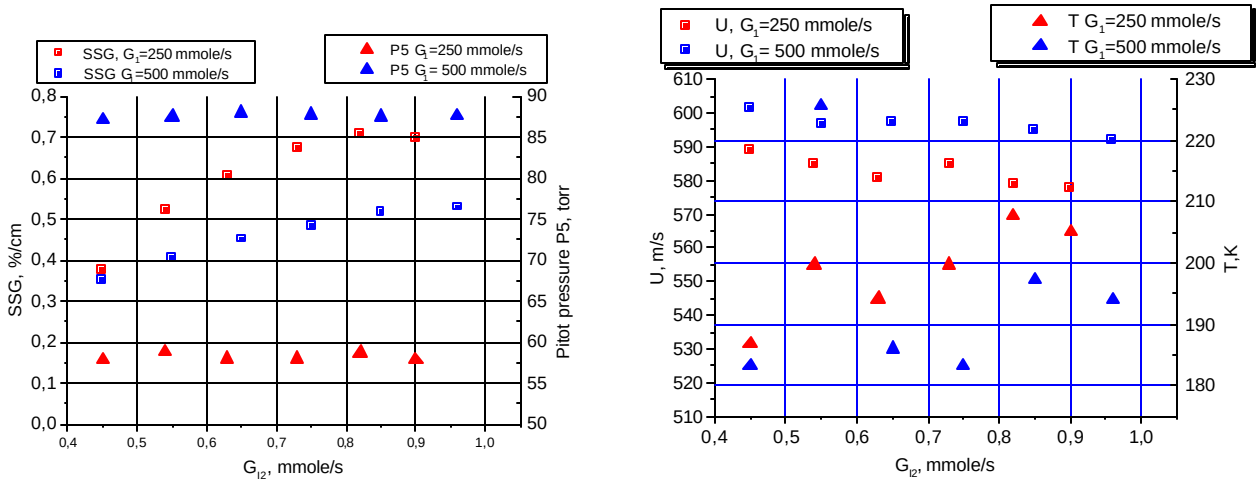

Fig.1.9 The dependencies of SSG, P5, T, U on iodine molar flow rate

G_1 (nitrogen)	250 and 500mmole/s
G_2 (nitrogen)	11 mmole/s
G_0	39.2 mmole/s
He dilution of chlorine	0:1
G_{I2}	**variable**
T(BHP)	-16C
normal probe beam direction	z=64mm, y=0

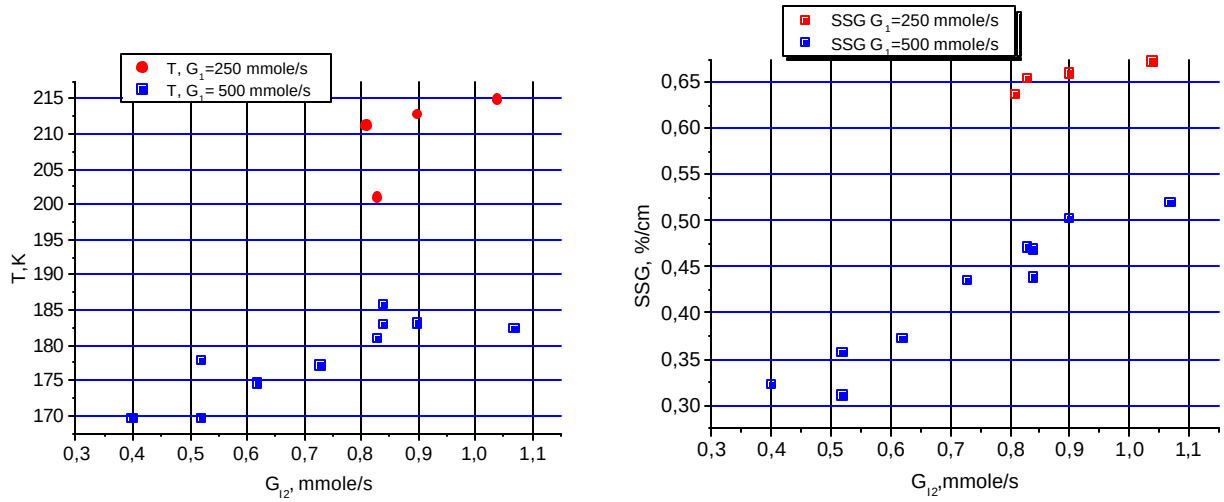

Fig. 1.10. The dependencies of SSG and T on iodine molar flow rate.

The values of SSG in measurements for oblique beam direction are slightly higher than for normal beam direction. In the first optical scheme the probe beam enters into active medium on the distance 81 mm apart from NB-1 and leaves active medium on distance 55 mm. But in second scheme the probe beam located at 64 mm apart from NB-1.

1.4.4 The dependence of SSG and T on distance Z from NB-1.

G_1 (nitrogen)	530mmole/s
G_2 (nitrogen)	11 mmole/s
G_0	39.2 mmole/s
He dilution of chlorine	0:1
G_{I2}	0.8 or 0.4 mmole/s
T(BHP)	-16C or –5.6C
normal probe beam direction, y=0	z=**variable**,

a **b**

Fig. 1.11. The dependence of SSG and T on distance Z from NB-1 for different G_{I2} and T(BHP)

G_1 (nitrogen)	270mmole/s
G_2 (nitrogen)	11 mmole/s
G_0	39.2 mmole/s
He dilution of chlorine	0:1
G_{I2}	0.8 mmole/s
T(BHP)	-16C or –5.6C
normal probe beam direction, y=0	Z=**variable**

Fig. 1.12. The dependence of SSG and T on distance from NB-1.

The SSG degrades with distance Z from NB-1. For higher G_I this degradation is stronger. For the same primary molar flow rate the degradation of SSG is stronger for higher G_{I2}. The increase of BHP temperature up to –5.6C doesn't result in intensification of SSG degradation.

Our preliminary conclusion: the degradation of SSG is due to iodine condensation or attachment to small ice particles. When the primary nitrogen flows out from nozzle it turns iodine jets into direction of $O_2(^1\Delta)$ flow. Because the local concentration of $O_2(^1\Delta)$ and I2 in the jets near NB-1 are very high the dissociation is very fast. After that the intense turbulent mixing of $I2+O_2(^1\Delta)$ with primary N2 takes place and the the static temperature, local concentrations of O_2, H_2O, residual I_2 fall dawn quickly similar as in the supersonic nozzle.

The flow is supersaturated by iodine vapors. The saturated iodine pressure at temperature ~200K has value of the order of 10^{-6} torr but the real partial iodine pressure is of the order of 0.01 torr. The three particles collisions I+I2+M at higher MNP are faster also. The iodine clusters may be produced also in the region where I2 flow contacts with primary N2 flow. After mixing I atoms can be captured by these small iodine clusters or by ice particles in the oxygen jets. For higher I2 or N2 flow rates this effect will be more intense. Heterogeneous condensation I_2 and attachment iodine atoms require much less values of the iodine supersaturation. The condensation shock wave must not be looking in the real situation.

1.4.5. Operation of NB-1 with dilution of chlorine with helium.

It was found in the previous experiments that the rise of G_1 leads to choking of the oxygen flow in JSOG, the decrease gas velocity in JSOG and $O_2(^1\Delta)$ losses in reaction zone. The mixture of Cl2 with Helium should be supplied to JSOG to prevent $O_2(^1\Delta)$ losses. The total pressures P1, P2 increase in this case but partial oxygen pressure in the JSOG and plenum decreases with the rise of helium molar flow rate due to improving the gas conductivity of the nozzles. The $O_2(^1\Delta)$ yield increases with the rise of helium molar flow rate because $p\tau$ parameter decreases.

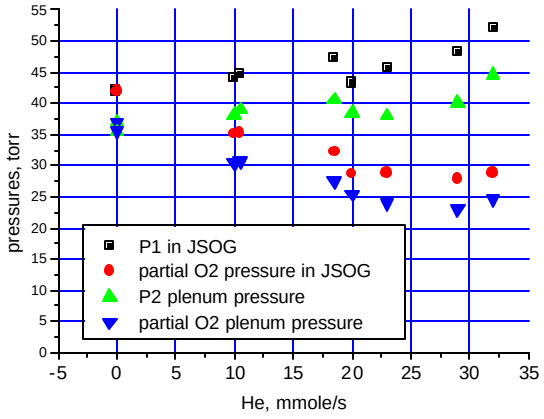

Fig. 1.13. Dependence of pressures on helium molar flow rate.

G_1 (nitrogen)	500mmole/s
G_2 (nitrogen)	11 mmole/s
G_0	39.2 mmole/s
He dilution of chlorine	variable
T(BHP)	-16C
normal probe beam direction, y=0	

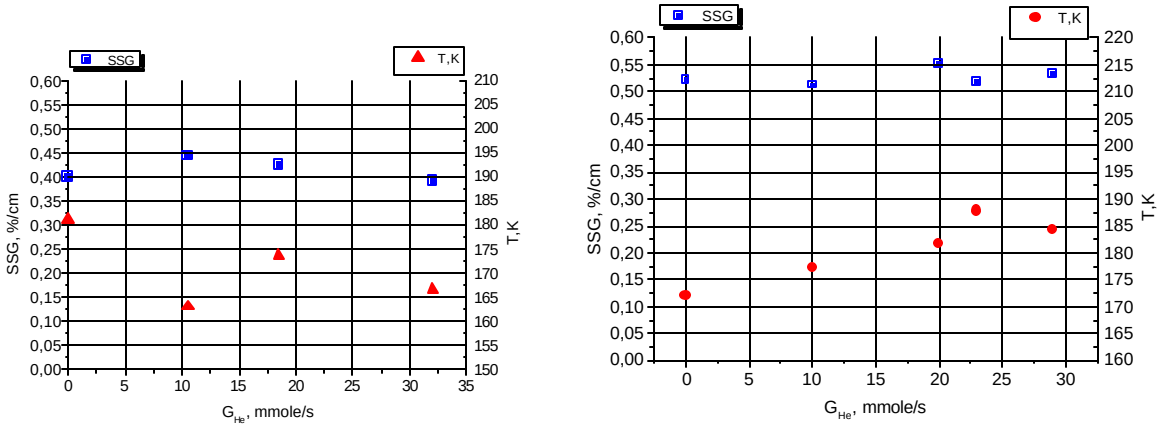

a) b)

Fig.1.14. Dependence of SSG and T on Helium dilution of chlorine.
a) set-up B, G_{I2}=0.55 mmole/s; b) set-up B, G_{I2}=0.8 mmole/s

The SSG demonstrates the weak dependence on He dilution. It is strange from the first point of view because $O_2(^1\Delta)$ yield increasing was expected. May be the absolute velocity of $O_2(^1\Delta)$+He flow is higher than for pure $O_2(^1\Delta)$ and thus contact time of $O_2(^1\Delta)$+He and N2+I2 jets at high pressure is shorter than in the case of chlorine undiluted with helium. Another reason of the decrease of iodine dissociation rate may be lower $O_2(^1\Delta)$ partial pressure in the $O_2(^1\Delta)$+He jets.

1.4.6 Operation of NB-1 with primary argon buffer gas.

The using of more heavy Argon instead of nitrogen as a primary buffer promised the rise Pitot pressure due to increasing momentum of the ejecting gas. But experiments results demonstrate the increase of static pressure in the cavity without changing Pitot pressure. As a result the Much M number is lower for Ar than for nitrogen buffer gas.

Primary gas	Molar flow rate Mmole/s	P3 Torr	P5 Torr
Nitrogen	250	8.5	55
Argon	250	10	50
Nitrogen	500	10.5	90
Argon	500	14.5	92

The absolute gas velocity was lower also (argon heavier than nitrogen) (Fig.1.15). The measured gas temperature is close to the temperature in the case of nitrogen primary buffer gas. Such behavior may be explained by the higher specific heat ratio γ_{Ar} =1.67. The noble gases produce the jets with higher initial Mach number at the same throat and outlet cross section squares in the nozzle bank. The interaction of these jets in the space between iodine injector tubes produces at larger Mach number the system of more intense shock waves and increases the pressure losses.

G_1 (argon)	250 s or 500 mmole/
G_2 (nitrogen)	11 mmole/s
G_0	39.2 mmole/s
G_{I2}	variable
He dilution of chlorine	0:1
T(BHP)	-16C
oblique probe beam direction, y=0	

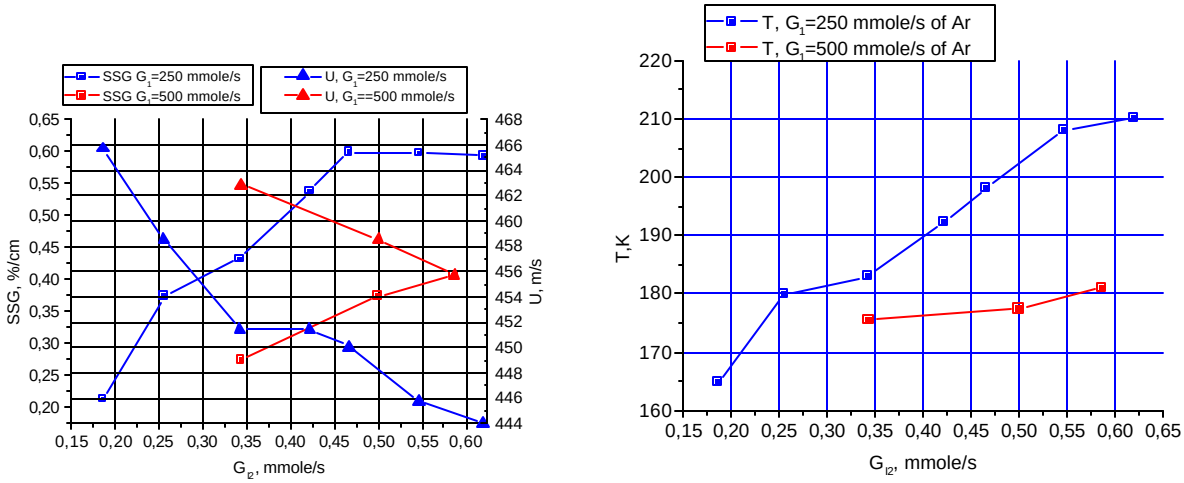

Fig. 1.15 The dependence of SSG, absolute gas velocity and T on G_{I2}.

The SSG degrades with the increase of distance from NB-1 (Fig.3.11).

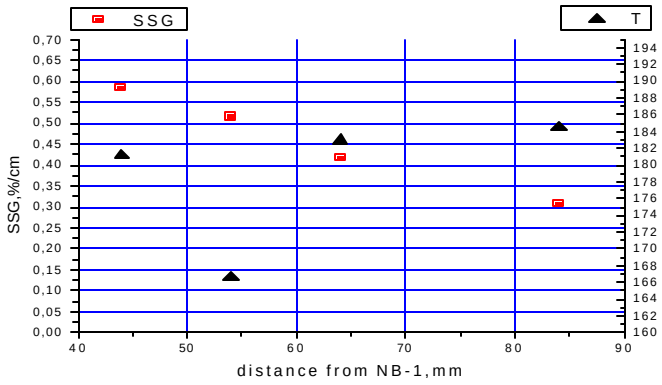

Fig.1.16. Dependence of SSG and Tm on distance from NB-1.

1.5. PARAMETERS OF THE GAS FLOW FOR NOZZLE BANK NB-2.

The sketch of nozzle bank NB-2 is shown in Fig. 1.17.

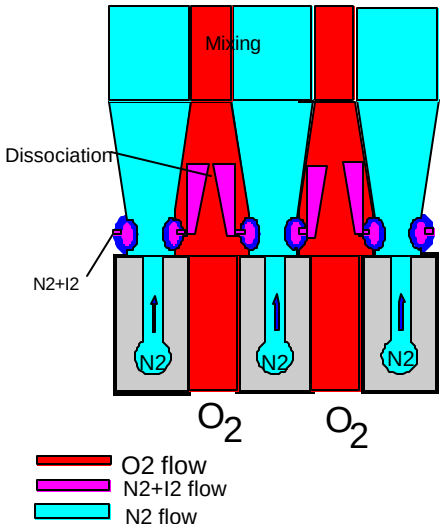

Fig.1.17. The sketch of NB-2.

Brief description. NB-2 consists of 7 slits (2.5x15 mm) for $O_2(^1\Delta)$, the distance between centers of slits D= 6.5 mm, 8 rows with 7 cylindrical holes ∅1 mm for the primary N2, 14 tubes with 15 holes ∅0.5mm in each tube for N2+I2. The N2+I2 flowed into tubes through both sides for more uniform injection of iodine. The N2+I2 flow is injected **perpendicular** to the $O_2(^1\Delta)$ flow. The primary nitrogen also flowed into injector through both sides for uniform injection in Y direction.

1.5.1 The dependence of gas flow parameters on primary nitrogen molar flow rate.

G_1 (nitrogen)	variable
G_2	11 mmole/s
G_0	39.2 mmole/s
G_{I2}	0.45 mmole/s
He dilution of chlorine	0:1
T(BHP)	-16C
oblique probe beam direction, y=0	

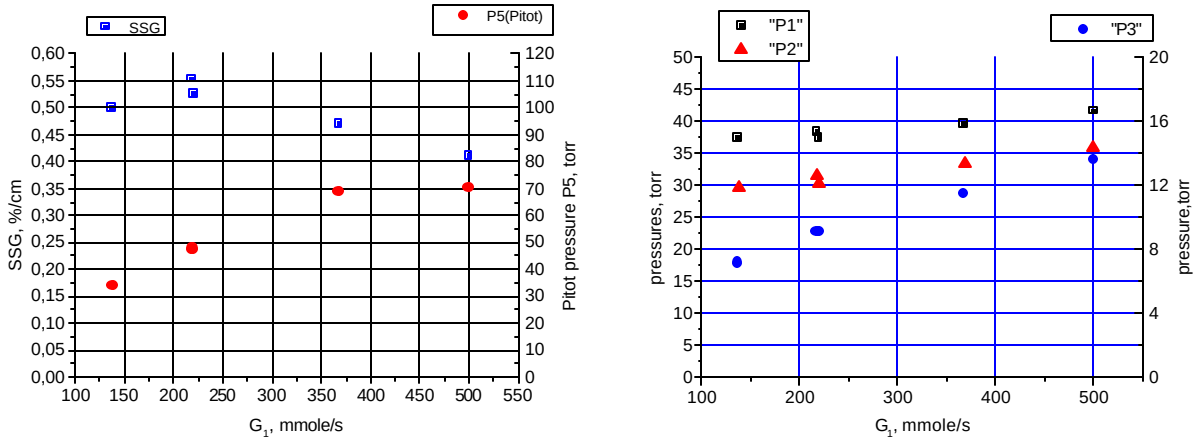

Fig. 1.18. Dependence of SSG, pressures P1, P2, P3, P5 on MNP

The effect of oxygen flow choking exists for NB-2 also. But this effect is lower than for NB-1. The pressure P3 is higher, P5 is lower than pressures for NB-1 for the same G_1. Thus Much number of flow is lower than for NB-1. As a result the gas velocity is lower but temperature is higher than for NB-1.

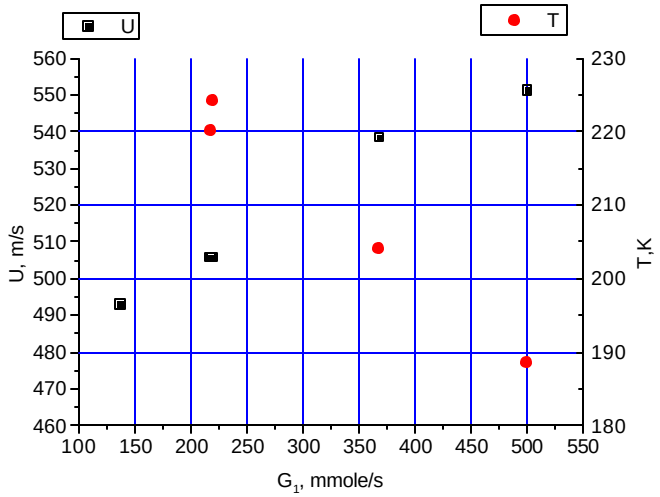

1.19.The dependence of gas velocity and temperature on G_1

1.5.2 The dependence of SSG and T on iodine molar flow rate G_{I2}.

G_1 (nitrogen)	250 or 500 mmole/s
G_2	11 mmole/s
G_0	39.2 mmole/s
G_{I2}	variable
He dilution of chlorine	0:1
T(BHP)	-16C
normal probe beam direction, y=0	

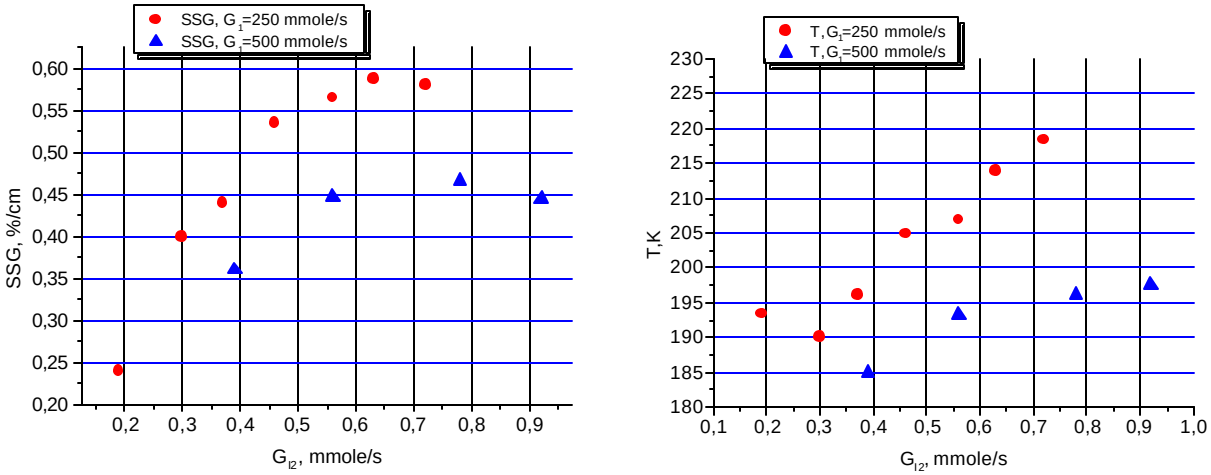

Fig. 1.20 The dependence of SSG and T on iodine molar flow rate MI2.

The SSG for NB-2 is higher than for NB-1 for the same G_{I2}. But maximum SSG is lower than for NB-1. In NB-2 iodine is injected perpendicular to oxygen flow. The residual time for high pressure $O_2(^1\Delta)$+I2 mixture is longer than for NB-1. The efficiency of iodine dissociation is better than for NB-1. As a result the SSG higher than for NB-1. The video showed that bright yellow flame in the case of NB-2 became very homogeneous and much shorter than in the case of NB-1. Simultaneously high local iodine and water vapor concentration (I, I_2, H_2O) leads to quenching of $O_2(^1\Delta)$. The quenching of $O_2(^1\Delta)$ at high G_{I2} so intense that result in degradation of SSG.

15.3. The dependence of SSG and Tm on distance from NB-2.

G_1 (nitrogen)	250 or 500 mmole/s
G_2	11 mmole/s
G_0	39.2 mmole/s
G_{I2}	0.56 mmole/s
He dilution of chlorine	0:1
T(BHP)	-16C
normal probe beam direction, y=0	

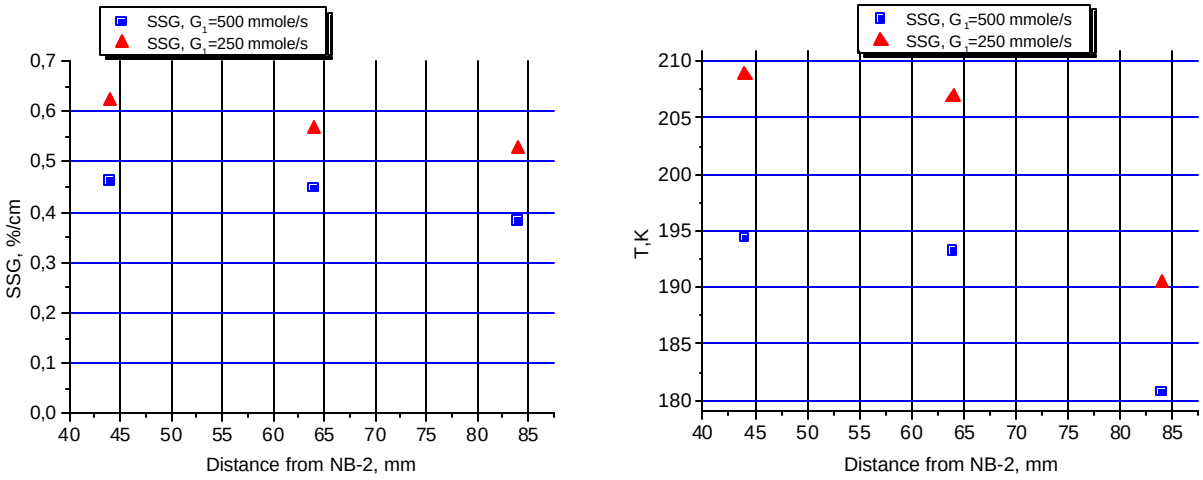

1.21. The dependence of SSG and T on distance from NB-2.

The SSG degrades along gas flow not so fast like in the case of NB-1. But the "measured temperature" T drops are essentially. There may be two effects. First: the hot $O_2(^1\Delta)$+I mixture mixes with cold N2 flow. Second: the turbulent pulsation dumps along gas flow what leads to narrowing of Doppler width W_D. The inversion population drops are more considerable than SSG (Fig.1.22.).

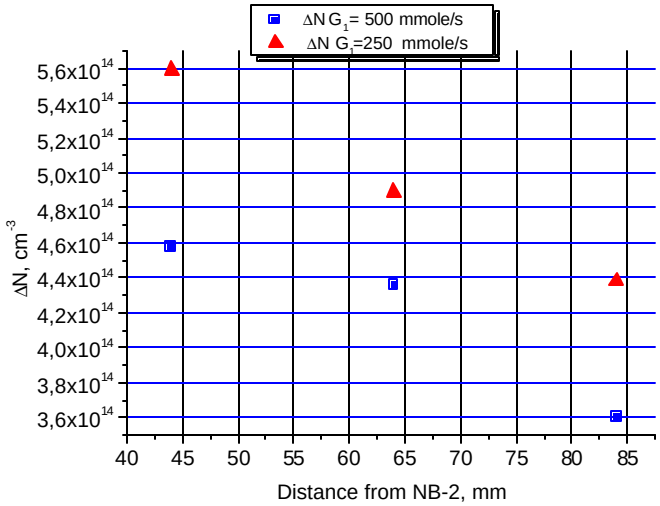

Fig.1.22 The dependence of inversion density on the distance from NB-2.

1.5.4. The operation of NB-2 with dilution of chlorine with Helium.

The dilution of chlorine with Helium was used to decrease residual time of high pressure mixture $O_2(^1\Delta)$+I2. Simultaneously the partial pressure of Cl2 and residual time in SOG were decreased also (Fig.1.23). It was measured that gas velocity U, P3 and P5 didn't depend on G(He) practically at used dilutions.

G_1 (nitrogen)	250 mmole/s
G_2	11 mmole/s
G_0	39.2 mmole/s
G_{I2}	0.45 mmole/s
He dilution of chlorine	Variable
T(BHP)	-16C
normal probe beam direction, y=0	Set-up-B, y=0

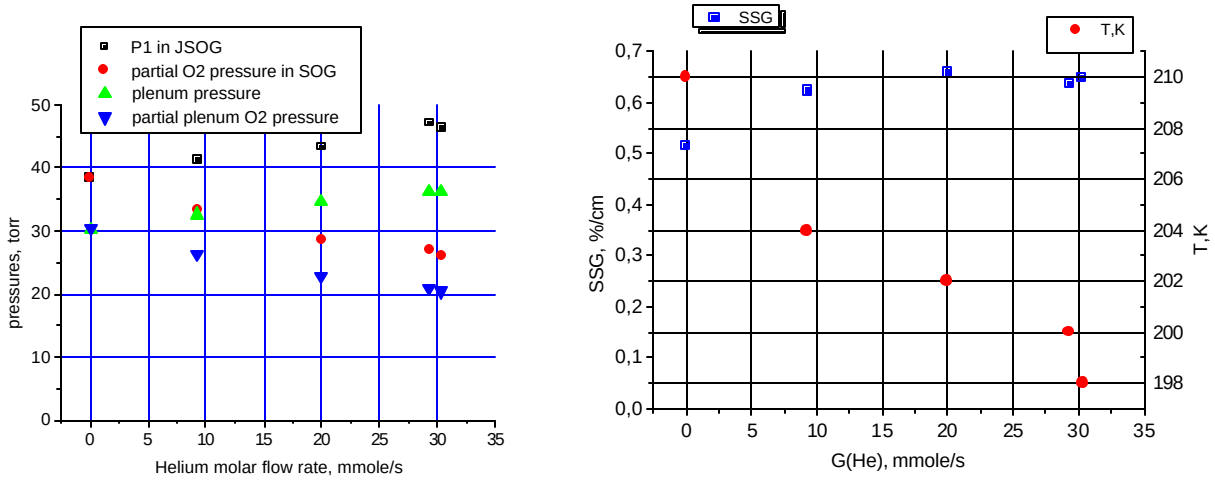

Fig.1.23. The dependence of pressures, SSG and gas temperature on Helium molar flow rate.

The dependence of SSG and T on iodine flow rate when Cl_2 diluted by Helium(Fig.1.24).

G_1 (nitrogen)	250 mmole/s
G_2	11 mmole/s
G_0	39.2 mmole/s
G_{I2}	variable
He dilution of chlorine	20mmole/s
T(BHP)	-16C
normal probe beam direction, y=0	Set-up-B, y=0

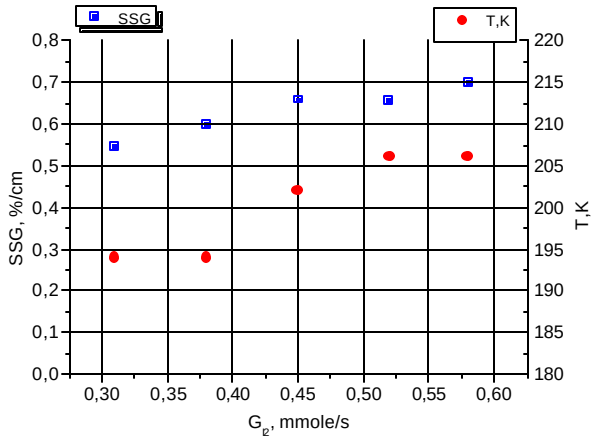

Fig.1.24.Dependence of SSG and T on iodine molar flow rate.

Hence the dilution of chlorine by helium results in increase of SSG and decrease of temperature..

1.6. PARAMETERS OF THE GAS FLOW WITH NOZZLE BANK NB-5.

The sketch of NB-5 is shown in Fig.1.25. Brief description. NB-5 consists of 7 slits (2.5x15 mm) for $O_2(^1\Delta)$, the distance between centers of slits 6.5 mm, 8 rows with 7 conical nozzles with throat ∅0.7 mm , ∅2 mm output, angle of expansion 20° for primary N2, 14 slits with height 0.5 mm for N2+I2. Unfortunately the iodine+N2 mixture flowed into tubes only from one side of tube and N2 primary flowed into the nozzle from one side also. It was due to specific design of NB-5.

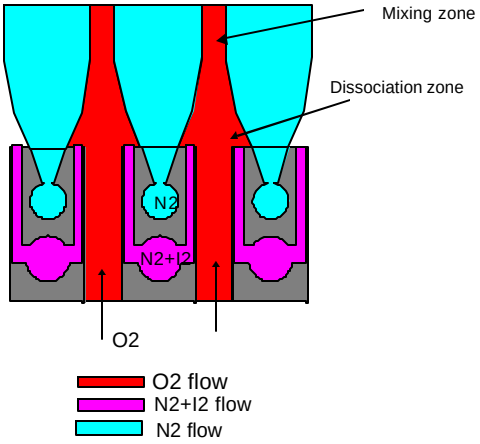

.

Fig. 1.25. The sketch of NB-5

1.6.1. Dependence of gas flow parameters on primary nitrogen molar flow rate MNP.

G_1 (nitrogen)	variable
G_2	11 mmole/s
G_0	39.2 mmole/s
G_{I2}	0.5mmole/s
He dilution of chlorine	zero
T(BHP)	-16C

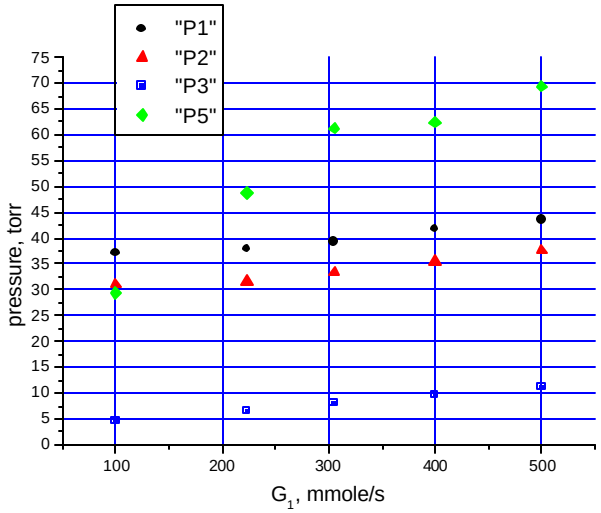

Fig.1.26.Dependencies of the measured pressures on primary nitrogen molar flow rate.

These dependencies were obtained for G_1=11 mmole/s and they change slowly on iodine molar flow rate. The absolute gas velocities U=530 m/s and U=550 m/s were obtained for G_1=250 mmole/s and G_1=500 mmole/s accordingly.

1.6.2. The dependence of SSG and T on G_{I2}.

G_1 (nitrogen)	250 or 500 mmole/s
G_2	11 mmole/s
G_0	39.2 mmole/s
G_{I2}	variable
He dilution of chlorine	0
T(BHP)	-16C
oblique probe beam direction, y=0	

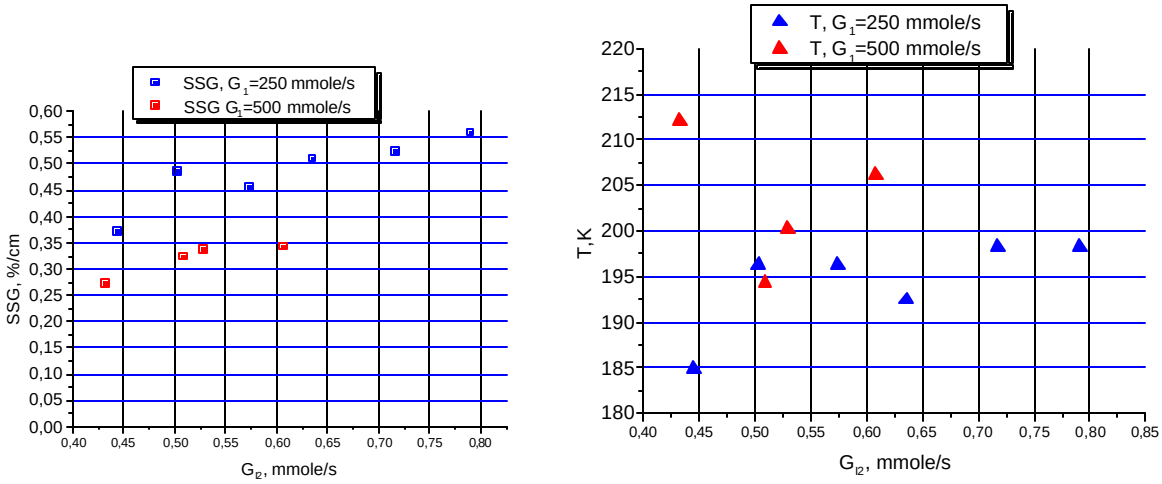

Fig.1.27. Dependencies of SSG and T on iodine molar flow rate G_{I2}

It was strange that T is higher for higher G_1.

1.6.3. Dependence of gas flow parameters on distance from NB-5.

G_1 (nitrogen)	270 mmol/s
G_2	11 mmole/s
G_0	39.2 mmole/s
G_{I2}	0.64 mmole/s
He dilution of chlorine	Zero
T(BHP)	-16C
normal probe beam direction, y=0	Set-up-A, x-variable, y=0

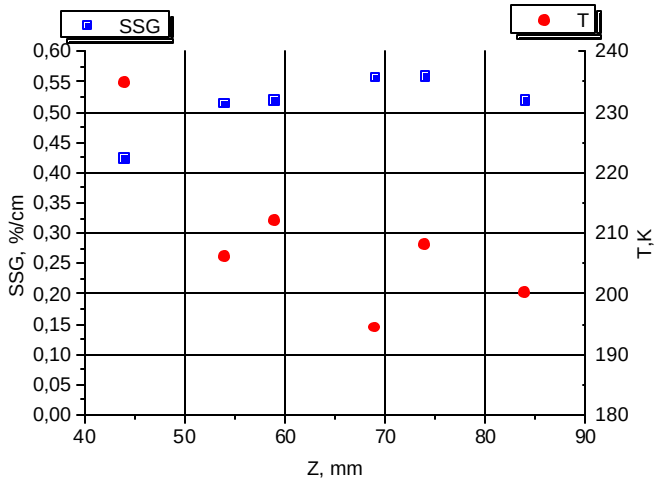

Fig. 1.28. Dependencies of gas flow parameters on the distance from NB-5.

1.6.4. Dependence of gas flow parameters on distance Y from the center of flow.

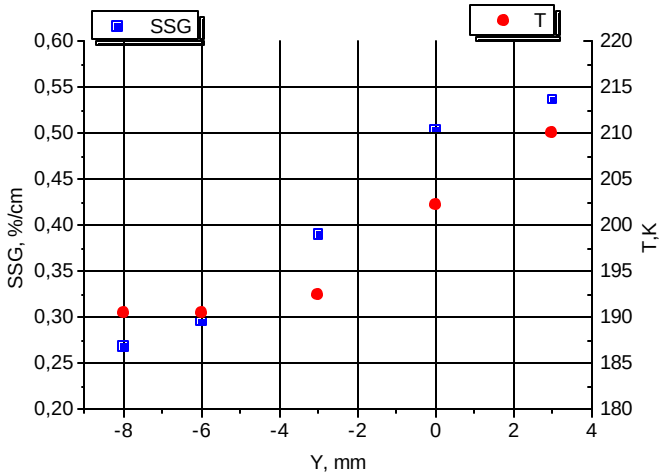

Fig.1.29. Dependence of gas flow parameters on the distance Y from the center of flow.

The strong asymmetric dependence of SSG and T on Y is due to not uniform injection of I2 and primary N2. The I2+N2 was supplied only from the left side (Y<0) of the injection tube but primary N2 was supplied nozzle only from the right side (Y>0) (see fig.1.30).

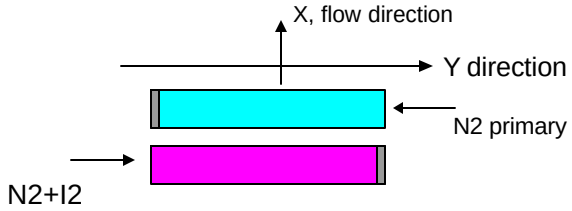

Fig.1.30. The supply of NB-5 by N2+I2 and primary N2

The given realization of the NB-5 was not successful and further experiments with it have been stopped.

1.7. PARAMETERS OF THE GAS FLOW FOR NOZZLE BANK NB-3 AND NB-4.

The cold aerodynamic experiments only were made with these both nozzle banks.

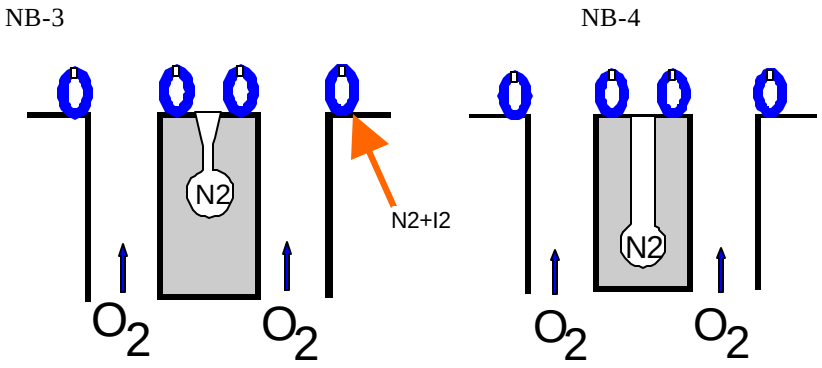

Fig.1.31. Sketch of NB-3 and NB-4

Brief description of NB-3. NB-3 consists of 7 slits (2.5x15 mm) for $O_2(^1\Delta)$, the distance between centers of slits was 6.5mm, 8 rows with 8 conical nozzles with throat ∅0.5 mm , ∅1 mm output, angle of expansion 20° for primary N2, 14 tubes with 15 holes ∅0.5mm in each tube for N2+I2. The N2+I2 flowed into tubes from both sides for more uniform injection of iodine. The N2+I2 flow is injected parallel to the $O_2(^1\Delta)$ flow. The primary nitrogen also flowed into injector from both sides for uniform injection in Y direction. **In the NB-3 nozzles for primary nitrogen are conical instead of cylindrical in NB-1.** This design should provide the weakening of the shock waves' system in the space between iodine tubes and the increase initial momentum of the ejecting nitrogen due to higher stagnation pressure (less total throat cross section square).

Brief description of NB-4. NB-4 consists of 7 slits (2.5x15 mm) for $O_2(^1\Delta)$, the distance between centers of slits 6.5 mm, 8 rows with 8 cylindrical holes ∅1.5 mm for primary N2, 14 tubes with 15 holes ∅0.5mm in each tube for N2+I2.
The N2+I2 flowed into tubes from both sides for more uniform injection of iodine. The N2+I2 flow is injected parallel to the $O_2(^1\Delta)$ flow. The primary nitrogen also flowed into injector from both sides for uniform injection in Y direction.
In the NB-4 nozzles for primary nitrogen are 1.5 mm in diameter instead of 1 mm in NB-1. This design gives possibility to decrease initial stagnation pressure of the ejecting nitrogen and to change the shock waves' system in the space between iodine tubes to weaken choking effect.

1.7.1. Results of cold aerodynamic test of NB-3.

Air (instead of chlorine) with flow rate of 40 mmole/s through JSOG was used in the cold experiments, secondary N2 flow rate was equal to 11 mmole/s. BHP jets were absent in the JSOG.

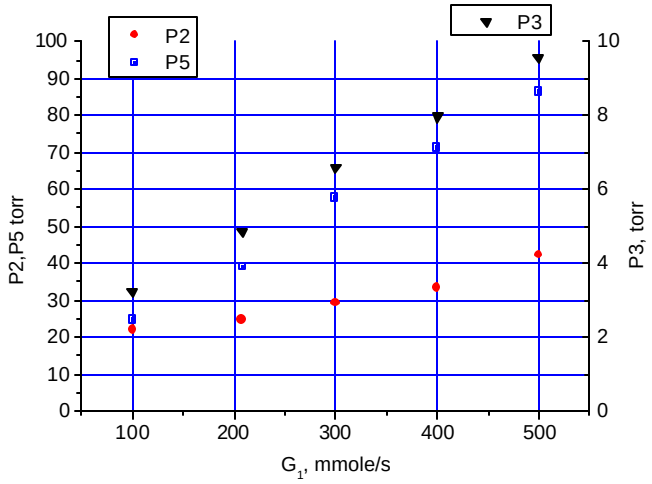

Fig.1.32. The dependence of pressures on primary nitrogen molar flow rate MNP.

The ratio $P_5/P_3 \approx 9$ and $P_2 > 30$ torr for $G_1 > 300$ mmole/s were reached in these tests. It means producing gas flow with high Much number (approximately 2.6) but with strong choking of flow from JSOG by primary nitrogen. Thus NB-3 is worse than NB-1 (the same Mach number but stronger choking). The $O_2(^1\Delta)$ should be lower for NB-3 due to higher P_2 and P_1. For this reason hot test of NB-3 were not made. This nozzle bank may give good results at dilution chlorine by helium.

1.7.2. Results of cold aerodynamic test of NB-4.

Air (instead of chlorine) with flow rate of 40 mmole/s through JSOG was used in the cold experiments, secondary N2 flow rate was equal to 11 mmole/s. BHP jets were absent in the JSOG.

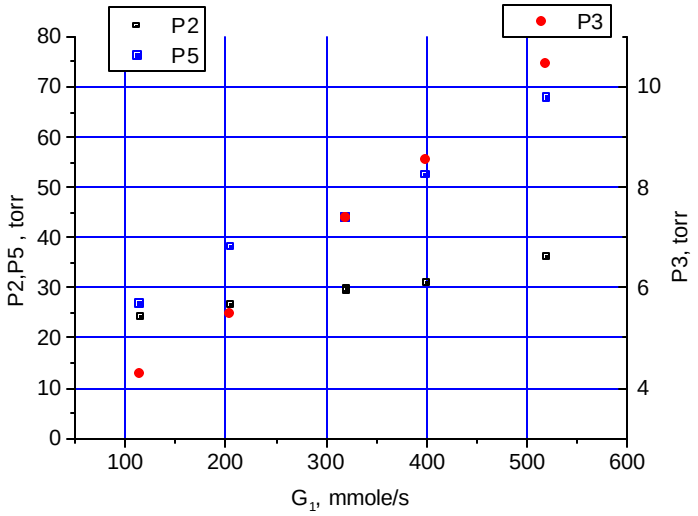

Fig.1.33. The dependencies of the different pressures on primary nitrogen molar flow rate.

The ratio $P_5/P_3 \approx 6$ and $P_2 \approx 30$ torr for $G_1 \approx 400$ mmole/s were reached in these tests. It means producing gas flow with low Much number (near 2) and not so strong choking of flow from JSOG by primary nitrogen. Thus NB-4 is worse than NB-1 (lower Mach) and NB-2(stronger choking). For this reason hot test of NB-4 were not made.

1.8. SUMMARY OF COMPARISON NOZZLE BANK DESIGNS

The parameters of active medium produced by three best versions of nozzle banks were tested using probe laser diagnostics. These nozzle banks provide high Much number, high gain, low temperature and high recovered pressure of active medium in the laser cavity. It was found that turbulent pulsation cause additional broadening of gain line but simultaneously turbulent pulsation provides fast mixing of three gas flows. The best parameters (highest SSG+ highest Pitot pressure) active medium is presented in Table.

Conditions	Parameter	NB-1	NB-2 (for G_{I2}=0.6 mmole/s)	NB-5
G_1=250 mmole/s G_2=11 mmole/s G_{I2}=0.8 mmole/s G_0==39.2 mmole/s T(BHP)=-16C	SSG, %/cm (Z=64mm)	0.65	0.6	0.55
	Gas velocity, m/s	~580	~510	530
	Temperature T, K	~210	~210	200
	Pitot pressure P5,torr	~58	~50	50
	Static pressure P3,torr	~8.5	~10	10
G_1=500 mmole/s G_2=11 mmole/s G_{I2}=0.8 mmole/s G_0=39.2 mmole/s T(BHP)=-16C	SSG, %/cm	0.5	0.45	0.35
	Gas velocity, m/s	~600	~550	550
	Temperature T, K	~180	~195	210
	Recovered pressure P5,torr	~90	~70	70
	Static pressure P3,torr	~11	~14	14

Only aerodynamic experiments with NB-3 and NB-4 were performed. The choking effect for NB-3 was very strong. The recovered pressure for NB-4 is lower than for NB-1.

Thus the active medium of COIL with high gain, high recovered pressure and low temperature can be produced by NB-1 and NB-2.

1.9. A MORE DETAIL ANALYSIS OF SOME RESULTS OF SMALL SIGNAL GAIN MEASUREMENTS ON A SUPERSONIC COIL WITH AN ADVANCED NOZZLE BANK.

The dependence of SSG and temperature on iodine molar flow rate G_{I2} is presented in fig.1.34. The SSG and temperature grow up to G_{I2} =1 mmole/s. The measurements showed that absolute gas velocity and Mach number monotonically decrease with increase of G_{I2}. This fact is evident because the increase of G_{I2} results in acceleration of chemical reactions and heat release.

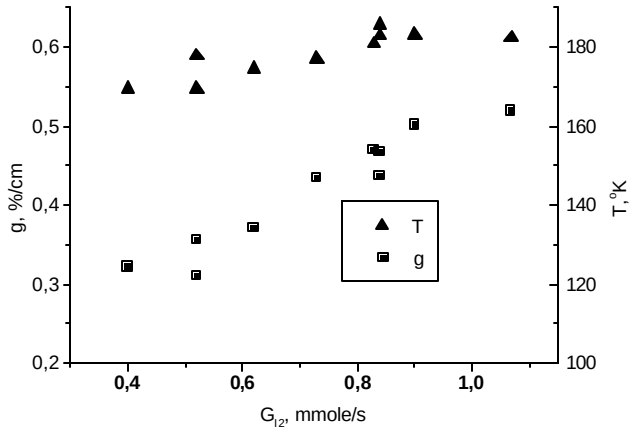

Fig.1.34. **The gain and temperature as a function of iodine molar flow rate G_{I2}. G_1=530 mmole/s, G_2=11 mmole/s, t=-16°C.**

The dependence of some parameters on primary nitrogen molar flow rate G_1 are presented in fig.1.35,1.36. The increase of G_1 results in a decrease of temperature and SSG, a raise of gas velocity, Mach number and Pitot pressure P_2. The highest absolute gas velocity U=615 m/s have been obtained for G_1=530 mmole/s. These data shows that the stagnation gas temperature T* decreases with increase of G_1 but total heat power Q increases. It was found that the raise of G_1 from 163 mmole/s to 530 mmole/s results in increase of plenum pressure from 25 torr to 34.5 torr. Hence the real throat for the oxygen flow is located downstream from the nozzle bank and its cross section decreases with increase of G_1. This aerodynamic throat for oxygen flow is formed by expanding supersonic jets of primary nitrogen. First of all the raise of G_1 results in increase of $O_2(^1\Delta)$ losses during oxygen transport between JSOG and nozzle bank. Another reason is the increase of $O_2(^1\Delta)$ losses between nozzle bank and aerodynamic throat where reactions between $O_2(^1\Delta)$ and iodine occur.

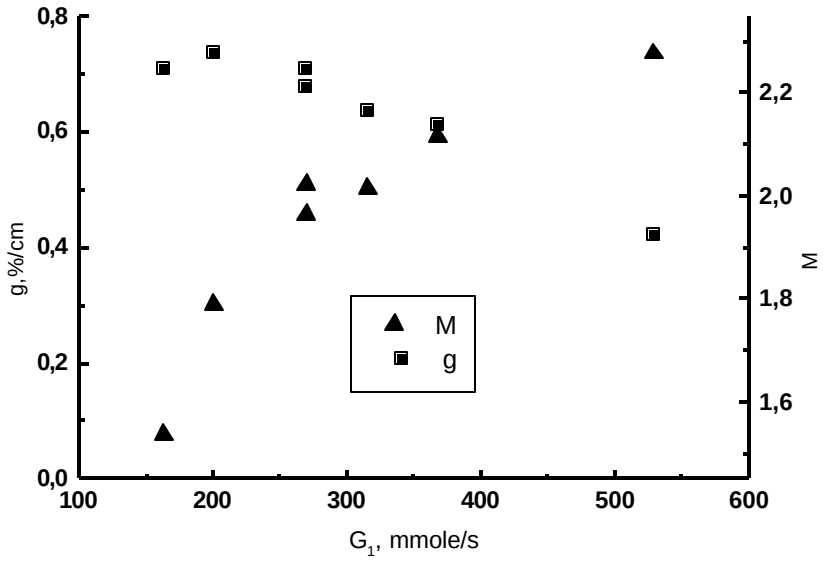

Fig.1.35. **The gain and Mach number as a function of primary nitrogen molar flow rate G_1. G_2=11 mmole/s, G_{I2}=0.8 mmole/s, t=-16°C.**

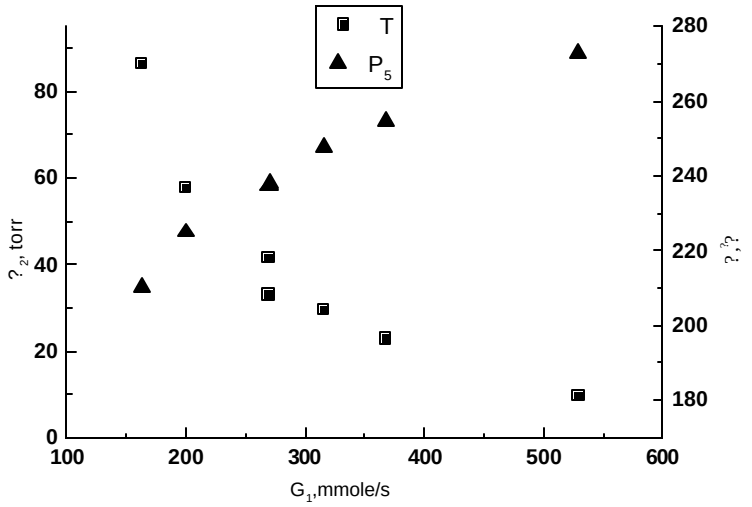

Fig.1.36. **The temperature and Pitot pressure as a function of primary nitrogen molar flow rate G_1. G_2=11 mmole/s, G_{I2}=0.8 mmole/s t=-16°C.**

The influence of BHP temperature on the active medium parameters are presented in fig.1.37,1.38. The essential decrease of the gain and increase of the static and stagnation temperatures with increase of BHP temperature is evidently due to the raise of the water vapor fraction in the oxygen flow. The increase of the heat release can be due as acceleration of chemical reaction involving water vapor as the increase of the heat release during water vapor condensation in supersonic flow. The initial average temperature of all three streams from the nozzle bank is estimated by the value ~300°K. The increase of BHP temperature from –20°C to –4°C results in increase of water vapor fraction in the oxygen flow in several times [6] but stagnation gas temperature increases only on 20°K. This increase is less than the increase of stagnation temperature from initial temperature 300°K to 375°K at BHP temperature –20°C. It means than main part of $O_2(^1\Delta)$ losses and heat release occurs as a result of chemical reaction involving rather iodine than water molecules.

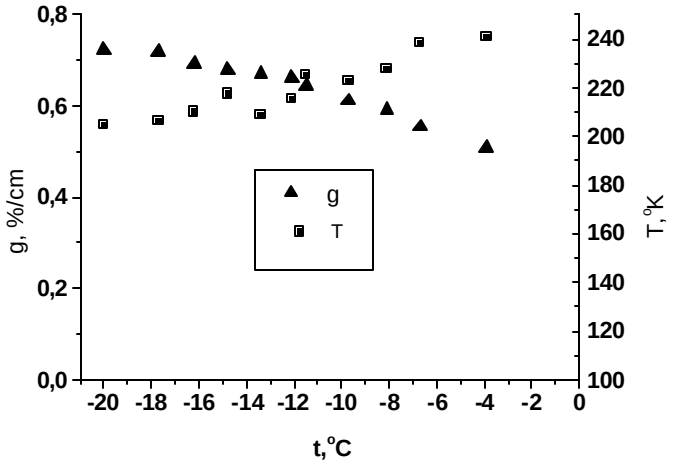

Fig1.37. **The gain and temperature as a function of BHP temperature. G_1=270 mmole/s G_2=11 mmole/s, G_{I2}=0.8 mmole/s.**

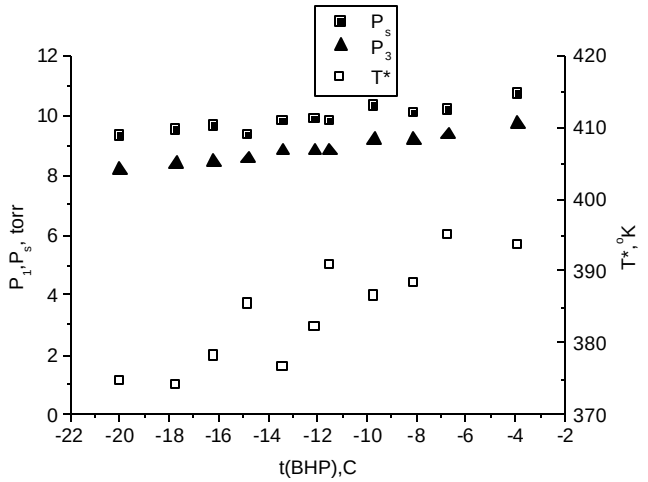

Fig.1.38. **The stagnation temperature T*, static P_s and wall pressure P_3 as a function of BHP temperature. G_1=270 mmole/s G_2=11 mmole/s, G_{I2}=0.8 mmole/s.**

The static pressure P_s was calculated from (11) in the assumption that molar ration $x_{N2}/x_{O2}=G_1/(G_0+G_1)$ that means the total mixing of all three streams flowed out from nozzle bank. The P_s and P_3 increase with the raise of BHP temperature that is due to the raise of gas temperature. The static pressure P_s is higher than the wall pressure P_3 but ratio $P_s/P_3 \approx 0.89$ doesn't depend on BHP temperature.

As expected, when the probe laser beam was directed transversely to the gas velocity vector ($\varphi=0°$) the splitting of the spectral line was absent. The dependence of gain, temperature and calculated static pressure P_s along the gas stream are presented in fig.1.39-1.41. The gas temperature is essentially constant along the flow direction but static pressure decreases linearly with the distance from the nozzle exit plane. In fact, the effect is stronger for the higher primary nitrogen flow rate. A faster drop of gain than pressure along the gas stream means that gain drop can not be explained only by expansion of the gas flow. Using the values of Mach number M=2.27 for G_1=530 mmole/s and static pressure P_s=11.6 torr at the distance 84 mm the nozzle bank (13) gives the value of Pitot pressure P_5'=82.4 torr. This value is very close to the measured Pitot pressure P_5 =88.7 torr.

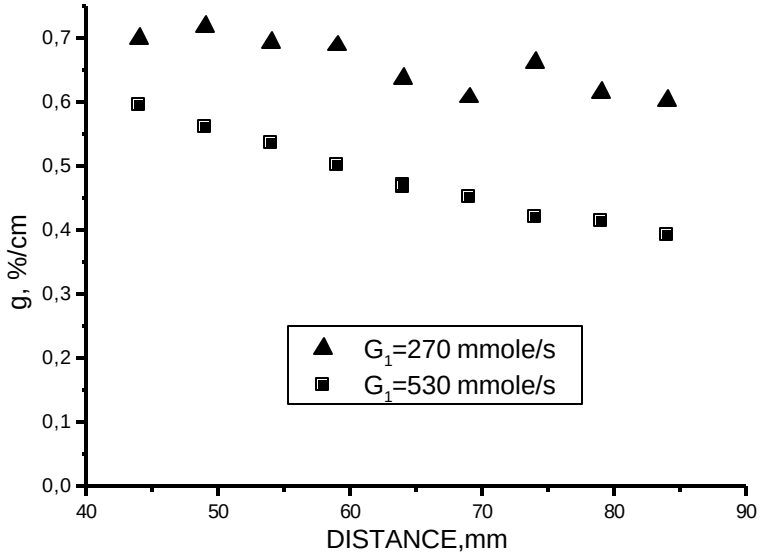

Fig.1.39. **The SSG as a function of distance from the nozzle bank. G_2=11 mmole/s, G_{I2}=0.8 mmole/s, t=-16°C.**

The probe laser measurements along gas flow have been performed also for higher BHP temperature t= –5,6°C and G_{I2}=0.8 mmole/s and for lower iodine molar flow rate G_{I2}=0.4 mmole/s and BHP temperature –16°C. In both cases the highest gain was achieved also at distances less than 44 mm from the nozzle bank and temperature was approximately constant along gas flow. It was found that the rate of the gain decrease along a gas flow didn't depend on G_{2I} and BHP temperature.

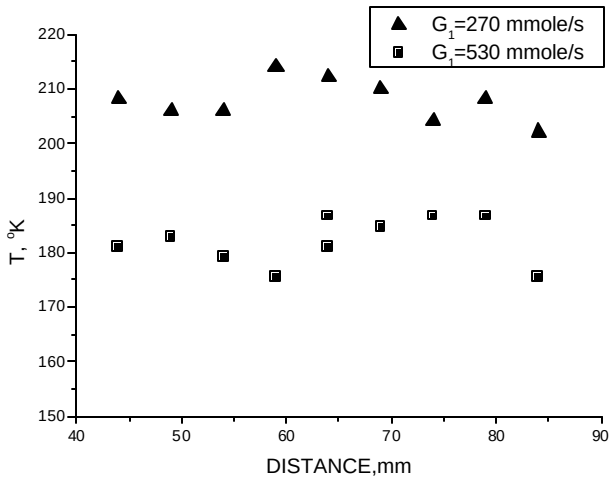

Fig.1.40. **The temperature as a function of distance from the nozzle bank. G_2=11 mmole/s, G_{12}=0.8 mmole/s, t=-16°C.**

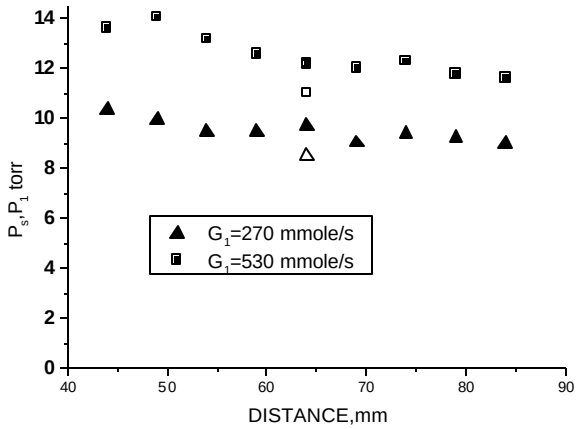

Fig.1.41. **The static pressure as a function of distance from the nozzle bank. G_2=11 mmole/s, G_{12}=0.8 mmole/s, t=-16C. Open symbols is the wall pressure at the distance 64 mm from the nozzle bank.**

1.10. DISCUSSION

The highest gain and low gas temperature establish on the distances less than 44 mm from the exit of the nozzle bank. The temperature of those parts of stream that contains atomic iodine is depends on the distance from the nozzle bank. The low gas temperature can not be explained only by supersonic expansion of oxygen+iodine flow. According to spectroscopic data for G_1=530 mmole/s the temperature T=181°K and static pressure P_s= 12.2 torr establish at distance 64 mm from nozzle bank. For the same gas flow conditions M=2.27, and wall pressure P_3=11 torr is slightly lower than static pressure determined from spectroscopic data. This data gives calculated stagnation pressure P*=145 torr. This value is much higher than plenum pressure of oxygen 34.5 torr and stagnation pressure of the secondary nitrogen flow (in experiment stagnation pressure of 11 mmole/s of secondary nitrogen equaled 60 torr). The high stagnation pressure of zones containing gain can be due only to momentum transfer from the high momentum stream of the primary nitrogen. The momentum transfer occurs simultaneously with heat and mass transfer between cold primary nitrogen supersonic flow and gain zones.

Hence the low temperature of gain zones is due to mass and heat transfer between oxygen-iodine stream and stream of primary nitrogen. The observed fast mass, heat and momentum transfer rate can't be explained only by molecular transfer mechanism. For rarified oxygen-nitrogen gas at pressure 11 torr the molecular transfer coefficient D is of the order of 10 cm^2/s. The estimated mixing distance is of the order of $L_m \approx (d^2/D)U \approx 700$ cm, where $d \approx 0.35$ cm is the distance between oxygen and nitrogen nozzles. This distance is much bigger than the observed distance of mixing.

The supersonic gas stream generated by ejector nozzle bank is characterized by a strong initial inhomogeneous distribution of the gas-dynamic parameters: velocity, pressure, temperature. The initial inhomogeneous distribution of gas-dynamic parameters results in generation the periodic and chaotic pulsation of the gas velocity, pressure and temperature. High Reynolds number of the flow ($Re \approx 5000$) and heat release in oxygen-iodine zones can intensify these pulsation. This

pulsation results in much faster heat, mass and momentum transfer. The fast mass transfer is supported by LIF experiments showed fast mixing of all three streams flowed out from nozzle bank [1]. The fast momentum transfer was supported also by measurements of Pitot pressure(fig.1.42). In these aerodynamic experiments the Pitot pressure distribution was measured in the center plane of the mixing chamber by Pitot tube 2 mm in diameter. The oxygen flow was replaced by nitrogen flow of 39.2 mmole/s. It was found that ratio of average Pitot pressure deviation to the average Pitot pressure across gas flow decreases from 30% to 7% when the distance increases from 40 mm to 90 mm from the nozzle bank.

The fast mixing is accompanied by chaotic transverse pulsation of gas velocity. The transverse velocity pulsation leads to additional broadening of gain line because of Doppler effect. The additional broadening of the gain line shape may be caused by wave processes on the contact borders of the jets also. The high pressure primary nitrogen jets expand and generate intense transverse momentum which provides compression of the oxygen and N_2+I_2 jets which tends to promote choking of the flow downstream of the minimum geometric cross sectional area (ie. the nozzle bank). The static oxygen pressure in this aerodynamic throat is higher than the nitrogen pressure. The oxygen jets then expand to become supersonic which compresses the nitrogen jets. The compressing and decompressing of jets can be repeated many times along gas flow [7]. In connection with this the correct interpretation of data obtained from the spectroscopic measurements occurs. The distribution of transverse velocity U_T can contain a Gaussian component

$$P(U_T) = \frac{1}{U_0}\sqrt{\frac{\ln 2}{\pi}}\exp\left(-\left(\frac{U_T}{U_0}\right)^2 \ln 2\right)$$

where U_0 is the characteristic velocity. It gives the overestimation of the gas temperature on $\Delta T(°K)=(U_0/9.53)^2$, where U_o is in (m/s). For example the transverse velocity U_0 of the order of 30 m/s results in ~10°K overestimation of the gas temperature. The possibility of turbulence in COIL active medium with pulsation transverse velocity of the order of 20% of the streamwise velocity have been predicted in [8].

The decrease of the SSG with distance from the nozzle exit plane may be partially explained by the gas flow expansion and pressure drop (fig.1.41). This, however, is insufficient to explain the decrease in the small signal gain along the flow direction. The kinetics of the excited state quenching of oxygen and iodine at low temperatures are poorly understood. Analysis using room temperature rate constants for the quenching of O_2 ($^1\Delta$) and exited iodine atoms cannot explain the observed drop in the SSG along the flow direction. At low gas temperatures the homogeneous condensation of water vapor and the attachment of iodine atoms to the surface of the small ice particles may play a substantial role. Water vapor and iodine condensation on BHP aerosol particles can also take place.

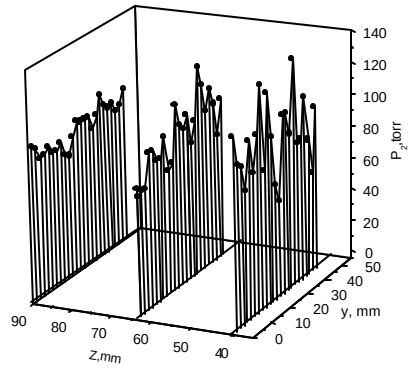

Fig.1.42. The Pitot pressure distribution. G_1=50 mmole/s, G_2=11 mmole/s, G_0(nitrogen)=9.2 mmole/s, G_{I2}=0. y-direction across the flow, z-direction along the flow

It was found that the static pressure calculated from (11) is slightly higher than the wall pressure for given experimental conditions. One of the reasons of this discrepancy is the overestimation of the gas temperature from (7). Another possible reason of the pressure difference is the existence of shock and expansion waves in the mixing chamber.

The compression of oxygen flow and secondary nitrogen flow by primary nitrogen jets plays a very important role in the formation of gain in the present nozzle bank. The compression leads to the formation for oxygen-iodine flow of aerodynamic throat located downstream nozzle bank. It seems to us that the main part of molecular iodine dissociated in the region between iodine injection and aerodynamic throat cross sections. The chemical reactions that occur in dissociation region results in O_2($^1\Delta$) losses and heat release. The optimization of position and size of this aerodynamic throat is the key to achieve the high gain with minimal losses of O_2($^1\Delta$). This situation is analogous to optimization of the iodine injection point and the throat size in COIL with slit nozzle [9, 10].

1.11. CONCLUSION

Tunable Diode laser spectroscopy has been used to interrogate the gain in the COIL active medium. A detailed analysis gives not only the SSG and temperature but other important parameters of the supersonic flow. The absolute gas velocity, static pressure, gas temperature of the gain medium generated by an advanced ejector nozzle bank have been determined from spectroscopic data. At absolute gas velocity ~600 m/s the maximum gain and low temperature are achieved at distances less 44 mm from the nozzle bank. The fast cooling and high stagnation pressure of the oxygen-iodine flow are evidence of fast mass, heat and momentum transfer between primary nitrogen and oxygen-iodine flows. The gas temperature is approximately constant along a gas flow. It was found that gain drops along gas flow faster than the pressure caused by expansion of flow in mixing chamber. The ejector nozzle bank produces a gain medium with high Mach number M=2.27, low gas temperature~180K° , high small signal gain $\approx 5\times10^{-3}$ cm^{-1}, high potentially recovered pressure of the order of 100 torr at primary nitrogen molar flow rate 530 mmole/s. The static pressure of supersonic flow determined from the spectroscopic data is slightly higher than the wall pressure. The decrease of primary nitrogen molar flow rate down to 270 mmole/s increases of the gain up to 7×10^{-3} cm^{-1} but increase the gas temperature to 220°K. The rise of BHP temperature from –20°C to –4°C leads to the gain decrease in 1.4 times, increase of the gas temperature and static pressure.

Fast transfer phenomena in the gain medium generated by ejector nozzle bank is due to generation of a transverse component of stream velocity that cause additional broadening of gain line. In this situation the calculated gas temperature and static pressure are overestimated.

REFERENCES

[1] G.D. Hager, T.G. Madden, V.D. Nikolaev, M.V. Zagidullin, "An efficient supersonic COIL with more than 200 torr of the total pressure in the active medium", in *31st AIAA Plasmadynamics and Lasers Conference*, 19-22 June 2000, Denver, Colorado, USA, AIAA Paper 2427-2000;

[2] R.F.Tate, B.S.Hunt, C.A. Helms, K.A. Truesdell, G.D. Hager, "Spatial gain measurements in a chemical oxygen iodine laser (COIL)", *IEEE J.Quantum Electronics*, vol. 31, pp. 1632-1636 , 1995

[3] T.L. Henshow, T.J. Madden, J.M. Herbelin, G.C. Manke, B.T. Anderson, R.F.Tate, G.D. Hager, " Measurements of gain on the 1.315 μm transition of atomic iodine produced from the $NCl(a^1\Delta)$ energy transfer laser", *SPIE*, vol. 3612, pp. 147-156, 1999

[4] S.J. Davis, W.J.Kessler, M. Bachmann, "Collisional broadening of absorption lines in water and atomic iodine relevant to COIL diagnostics", *SPIE*, vol. 3612, pp. 157-166, 1999

[5] V.D. Nikolaev, M.I. Svistun, M.V. Zagidullin, N.A.Khvatov "The temperature dependence of pressure broadening of $^2P_{1/2}$-$^2P_{3/2}$ transition of atomic iodine" *Quantum Electronics*, vol 31, pp. 373-376, 2001

[6] D.Furman, B.D.Barmashenko, S.Rosenwaks. "Diode-laser based absorption spectroscopy diagnostics of a jet-type $O_2(^1\Delta)$ generator for chemical oxygen-iodine lasers", *IEEE Journal of Quantum Electronics*, vol.35, pp.540-547, 1999

[6] G.N. Abramovich, "Theory of the turbulent jets", Moscow, 1984, Nauka, p.51

[7] J.E.Scott, J.L. Shaw, K.A.Truesdell, G.D.Hager, C.A.Helms, AIAA-Design considerations for the chemical oxygen-iodine supersonic mixing nozzle. – *in 25th AIAA Plasmadynamics and Lasers Conferencf*., Colorado Springs, CO, June 20-22, 1994, *Paper 94-2436*,

[8] M.V.Zagidullin, V.D.Nikolaev, M.I.Svistun, N.A.Khvatov, N.I.Ufimtzev, «Highly efficient supersonic chemical oxygen-iodine laser with a chlorine flow rate of 10 mmole/s», *Quantum Electronics* , vol.27, pp. 195-199, 1997

[9] J.I.Galea, S.A.Orszag, K.R.Sreenivasan, "Time – dependent simulations of laminar and turbulent flows in COIL geometries," *in AIAA 31st AIAA Plasmadynamics and Lasers Conference*, 19-22 June 2000, Denver, CO, paper 2000-2572.

Part 2. AERODYNAMIC TESTS OF THE NEW EJECTOR NOZZLES

2.1. IMPROVEMENT OF DESIGN OF THE NOZZLE BANK CONSIDERING UP TO DATE UNDERSTANDING OF THE EXISTENT PHENOMENA.

NB-6, NB-7, NB-8 have been additionally designed and manufactured

NB-6. NB-6 consists of 5 slits (3.5x16 mm) for $O_2(^1\Delta)$ (flow 0), the distance between centers of slits 9.5 mm, 6 rows with 7 conical nozzles with throat ∅1 mm , ∅2 mm output, for primary N2 (flow 1), 10 tubes with 15 holes ∅0.5mm in each tube for N2+I2 (flow 2). The N2+I2 flowed into tubes from both sides for more uniform injection of iodine. The N2+I2 flow is injected parallel to $O_2(^1\Delta)$ flow. The primary nitrogen also flowed into injector from both sides for uniform injection in Y direction. The larger cross section of oxygen nozzle have been made to decrease choking effect.

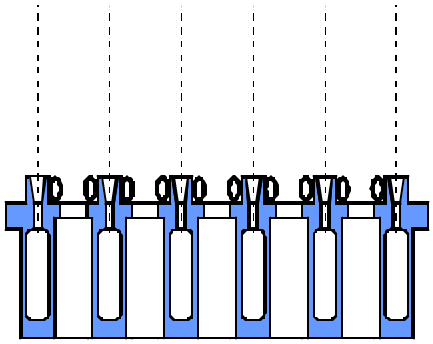

Fig.2.1
Axis of conical nozzles parallel to axis of mixing chamber

NB-7. NB-8 consists of 5 slits (3.5x16 mm) for $O_2(^1\Delta)$ (flow 0), the distance between centers of slits 9.5 mm, 6 rows with 7 conical nozzles with throat ∅1 mm , ∅2 mm output, for primary N2 (flow 1), 10 tubes with 15 holes ∅0.5mm in each tube for N2+I2 (flow 2). The N2+I2 flowed into tubes from both sides for more uniform injection of iodine. The N2+I2 flow is injected parallel to $O_2(^1\Delta)$ flow. The primary nitrogen also flowed into injector from both sides for uniform injection in Y direction. The larger cross section of oxygen nozzle have been made to decrease choking effect.

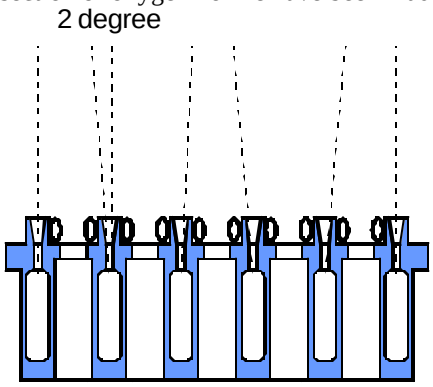

Fig.2.2
Axis of conical nozzles turned on 2 degree relative to the axis of mixing chamber. In the next row of conical nozzles the direction nozzles axis are reversed. The axis of the extreme nozzle parallel to the chamber axis.
Designed of NB-7 was not correct and no test have been made with NB-7.

NB-8. NB-8 consists of 5 slits (3.5x16 mm) for $O_2(^1\Delta)$ (flow 0), the distance between centers of slits 9.5 mm, 6 rows with 7 conical nozzles with throat ∅1 mm , ∅2 mm output, for primary N2 (flow 1), 10 tubes with 15 holes ∅0.5mm in each tube for N2+I2 (flow 2). The N2+I2 flowed into tubes from both sides for more uniform injection of iodine. The N2+I2 flow is injected parallel to $O_2(^1\Delta)$ flow. The primary nitrogen also flowed into injector from both sides for uniform injection in Y direction. The larger cross section of oxygen nozzle have been made to decrease choking effect.
The axis of the 4 conical central nozzles for primary nitrogen are turned on 2degree, the axis of the extreme nozzles are parallel to the chamber axis. The axis of the next 4 lower central nozzles are turned on 2 degree in the reverse direction. Hence 4 of 7 nozzles in one row are turned on 2 degrees in right direction and 3 of 7 nozzles in left direction.

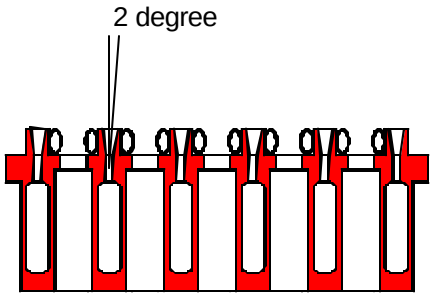

Fig.2.3

2.2. 'COLD' GAS DYNAMIC TESTS OF NEW DESIGN OF THE NOZZLE BANK USING THE SPECIAL RESONATOR CAVITY WITHOUT THE MIRROR TUNNELS.

Results of 'cold' gas dynamic tests.

The next parameters have been measured: P2-oxygen plenum pressure, P3-static wall pressure at the distance 64 mm from the nozzle bank, Pitot pressure P5 at the distance 90 mm from the nozzle bank in the center of the mixing chamber. M-mach number of flow. The results of experiments for G_1~500 mmole/s of primary nitrogen (flow 1), G_0=39.2 mmole/s of air (flow 0) through oxygen nozzles and G_2=11 mmole/s of secondary nitrogen (flow 2) are presented in Table .

Nozzle bank	G_1,mmole/s (flow 1)	P_2, torr	P_3, torr	P_5, torr	M
NB-1	516	30	8.8	78	2.54
NB-2	510	29.8	10.5	61	2.05
NB-3	500	42	9.56	86	2.57
NB-4	520	36	10.5	68	2.15
NB-5	495	30.5	8.1	65.4	2.42
NB-6	525 250	15.8 13.6	7.7 3.5	106 48.6	3.2 3.2

2.3. THE PITOT PRESSURE DISTRIBUTION.

The Pitot pressure distribution across (Z direction) and along flow(X direction) for nozzle banks NB-1, NB-6, NB-8 was measured in detail.

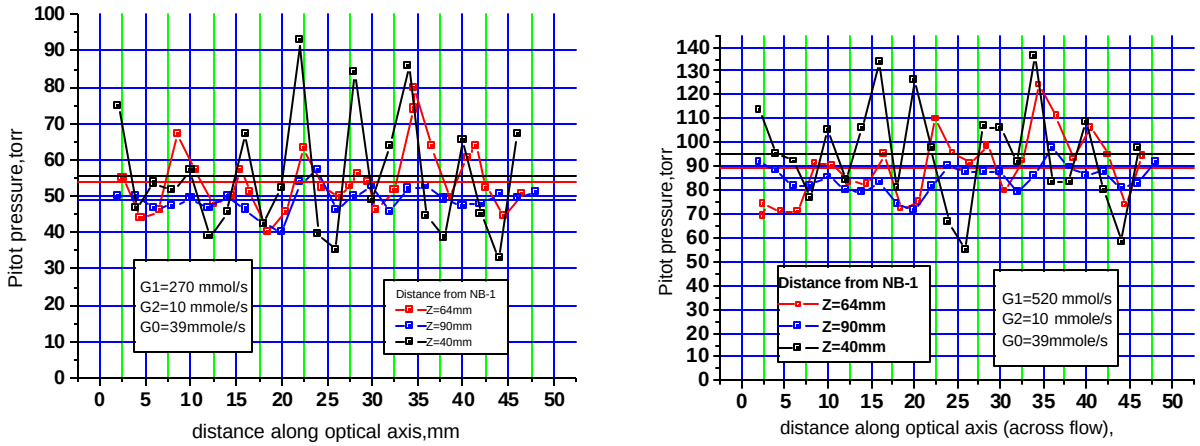

Fig. 2.4. The Pitot pressure distribution for NB-1.

The average Pitot pressure is shown by solid line. The ratio of the average Pitot pressure deviation to the average value is shown in Fig.2.5.

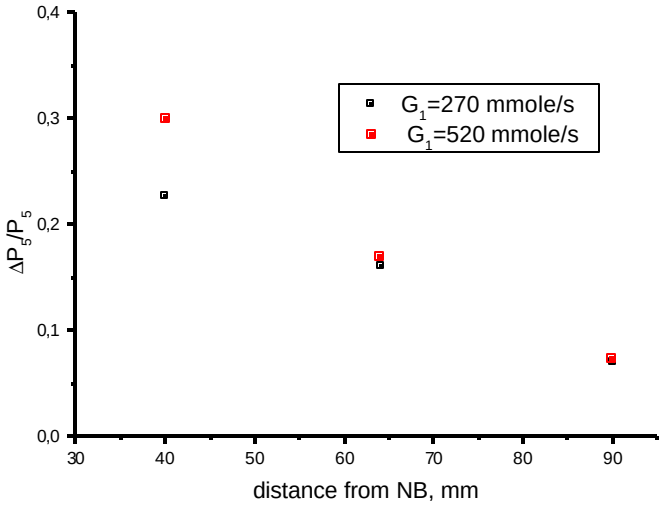

Fig.2.5 The damping of Pitot pressure deviation. (NB-1).

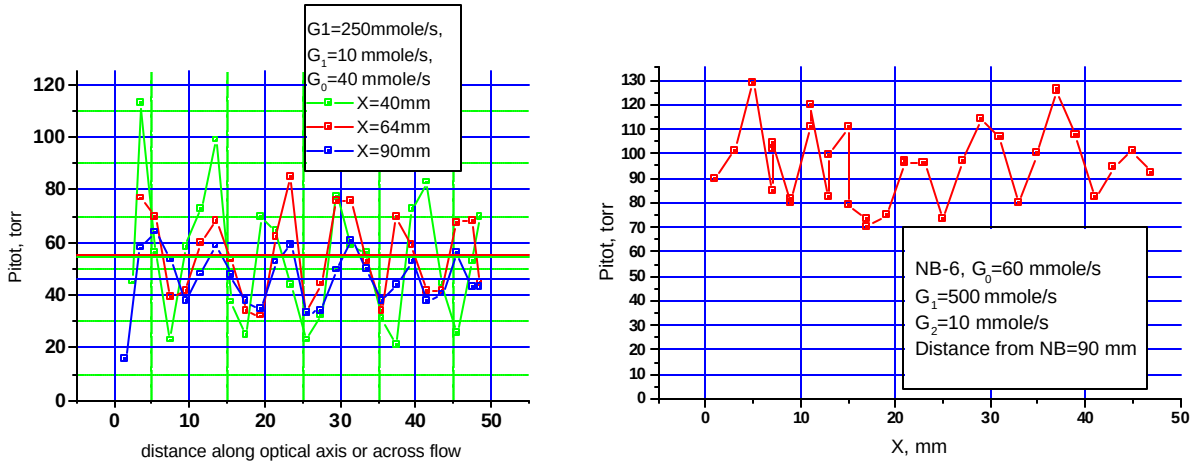

Fig.2.6. Pitot pressure distribution for NB-6 for low and high nitrogen molar flow rate through oxygen nozzles.

The damping of Pitot pressure deviation along gas flow for NB-6 is low than for NB-1.

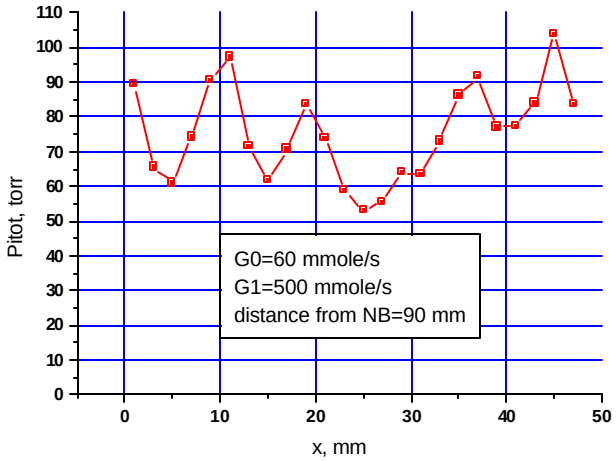

Fig.2.7 The Pitot pressure distribution across gas flow for NB-8.

The Pitot pressure distribution across gas flow for NB-1 is much smooth than for NB-6 and NB-8. It seems to us that more smooth distribution for NB-1 is due to a) smaller scale of oxygen nozzles, b) the cylindrical nozzles produce nitrogen jets with higher size than conical nozzles. The lower average Pitot pressure for NB-8 than for NB-6 is due to oblique direction of nozzle axis.

2.4. STUDY OF EFFICIENCY AND MIXING RATE OF IODINE USING LASER INDUCED FLUORESCENCE.

The Laser induced fluorescence (LIF) experiments to observe mixing of gas flows generated by NB-1, NB-2, NB-6, NB-8. The array of Ar-laser beams were produced by hologram. The direction of flow is perpendicular to the AR-laser beams and directed up. The yellow trace is molecular iodine emission. Higher yellow emission is higher iodine concentration. The appearance of dark traces in the upper part of LIF picture is due to low intensity of Ar-laser beams in upper part of mixing chamber because the upper beams corresponds to higher order of hologram interference. Single Ar-beam LIF experiments were also performed for better contrast of LIF picture.

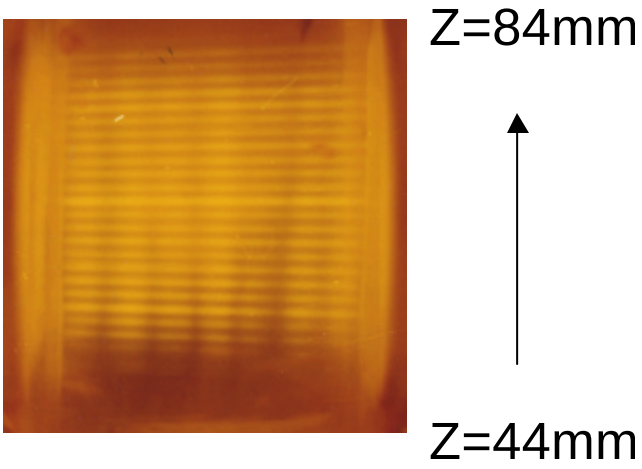

Fig.2.8. LIF picture in mixing chamber for NB-1. G_1=500 mmole/s, G_2=10 mmole/s, G_0=40 mmole/s.

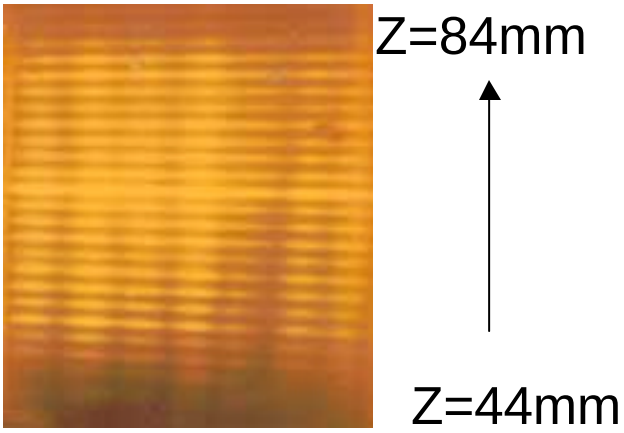

Fig.2.9. LIF picture in mixing chamber for NB-2. G_1=500 mmole/s, G_2=10 mmole/s, G_0=40 mmole/s

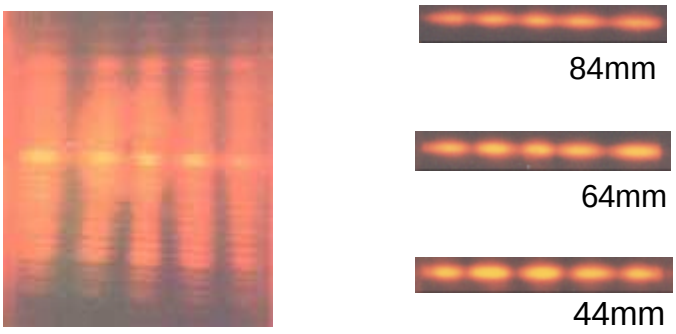

a b

Fig.2.10. LIF picture in mixing chamber for NB-6. G_1=500 mmole/s, G_2=10 mmole/s, G_0=60 mmole/s. a) iodine through oxygen nozzles, b)iodine through iodine nozzles

The LIF experiments showed that flow 2 is totally mixed with flow 0 from oxygen nozzles but primary nitrogen flow 1 is not totally mixed with flow 2. For nozzle bank NB-6 the additional LIF experiment was performed . A molecular iodine vapor were added to the nitrogen flow 0 through oxygen nozzles and through iodine nozzles only pure secondary nitrogen flow 2 was passed. The LIF pictures were practically identical.

Thus the LIF experiments showed that flow 2 is almost totally mixed with flow 0 but primary nitrogen 1 is not totally mixed with mixture of flows 0 and 2.

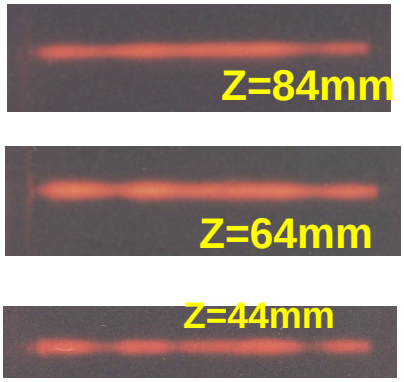

Fig.2.11. LIF picture in mixing chamber for NB-8. G_1=500 mmole/s, G_2=10 mmole/s, G_0=60 mmole/s.
These observations showed that mixing efficiency is better for NB-8, than for NB-6.

2.4.1. Summary

The Pitot pressure distribution and LIF observations showed that better mixing occurs when next actions are made:

1.Decrease of nozzle element scale,
2. Using cylindrical nozzles instead of conical or profiled nozzles.
3. Deflection of nozzle axis relative to the each other and relative chamber axis.

3. NEW COIL POWER EXTRACTION EXPERIMENT WITH EJECTOR NOZZLE BANK

3.1. New power extraction experiments with NB-1.

The output power in COIL experiments was measured from both mirrors. The total power is $W=W_1+W_2$, where W_{is} the output power from the first mirror, W_2 is the output power from the second mirror. The total mirror transmission is T1+T2.

3.1.1Dependence of output power and gain on the iodine molar flow rate.

G_1 (nitrogen)	270mmole/s
G_2 (nitrogen)	11 mmole/s
G_0	39.2 mmole/s
He dilution of chlorine	no diulution
T(BHP)	-16C
first mirror transmission T1	2.4%
second mirror transmission T2	0.8%

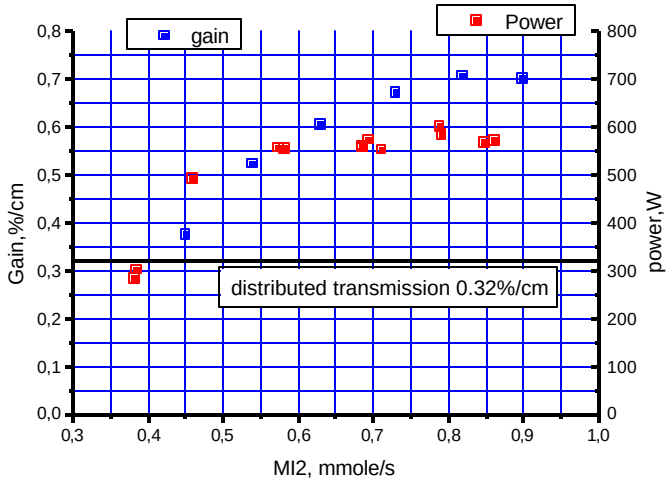

Fig. 3.1. Dependence of gain and output power on iodine molar flow rate.

G_1 (nitrogen)	530mmole/s
G_2 (nitrogen)	11 mmole/s
G_0	39.2 mmole/s
He dilution of chlorine	no diulution
T(BHP)	-16C
first mirror transmission T1	1.5%
second mirror transmission T2	0.8%

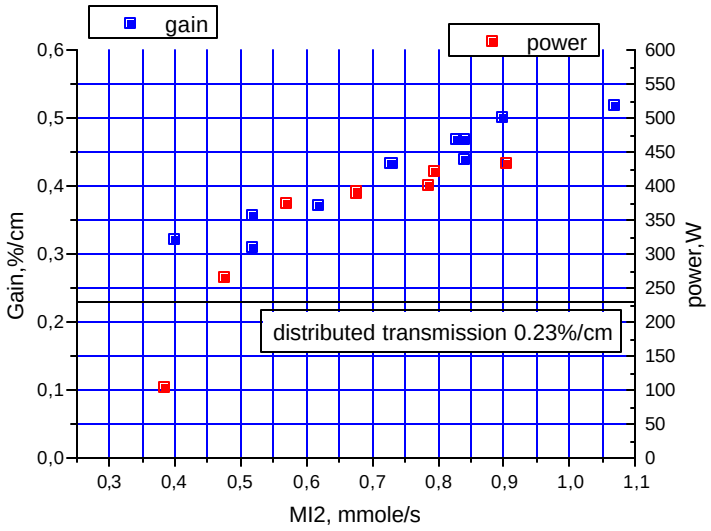

Fig. 3.2. Dependence of gain and output power on iodine molar flow rate.

The maximum power is achieved at iodine molar flow rate less than iodine molar flow rate at which maximum gain establishes.

3.1.2 DEPENDENCE OF OUTPUT POWER ON TOTAL MIRROR TRANSMISSION

G_1 (nitrogen)	270 or 530mmole/s
G_2 (nitrogen)	11 mmole/s
G_0	39.2 mmole/s
G_{I2}	
He dilution of chlorine	no diulution
T(BHP)	-16C

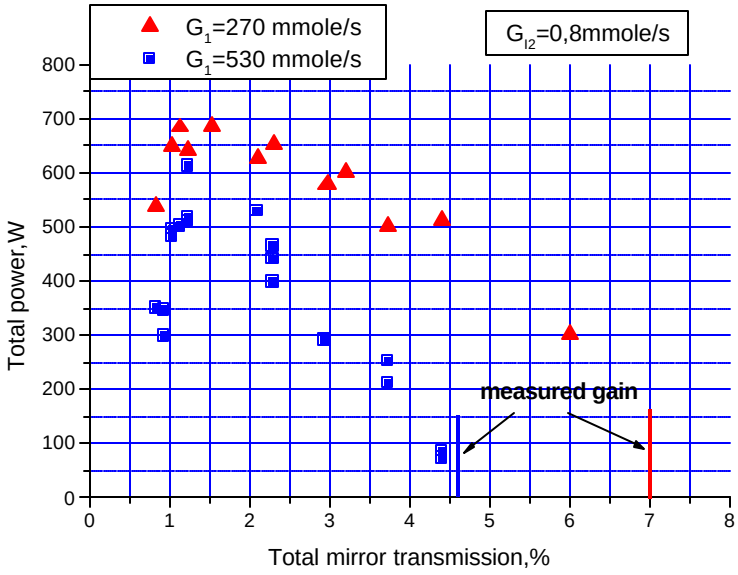

Fig.3.3. The dependence of output power on total mirror transmission.

The gain measured by probe laser is close to the gain at which output power vanishes.

3.1.3. COIL experiments with chlorine pre-diluted with Helium.

G_1 (nitrogen)	270 or 530mmole/s
G_2 (nitrogen)	11 mmole/s
G_0	39.2 mmole/s
G_{I2}	0.8 mmole/s
He dilution of chlorine	variable
T(BHP)	-16C
first mirror transmission T1	1.1%
second mirror transmission T2	0.14%

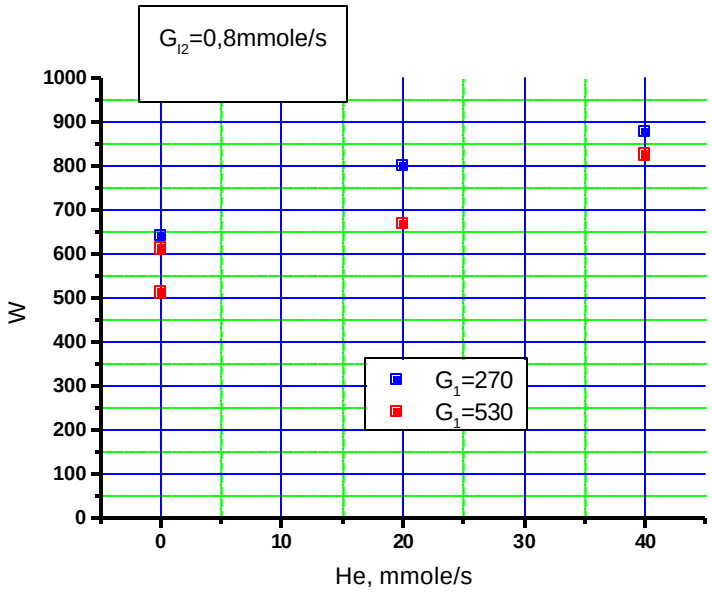

Fig.3.4. Dependence of ouput power on Helium molar flow rate

G_1 (nitrogen)	270 or 530mmole/s
G_2 (nitrogen)	11 mmole/s
G_0	39.2 mmole/s
G_{I2}	
He dilution of chlorine	40 mmole/s
T(BHP)	-16C

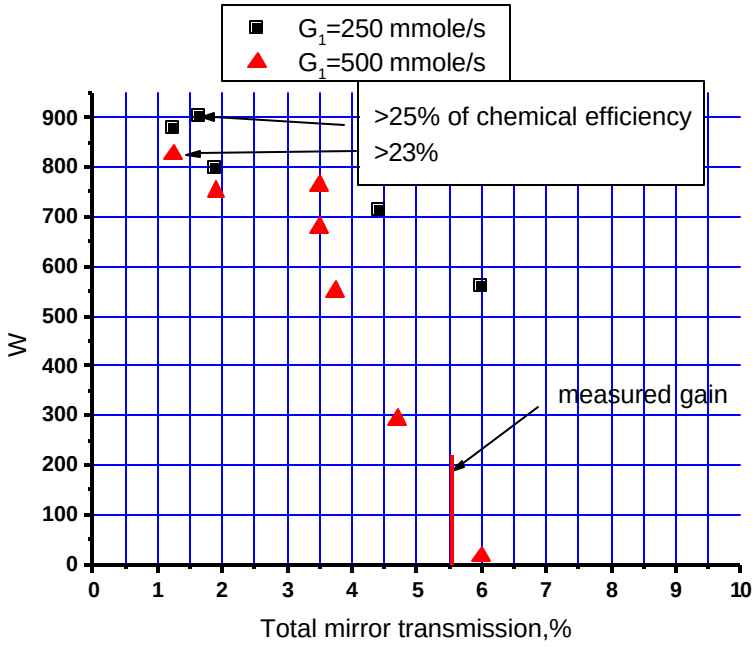

Fig.3.5. Dependence of output power on total mirror transmission.

The main conclusion from these experiments: the dilution of chlorine by Helium results in substantial power increase. But it was found that SSG didn't substantially increase (Part 1). Hence the dilution by He results in increase of $O_2(^1\Delta)$ yield but not gain.

3.2 NEW POWER EXTRACTION EXPERIMENTS WITH NB-2.

3.2.1. COIL Operation at G_1=270 mmole/s.

G_1 (nitrogen)	270 mmole/s
G_2 (nitrogen)	11 mmole/s
G_0	39.2 mmole/s
He dilution of chlorine	no dilution
T(BHP)	-16C
first mirror transmission T1	1.1%
second mirror transmission T2	0.14%

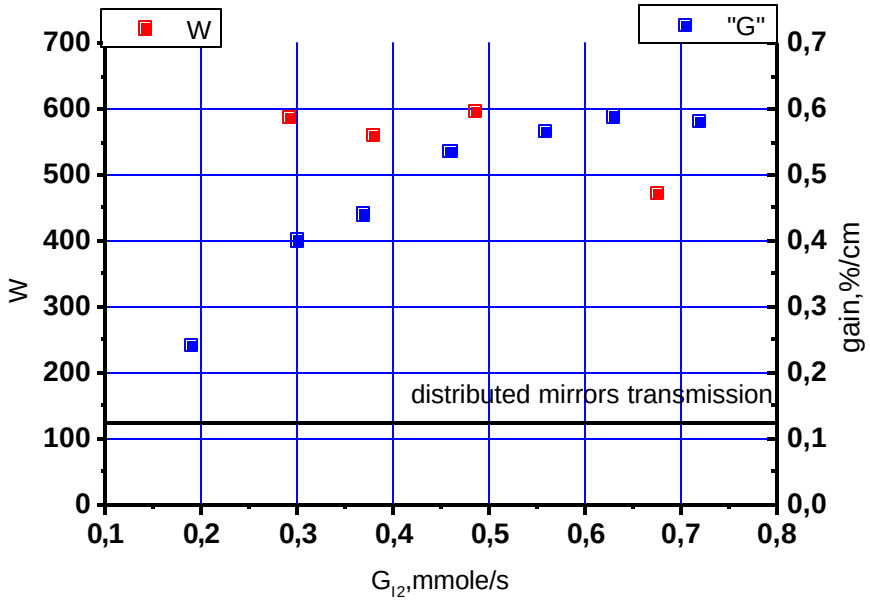

Fig.3.6. Dependence of gain and output power on iodine molar flow rate

The maximum power is achieved at much low G_{I2} than maximum gain. So to big losse of $O_2(^1\Delta)$ during formation of gain medium by NB-2.

G_1 (nitrogen)	270 mmole/s
G_2 (nitrogen)	11 mmole/s
G_0	39.2 mmole/s
G_{I2}	0.59 mmole/s
He dilution of chlorine	variable
T(BHP)	-16C
first mirror transmission T1	1.5%
second mirror transmission T2	0.8%

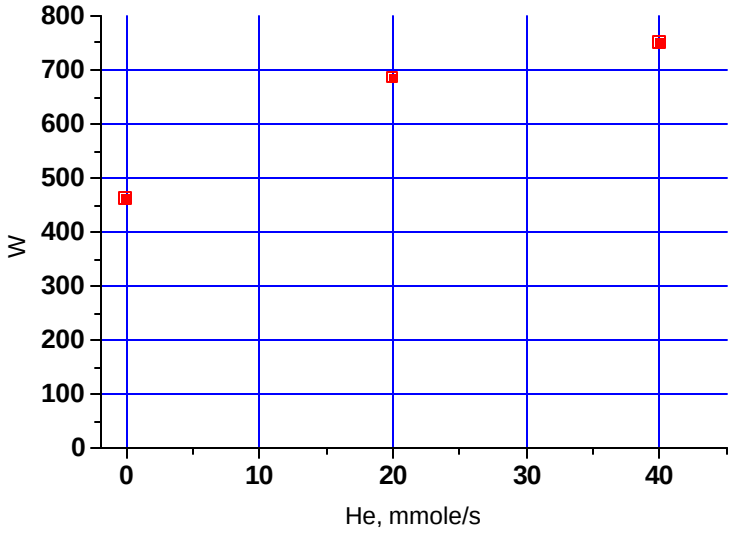

Fig.3.7.Dependence of output power on He dilution

G_1 (nitrogen)	270 mmole/s
G_2 (nitrogen)	11 mmole/s
G_0	39.2 mmole/s
G_{I2}	0.5 mmole/s
He dilution of chlorine	variable
T(BHP)	-16C

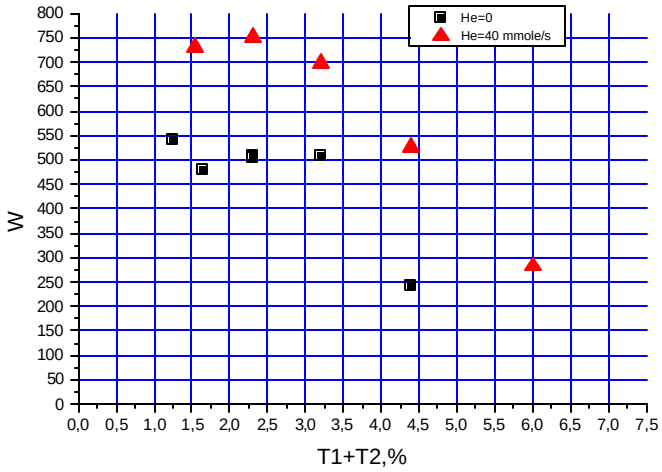

Fig.3.8. Dependence of power on the total mirror transmission

3.2.2. COIL operation at G_1=530 mmole/s.

G_1 (nitrogen)	530 mmole/s
G_2 (nitrogen)	11 mmole/s
G_0	39.2 mmole/s
G_{I2}	0.48 (optimal)
He dilution of chlorine	0
T(BHP)	-16C
first mirror transmission T1	1.5%
second mirror transmission T2	0.08%
OUTPUT POWER	**409 W**

G_1 (nitrogen)	530 mmole/s
G_2 (nitrogen)	11 mmole/s
G_0	39.2 mmole/s
G_{I2}	0.48 (optimal)
He dilution of chlorine	40 mmole/s
T(BHP)	-16C
first mirror transmission T1	1.5%
second mirror transmission T2	0.08%
OUTPUT POWER	**690 W**

3.3. COIL OPERATION WITH NB-6 AND NB-8.

In the next table the main results of power extraction with NB-6 and NB-8 are presented. The higher chlorine molar flow rate 56 mmole/s was in these experiments.

Parameter	NB-8	NB-6
G_0, mmole/s	56	56
G_1, mmole/s stagnation pressure, atm	500 3,3	500 3,5
G_2, mmole/s	10	10
Power without dilution by He Plenum pressure 44 torr	870W(17%)	654W(12.9%)
Power with dilution CL_2:He=1:1 Total Plenum pressure 53 torr Oxygen partial pressure 26.5 torr	956W(18.8%)	increase of Helium dilution results in power decrease for Cl_2:He 1:1 dilution 525W for Cl_2:He 1:0.5 dilution 624W

The decrease of power with increase of helium molar flow rate in the case of NB-6 we explain by shorter residence time of the oxygen-iodine mixture in the region between nozzle bank and aerodynamic throat.

3.4. CONCLUSION

The highest chemical efficiency have been achieved with NB-1 and helium dilution of chlorine. In the case of NB-2 the losses of $O_2(^1\Delta)$ are bigger than in the case of NB-2. Probably in the case of NB-6 the residence time of oxygen-iodine mixture at high pressure between nozzle bank and aerodynamic throat is short to achieve efficient dissociation of iodine. Another reason is much worse mixing of oxygen-iodine stream with primary nitrogen stream. Unfortunately the probe laser diagnostics experiments have not been performed with NB-6 and NB-8. The higher power with NB-8 than with NB-6 is due to better mixing of flows. The residence time between nozzle bank in the case of NB-6 is expected shorter than in the case of NB-8. It is proved by increase of power with increase of He dilution in the case of NB-8 and reverse dependence in the case of NB-6.

3.5. ANALYSIS OF POWER EXTRACTION.

The measurements of gas flow parameters, gain, singlet oxygen yield allow to predict output power and then compare it with real power obtained in power extraction experiments. In this section the results of measurements $O_2(^1\Delta)$ yield, chlorine utilization, gain, gas flow parameters, predicted and measured power for COIL with NB-1 are presented.

3. 5.1. $O_2(^1D)$ yield

In fig.3.9. the results of measurements of $O_2(^1\Delta)$ yield upstream of NB-1 (plenum yield). "Pressure*residence time" equals to the product of pressure in the JSOG and residence time. The measurements of $O_2(^1\Delta)$ were made according to following procedure. The photodetector measured spontaneous emission of $O_2(^1\Delta)$ in the volume in front of NB-1. The output from detector+amplifier is voltage V. that proportional to $O_2(^1\Delta)$ concentration. The partial oxygen pressure in front of NB-1 P_{O2} is easy calculated from chlorine and helium molar flow rates, total pressure and chlorine utilization. The changing of chlorine molar flow rate and dilution by Helium allowed to change the $p\tau$ parameter. The ration V/P_{O2} is proportional to $O_2(^1\Delta)$ yield $V/P_{O2} = AY$. The extrapolation of V/P_{O2} when $p\tau \to 0$ gives AY_d where Y_d is a detachment yield of $O_2(^1\Delta)$ from BHP. Hence the colibration constant of photodetector can be found if one knows value Y_d. Two values were assumed $Y_d=1$ and $Y_d=0.75$. The first value means that oxygen leaves BHP with 100% fraction of $O_2(^1\Delta)$. The detachment yield $Y_d=0.75$ is assumed are measured in several paper [1].

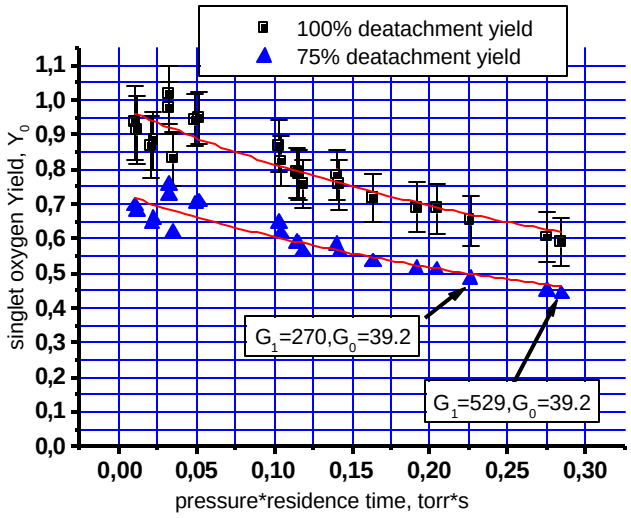

Fig. 3.9. $O_2(^1D)$ Yield from JSOG

The pointer in the fig.1 indicated the $O_2(^1\Delta)$ yiled in the case chlorine molar flow rate G_0=39.2 mmole/s and primary nitrogen molar flow rate G_1=270 mmole/s or G_1=529 mmole/s The higher $p\tau$ and lower yield for G_1=529 mmole/s is due to choking of the oxygen flow by primary nitrogen stream.

3.5.2. Calculation of gas flow parameters from spectroscopic measurements.

The gas stream temperature, velocity, Mach number, stagnation temperature have been calculated on the basis of spectroscopic measurements presented in Part 1. Additionally it is assumed of 100% mixing of three initial flows and uniformity of flow.

The total heat power release in the flow is calculated by

$$Q=(T^*-T_0)CG \quad (1)$$

where T* is the stagnation temperature calculated from (9) of Part1, C is the known molar heat capacity, G is the total molar flow rate, T_0=300K is the initial stagnation temperature (average temperature of three flows flowing out from NB-1) Some amount of heat power is due to water vapor condensation. We assume that water vapor molar flow rate is equal to $G_{H2O}=P_{H20}*G_0/P_1$ where P_{H20}=1.15 torr is the saturated water vapor pressure in JSOG at –16C. Also it is assumed that all water vapor condensed in the cold supersonic flow. The heat of water vapor condensation Q_c is calculated by

$$Q_c = G_{H2O}55.7(KJ/mole) \quad (2)$$

where 55.7 kJ/mole is the heat of water sublimation at 200K. The water vapor condensations results in increase of stagnation temperature

$$\Delta T^*_c = Q_c / CG \qquad (3)$$

The difference of heat power $Q-Q_c$ and stagnation temperature $\Delta T^* = T^* - T_0 - \Delta T^*_c$ is mainly due to quenching of $O_2(^1\Delta)$ because the main source of energy is $O_2(^1\Delta)$. Here we neglect excitation of vibration levels of molecules and heat of interhalogen reactions. Hence the fraction of $O_2(^1\Delta)$ that consumed for heating of flow is

$$\Delta Y_h = \frac{(Q - Q_c)}{G_0 U t 94.3} \qquad (4)$$

At low temperature (200K) the inversion ΔN is practically equal to the iodine atoms concentration. Hence approximately

$$N_I \approx \Delta N = \frac{8p}{A_{34} l^2} \int_{-\infty}^{\infty} g(n)\, dn \qquad (4)$$

Hence the number of dissociated iodine molecules is $\Delta N_{I2} = N_I/2$. It corresponds to the changing of the iodine molecule molar flow rate $\Delta G_{I2} = \Delta N_{I2} US$, where S is the cross section of the chamber, U is the gas velocity. The number of $O_2(^1\Delta)$ molecules consumed for the break of the I_2 bound is

$$\Delta Y_b = \frac{0.5 N_I S U \cdot 148.6}{G_0 U t \cdot 94.3} \qquad (5)$$

148.6 J/mole is the dissociation energy of I_2.
Thus total $O_2(^1\Delta)$ losses is

$$\Delta Y_{los} = \Delta Y_b + \Delta Y_h. \qquad (6)$$

The inlet $O_2(^1\Delta)$ fraction in the flow is given by

$$Y = Y_0 - \Delta Y_{los} \qquad (7)$$

.

To predict the output power the simplest model of Fabry-Perot resonator with infinite mirror along gas flow will be used. The predicted power is calculated by

$$W = G_0 90.6 \cdot U t \cdot \frac{t}{t + a} \cdot (Y - Y_{Th}) \qquad (8)$$

where Y_{Th} is the threshold $O_2(^1\Delta)$ fraction at which gain is equal to the distributed losses of the laser cavity $g_{th} = (t+\alpha)/2L$, L=5 cm is the gain length, t is the total mirror transmission, α is the nonresonant losses, 90.6 J/mmole is the energy of 1 mmole of $O_2(^1\Delta)$.
The Y_{Th} is given by

$$Y_{Th} = \frac{2(g_{th} / s N_I) + 1}{2K_{eq} + 1 - 2(K_{eq} - 1)(g_{th} / N_I s)} \qquad (9)$$

where $\sigma = \frac{7}{12} \frac{A l^2}{8p} V(0)$ is the emission cross section, that can be defined from

$$g = s \frac{(Y - Y_{th})(K_{eq} + 0.5)}{(K_{eq} - 1) Y + 1} N_I \qquad (10)$$

where g is the measured peak SSG, $Y_{th} = (2K_{eq}+1)^{-1}$.

Finally output power is given by

$$W = G_0 \cdot U t \cdot 90.6 \frac{t}{t + a} (Y - Y_{th}) \left[1 - \frac{g_{th}}{g} \left[1 - \frac{g_{th}}{g_0} \frac{Y - Y_{th}}{Y + (K_{eq} - 1)^{-1}}\right]^{-1}\right] = G_0 \cdot U t \cdot 90.6 (Y - Y_{th}) h_{FP} \qquad (10)$$

where

$$h_{FP} = \left[1 - \frac{g_{th}}{g}\left(1 - \frac{g_{th}}{g_0}\frac{Y - Y_{th}}{Y + (K_{eq} - 1)^{-1}}\right)^{-1}\right] \qquad (11)$$

is the extraction efficiency of Fabry-Perot resonator with infinite mirrors.

The chemical efficiency

$$h_c = (Y - Y_{th}) \cdot Ut \cdot h_{FP} \quad (12)$$

3.5.3. Estimated and measured chemical efficiencies.

The analysis will be performed for COIL with NB-1 for two primary molar flow rates. The calculations have been performed for detachment yield 75%. Results of calculations for detachment yield 100% are presented in brackets.

Input Parameter		
Nozzle bank	NB-1	NB-1
G_0, mmole/s	39.2	39.2
G_1, mmole/s	270	530
G_2, mmole/s	11	11
G_{I2}, mmole/s	0.81	0.81
The cross section of flow , S, cm^2	10	10
Mirror transmission, %	1.14	1.14
Nonresonant losses (estimation),%	0.5	0.5
Mixing efficiency (assumed)	100	100
Geometry efficiency	100	100
Y_0, %	51(67)	45(60)
Chlorine utilization Ut ,%	95	95
Power (experiment)	683	612
Chemical efficiency η_c	0.192	0.172

Output (measured values)		
g, % $\Delta N \approx N_I$, cm^{-3}	7 10^{15}	4.2 7×10^{14}
U, m/s	580	610
T, K	207	181

Calculated parameters		
Mach number	2.02	2.25
T*, K	378	369
T_0, K	294	295
ΔT^*_c, K	9.7	4.3
$O_2(^1\Delta)$ Heat losses ΔY_h	0.20	0.35
$O_2(^1\Delta)$ losses to break bond I-I ΔY_b	0.02	0.015
inlet $O_2(^1\Delta)$ fraction $Y=Y_0-\Delta Y_h-\Delta Y_b$	0.29(0.45)	0.085(0.23)
Threshold $O_2(^1\Delta)$ fraction $Y_{th}=(2K_{eq}+1)^{-1}$	0.088	0.068
Extraction efficiency η_{FP} ,%	0.59(0.60)	0.44(0.50)
Predicted chemical efficiency $\eta=(Y-Y_{th})\times Ut\times\eta_{FP}$	0.12(0.22)	0.1(0.084)

The predicted chemical efficiency is close to measured only for G_1=270 mmole/s and for assumption than $O_2(^1\Delta)$ yield from JSOG is close to 67%. The predicted power for G_1=530 mmole/s is much less than measured for both assumption about $O_2(^1\Delta)$ yield from JSOG. It means that some assumptions were not correct. Let' consider what kind of assumption result in underestimation of power. First of all it is overestimation of $O_2(^1\Delta)$ losses. Second is underestimation of power extraction efficiency. The overestimation of $O_2(^1\Delta)$ losses can be due to assumption (1). The ratio (1) means that all part of gas stream has the same temperature defined from spectroscopic measurements. This assumption can be not correct in the case of G_1=530 mmole/s. Hence the $O_2(^1\Delta)$ losses calculated from (4) can be overestimated. The another reason of overestimation is the underestimation of heat power caused by water vapor condensation. If the carryout of BHP aerosol takes place then the heat of condensation (freezing) will be higher and ratio (4) will give lower losses of $O_2(^1\Delta)$.

The underestimation of power extraction also can exsists. We don’t know the exact value of nonresonant losses. But the value of extraction efficiency of the order of 0.5 for small gain length COIL is reasonable value and comparable with extraction efficiency obtained in another works.

4. THE TEMPERATURE DEPENDENCE OF PRESSURE BROADENING OF $^2P_{1/2}$-$^2P_{3/2}$ TRANSITION OF ATOMIC IODINE

4.1 INTRODUCTION

Pressure broadening of the $^2P_{1/2}$-$^2P_{3/2}$ transition in atomic iodine has been extensively studied in conjunction with the photodissociative iodine laser [1-5]. Measurements of pressure broadening coefficients have been performed for room and higher temperatures. In [4] the predicted inverse temperature dependence of the pressure broadening coefficients was in agreement with measurements in the temperature range 300°-1000°K. In a supersonic COIL with a cavity pressure of 10 torr and temperatures lower 200°K the broadening of the gain spectrum by pressure and by the Doppler effect are comparable. High resolution tunable diode laser spectroscopy has recently been used to obtain high resolution scans of the $^2P_{1/2} - {}^2P_{3/2}$ transition in atomic iodine [6-7]. For example in [7] the atomic iodine transition $^2P_{1/2}$-$^2P_{3/2}$ was resolved with an accuracy 6 MHz and pressure broadening coefficients were measured for nitrogen, helium, and oxygen at room temperature.

The line shape of the gain/(absorption) on the strongest hyperfine transition $^2P_{1/2}(F=3)\rightarrow{}^2P_{3/2}(F=4)$ in atomic iodine is a Voigt function which is a convolution of a gaussian G with FWHM W_D and the lorenzian L with FWHM W_L

$$g(X) = \Delta N \frac{A_{34} l^2}{8p} L(X) * G(X) = \Delta N \frac{A_{34} l^2}{8p} V(X\ \ ) =$$

$$\Delta N \frac{A_{34} l^2}{8p} \sqrt{\frac{\ln(2)}{p}} \frac{W_L}{pW_D} \int_{-\infty}^{\infty} \frac{\exp\left(-Z^2 4\ln 2 / W_D{}^2\right)}{(X-Z)^2 + \left(\frac{W_L}{2}\right)^2} dZ \qquad \textbf{(1)}$$

where V(X) is the Voigt function, the integral of V(X) is normalized to 1, $X=\nu-\nu_o$ is the frequency relative the center of the line, ΔN is the inversion density, A_{34} is the Einstein coefficient, and λ=1.315μm wavelength.

The FWHM of the Gaussian is $W_D(MHz) = 14.49\times\sqrt{T}$, where T is the gas temperature. The FWHM of Lorenzian is proportional to partial pressure of the gas components and is additive: $W_L=\Sigma\alpha_i P_i f_i(300/T)$, where α_i is the pressure broadening coefficient of the i^{th} gas component for T=300°K, P_i is the partial pressure of the i^{th} component and $f_i(1)=1$. The Lorenz theory of pressure broadening predicts growth of the function f_i (300/T) with a decrease in temperature. If the interaction potential has the form $V(R) = CR^{-N}$ that results in a resonance frequency shift [8] then f $(300/T) = (300/T)^{\gamma}$ where $\gamma = (N+1) / 2(N-1)$. For example if N=3 then γ=1, N=6, γ=0.7. In the approximation of hard sphere collisions $N\rightarrow\infty$ and one obtains γ=0.5. Previous work has used approximations of γ=1(N=3) or γ=0.5($N\rightarrow\infty$) for the description of the temperature dependence of pressure broadening in the $^2P_{1/2}\rightarrow{}^2P_{3/2}$ transition of atomic iodine [4]. If the approximate assumption is made that the interaction potential has the same dependence on R for all collisions the FWHM is $W_L=(300/T)^{\gamma}\sum\alpha_i P_i$. Here we assume an identical frequency shift for all collision partners. On the basis of this assumption the temperature dependence of the pressure broadening was obtained for the temperature range 220-340°K for oxygen nitrogen mixtures.

4.2. EXPERIMENT

The cold gas medium with atomic iodine was prepared in a similar manner as the active medium in a subsonic COIL. This method is described in [9]. The experimental set-up is similar to that described in [10] and is presented in fig.1. The $O_2(^1\Delta)$ was generated in a jet singlet oxygen generator from the reaction between the gaseous chlorine and the BHP jets. The chlorine utilization U ≈ 95%. The temperature of the BHP jets was –16°C. In the mixing chamber the primary nitrogen mixes with the oxygen flow. The secondary nitrogen with iodine vapor was then mixed with the oxygen flow. The secondary nitrogen with iodine vapor was then mixed with primary O_2 +N_2 flow. The mixing and chemical result in the dissociation of molecular Iodine. The active mixture then flows into a chamber with cross section 50×28 mm. The side walls of the chamber are divergent with and angle of 3°. The probe laser beam was introduced into the chamber to scan the Iodine gain/(absorption) line.

The gas temperature in the chamber was varied by

a) temperature of primary nitrogen
b) molar flow rate of primary nitrogen
c) iodine molar flow rate

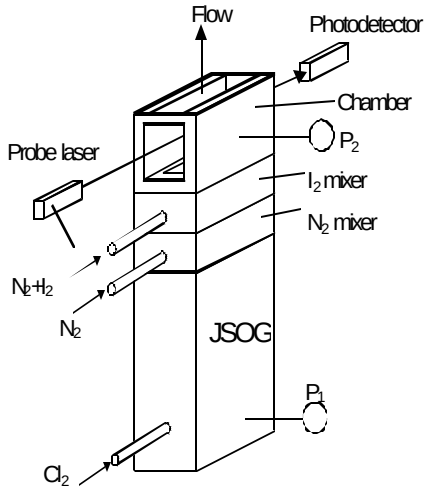

Fig.1: **Schematic Drawing of the Experimental device used for measuring Iodine line profile.**

To achieve low gas temperatures the primary nitrogen was passed through a copper spiral placed in a liquid nitrogen bath. The variation of the cold primary nitrogen molar flow rate allowed a changes the gas temperature in the cavity. The variation of the iodine molar flow changes the heat release in the gas flow which can also cause the cavity temperature to vary.

The cavity chamber was pumped by a mechanical pump with capacity 125 l/s. Under these conditions the gas flow in the chamber was subsonic. The pressures were measured with an accuracy 1%. The experiments were performed at pressures (>10torr) in the cavity chamber to achieve substantial gain/(absorption) in the wings of the line-shape where the lorentzian plays a dominant role. Only under these conditions is the deconvolution of Voight line shape reliable.

The high resolution spectra were with a tunable diode laser system developed by (Physical Science Inc). The hardware and software provided for the acquisition and storage of gain profiles with a tunning range ±1500MHz relative line center. The spectral line-shape of the probe beam was a lorenzian with W_p (FWHM)=8 MHz.

4.3. RESULTS

In fig.2 an example of a gain profile is presented. In this case gain was observed. Under different experimental conditions absorption was observed. Typically absorption was observed when the primary nitrogen was at the room temperature and the iodine molar flow rate was high. The resolution of the spectrum results in the determination of the Gaussian parameter W_D and the Lorenzian parameter W_{L1}. The pressure broadened line width was calculated as $W_L = W_{L1}-W_P$. Table [1] summarizes the experimental results. The error for W_D and W_{L1} was 2% and 4% respectively. The errors were due to noise in the spectra.

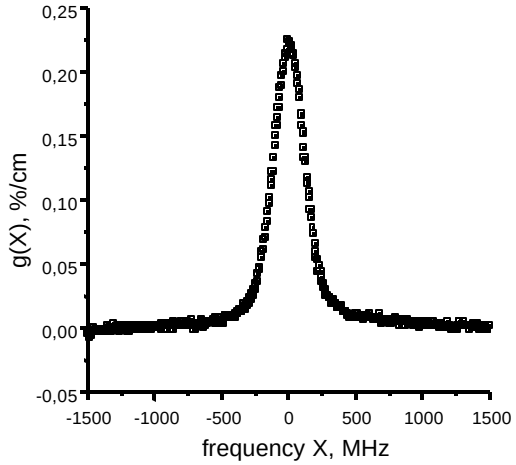

Fig.2: **Example of Iodine gain line profile.**

In table 1 the partial pressures of the gas components are presented. The gas composition was estimated in the following manner. The gas consists primarily of nitrogen, oxygen and residual chlorine with small amounts of water vapor, atomic, and molecular iodine. The partial pressures of oxygen and chlorine are given by $P_{O2}=P_2M_{CL2}U/M$, $P_{CL2}=P_2M_{CL2}(1-U)/M$. The partial pressure of nitrogen is given by $P_{N2}=P_2(M_{N2S}+M_{N2P})/M$. The water vapor partial pressure inside the JSOG is approximately P_{JSOG}=1.5 torr for the BHP temperature –16°C. The ratio of the water vapor

pressure in the JSOG to P_1 should be close to the ratio of the partial pressure of water vapor in the chamber to the partial pressure of oxygen+chlorine or $P_{H2O}=(P_S/P_1)(M_{CL2}/M)P_2$. The most difficult to estimate separately are the partial pressures of molecular and atomic iodine. Because the iodine molar flow rate did not exceed 0.3 mmole/s the pressure broadening of the line by atomic and molecular iodine was neglected.

The FWHM for the pressure broadening is given by:

$$W_L = f(300/T)\Sigma\alpha_i P_i, \qquad \textbf{(2)}$$

The pressure broadening coefficients for T=300°K are presented in Table 2.
Table 2. Therefore in our case

$$W_L=(5P_{O2}+5.5P_{N2}+6.2P_{CL2}+20.6P_{H2O})\, f(300/T) \qquad \textbf{(3)}$$

We assume that $f(300/T)=(300/T)^{\gamma}$ and $W_L=(W_{L1}-8)$ and rewrite equation (3) as:

$$f\left(\frac{300}{T}\right)=\left(\frac{300}{T}\right)^{g}=\frac{W_{L1}-8}{\left(5P_{O_2}+5.5P_{N_2}+6.2P_{CL_2}+20.6P_{H_2O}\right)} \qquad \textbf{(4)}$$

The dependence of f(300/T) is presented in fig.3. The best fit to $(300/T)^{\gamma}$ results in a value of γ=0.82. Further analysis has shown that values of γ in the range of $0.75<\gamma<1$ also place $(300/T)^{\gamma}$ in the range of experimental errors. Thus the experimental data can be described by temperature dependence of pressure broadening by the function $(300/T)^{\gamma}$ where $.75<\gamma<1$. To further refine the value of γ it will be necessary to perform experiments at gas temperatures lower 200K°. These results can be used for estimation of static pressure in the supersonic flow.

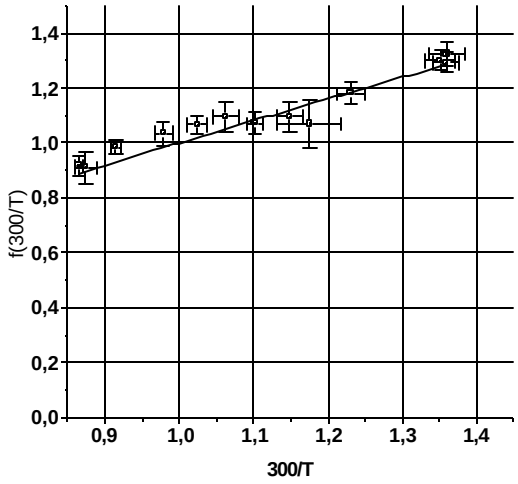

Fig.3:
Dependence of f(300/T) on temperature and fitting with the function $(300/T)^{g}$.

Table 1. Summary of experimental results.

M_{CL2}	M_{N2P}	M_{N2S}	P_1	P_2	P_{N2}	P_{O2}	P_{CL2}	P_{H2O}	W_D	W_{L1}	T
10	60.6	10	17.7	14.2	12.4	1.59	0.088	0.100	215	112	220
10	52.6	10	16.3	13.1	11.3	1.62	0.090	0.111	215	102	220
10	62.3	10	18.4	14.6	12.8	1.60	0.089	0.096	216	113	222
10	60.6	10	20.2	14	12.3	1.56	0.087	0.086	226	99	243
10	60.6	10	18.3	14	12.3	1.56	0.087	0.095	231	91	254
10	41.6	10	16.6	11.1	9.3	1.62	0.090	0.109	234	76	261
10	41.6	10	16.6	11	9.2	1.61	0.089	0.108	239	74	272
10	48	10	16.7	12	10.2	1.59	0.088	0.106	243	81	281
20	69.2	10	24.1	17	13.6	3.08	0.171	0.142	248	108	293
20	41.6	10	18.3	12.8	9.2	3.22	0.179	0.195	254	82	307
10	69.7	10	22.2	15.4	13.7	1.55	0.086	0.077	262	92	327
10	48	10	17.1	12	10.2	1.59	0.088	0.103	268	69	342
10	48	10	17.3	12	10.2	1.59	0.088	0.102	270	69	347

M_{CL2} – chlorine molar flow rate through the JSOG, M_{N2P}, M_{N2S}, athe molar flow rates of primary and secondary nitrogen, P_1, P_2, are the pressures in JSOG and in the cavity chamber, P_{CL2}, P_{O2}, P_{N2}, P_{H2O}, are the estimated partial pressures of chlorine, oxygen, nitrogen, and water vapor. T = (WD/14.49) is the gas temperature.

Table 2. Pressure broadening coefficients for temperature 300°K.

Gas	α_i (MHz/torr)	Ref.
O_2	5	7
N_2	5.5	7
Cl_2	6.3	11
H_2O	20.6	11
I_2	10.5	4
I	4.4	4

References

1. Zuev V.S.., Katulin V.A. et al. JETF, 62, 1673 (1972)
2. Patrick T.D., Palmer R.E.. *J.Chem.Phys*., 62, 3350 (1975)
3. Neuman D.K., Clarck P.K., Shea R.F., Davis S.J.. *J.Chem.Phys*., 79, 4680 (1983)
4. Engelman R.,.Palmer B,.Davis S.J. *J.Opt.Soc.Am*., 73, 1585 (1983)
5. Cerny D., Aubert-Frecon M., Basic R., Bussery B., Nota M., Verges J.. *SPIE Proc.*, 1031, 312 (1988)
6. Tate R.F., Hunt B.S., Helms C.A., Truesdell K.A., Hager G.D.. *IEEE J.Quantum Electronics*, 31, 1632 (1995)
7. Davis S.J., Kessler W.J., Bachmann M.. *SPIE Proc*., 3612, 157 (1999)
8. Vainstein V.A., Sobelmann I.I., Yukov E.A. Excited atoms and broadening of spectral lines. (M., Nauka 1979 p.253).
9. M.V.Zagidullin, V.D.Nikolaev, M.I.Svistun, N.A.Khvatov . Quantum Electronics 28, p.400-402 (1998)
10. M.V.Zagidullin, V.D.Nikolaev, M.I.Svistun, N.A.Khvatov . Quantum Electronics 30, p.161-166(2000)
11. Carroll D.L. *AIAA Journal*, 33, 1454 (1995)

5. CALCULATION OF GASDYNAMIC PARAMETERS OF THE ACTIVE MEDIUM IN THE CAVITY OF THE 3-NOZZLES EJECTOR COIL.

Consider the ejector mixing chamber of the COIL with the constant cross section square. There are three nozzle types in the inlet cross section for injection: 1- pure nitrogen with very high stagnation pressure, 2- oxygen, 3- nitrogen with iodine vapor. Denote by indexes 4 - gas parameters of the completely mixed stream, 5 – gas parameters after straight shock wave. All nozzles are sonic nozzles and throat cross sections are inlet cross sections of the mixing chamber. The total cross section square of the all three nozzles $F_{01}+F_{02}+F_{03}$ is less than cross section square of the mixing chamber F (cm^2).

At first it's necessary to determine the initial data:

universal gas constant: $R=8.314\cdot10^7$ erg/K•mole

adiabatic coefficients (ratios of the specific heat capacities): k_i

stagnation temperatures: T_{0i},

molar masses: mi, [molecular mass of the gas mixture with iodine vapor is determined as $m_3=(254P_I+28P_{N2})/(P_I+P_{N2})$, where P_I and P_{N2} are pressures in the iodine measuring cell,

specific heat capacities at constant pressure: $Ci=(R/mi)(k_i/(k_i-1))$], (i=1,2,3);

$C12= C_2/ C_1$; $C13= C_3/ C_1$;

the heat release in the mixing chamber due to iodine dissociation and $O_2(^1\Delta)$ quenching Q (in units of specific enthalpy of the pure N_2 stream),

Critical gas velocities: $$A_i = \sqrt{\frac{2RT_{0i}k_i}{m_i(k_i+1)}}$$

5.1. Adjustment initial stagnation pressures P_{0i}

The stagnation pressures and throat cross section square of the oxygen jet should be adjusted to provide the real molar flow rates of all gas components

$$g_i = 1.333\cdot10^6\sqrt{\left(\frac{k_i}{m_i R T_{oi}}\right)\left(\frac{2}{k_i+1}\right)^{\frac{k_i+1}{k_i-1}}}\,P_{0i}F_{0i}\ \text{(mmol/s)} \qquad (0)$$

(and mass flow rates: $G_i= 10^{-3}m_i g_i$)

due to the pressure losses in the ducts and real values of the N_2 and N_2+I_2 stagnation pressures are unknown. The thickness of the boundary layers in the oxygen slit and nitrogen cylindrical nozzles are unknown also. It's necessary to remark that the concrete calculation demonstrate very slowly dependence of the recovery pressure P_5 on values stagnation pressures at keeping of the mass flow rates or products $P_{0i}F_{0i}$. The static pressure P_4 and Mach number M_4 of the mixed stream depend on N_2 stagnation pressure because the coincidence of the calculated and experimental values of these static pressures and Mach numbers at zero iodine flow rate (Q=0) is major criterion of the choice N_2 stagnation pressure. Obviously the maximal cross section squares in the products $P_{0i}F_{0i}$ are restricted by real values. The adjusted initial values P_{0i} and F_{0i} are used for calculation of the reduced velocities $\lambda_i = V_i/V_{i\ crit}$, Mach numbers M_i, static pressure P and cross section squares F_i at the some (locking) cross section of the mixing chamber. Indeed, if the ratios of stagnation pressures P_{0i} (torr) of all streams to static pressure in the inlet cross section of the mixing chamber exceed critical value then all gas flows are expanded in contour nozzles such that static pressures of the all flows should be equalized in the nozzles' exit plane ($P_i = P$).

$$P_{01}p(l_1)=P_{02}p(l_2)=P_{03}p(l_3)\circ P \qquad (1)$$

but the sum of the cross section squares of these flows coincides with the cross section square of the mixing chamber F: $$F_1+F_2+F_3 = F_{01}/q(l_1)+F_{02}/q(l_2)+F_{03}/q(l_3) = F \qquad (2)$$

Denote $$X \circ 1-(k-1)l^2/(k+1),$$

then $$p(l)=[1-(k-1)l^2/(k+1)]^{k/(k-1)} \circ X^{k/(k-1)}, \qquad (3)$$

$$q(\lambda) = \left(\frac{k+1}{2}\right)^{\frac{1}{(k-1)}} \lambda\,[1-(k-1)\,\lambda^2/(k+1)]^{1/(k-1)} =$$

$$= \left(\frac{k+1}{2}\right)^{\frac{1}{(k-1)}} \sqrt{\frac{(1-X)(k+1)}{k-1}}\, X^{1/(k-1)} \circ q(X), \qquad (4)$$

The equations (1) and (2) give the possibility to determine gasdynamic parameters in this flow choking cross section. If $X_1 \circ 1-(k_1-1)/(k_1+1)\lambda_1^2$, (5)
then from equation (1)

$$X_2 \circ 1-(k_2-1)/(k_2+1)\lambda_2^2 = X_1^{j_1} (P_{01}/P_{02})^{(k_2-1)/k_2} \circ X_2(X_1) \qquad (6)$$

$$X_3 = X_1^{j_2} (P_{01}/P_{03})^{(k_3-1)/k_3} \circ X_3(X_1) \qquad (7)$$

where $j_1 = \frac{k_1(k_2-1)}{(k_1-1)k_2}$; $j_2 = \frac{k_1(k_3-1)}{(k_1-1)k_3}$.

Substitution (4)÷(7) into equality (2) gives equation

$$f(X_1) = F_{01}/q(X_1)+F_{02}/q(X_2(X_1))+F_{03}/q(X_3(X_1)) - F = 0 \qquad (8)$$

the root X_{1f} of which determines of $X_2=(X_{1f})^{j_1}(P_{01}/P_{02})^{(k_2-1)/k_2}$, $X_3=(X_{1f})^{j_2}(P_{01}/P_{03})^{(k_3-1)/k_3}$, reduced velocity $\lambda_i = ((1-X_i)(k_i+1)/(k_i-1))^{1/2}$, Mach numbers $M_i = \sqrt{\frac{2\lambda_i^2}{X_i(k_i+1)}}$, static pressure $P=P_{01}(X_{1f})^{k_1/(k_1-1)}$, cross section squares of the jets F_i and expansion ratio for each contour nozzle $F_i/F_{0i}=1/q_i=1/q_i(X_i)$. These parameters are served as the initial data for calculation of the gasdynamic parameters of the completely mixed stream.

5.2. Calculation gasdynamic parameters of the completely mixed stream.

Denote the ejection coefficients: $n_1=G_3/G_2$; $n:=G_2/G_1$; (9)
specific heat capacities at the constant pressure for mixed gas are:

$$C_4=(G_1C_1+G_2C_2+G_3C_3)/(G_1+G_2+G_3); \quad C14= C_4/C_1;$$

$$t_2=T_{02}/T_{01}; \; t_3=T_{03}/T_{01};$$

molar weight of the mixed gas: $m_4=(g_1m_1+g_2m_2+g_3m_3)/(g_1+g_2+g_3)$; (10)
adiabatic coefficient of the mixed gas:

$$k_4=1+(g_1+g_2+g_3)/(g_1/(k_1-1)+g_2/(k_2-1)+g_3/(k_3-1)) \qquad (11)$$

a) The conservation low of the mass flow rates:

$$G_4=G_1(1+n(1+n_1)); \; g_4=1000G_4/m4; \qquad (12)$$

b) The conservation of energy:

$$(G_1C_1T_{01}+G_2C_2T_{02}+G_3C_3T_{03}+Q^*)/G_1C_1T_{01}=(G_4/G_1)\,C14\,(T_{04}/T_{01})=$$
$$(1+n(1+n1))C14(T_{04}/T_{01})=1+n(t2C12+n1t3C13)+Q;$$

or $T_{04}= T_{01}(1+n(t2C12+n1t3C13)+Q)/(1+n(1+n1))C14$ (13)

where $Q=Q^*/G_1C_1T_{01}$ is dimensionless heat release in the mixing chamber.

c) The conservation of momentum with using gasdynamic functions $Z_i=\lambda_i+1/\lambda_i$:

$$G_4A_4Z_4k_4/(k_4-1) = G_1A_1Z_1k_1/(k_1-1)+G_2A_2Z_2k_2/(k_2-1)+G_3A_3Z_3k_3/(k_3-1)$$

$$Z_4 \circ (G_1A_1Z_1k_1/(k_1-1)+G_2A_2Z_2k_2/(k_2-1)+G_3A_3Z_3k_3/(k_3-1))/(G_4A_4k_4/(k_4-1)) = (\lambda_4+1/\lambda_4) \qquad (14)$$

or $\lambda_4^2 + Z_4\lambda_4 + 1 = 0$

This equation has two solutions: supersonic- $\lambda_4>1$ and subsonic (after straight shock wave) - $\lambda_5 = 1/\lambda_4$, where

$$\lambda_4=Z_4/2+(Z_4^2/4-1)^{1/2}; \qquad (15)$$

$$\lambda_5=Z_4/2-(Z_4^2/4-1)^{1/2}; \qquad (16)$$

Denote $X_4 \circ 1-(k_4-1)/(k_4+1)\lambda_4^2$;
then $T_4=T_{04}X_4$; (17)

$$q_4(X_4) \circ \left(\frac{k_4+1}{2}\right)^{\frac{1}{(k_4-1)}} \sqrt{\frac{(1-X_4)(k_4+1)}{k_4-1}}\, X_4^{1/(k_4-1)},$$

$$X_5 = 1-(k_4-1)/(k_4+1)\,\lambda_5^2;$$

$$q_5(X_5) = \left(\frac{k_4+1}{2}\right)^{\frac{1}{(k_4-1)}} \sqrt{\frac{(1-X_5)(k_4+1)}{k_4-1}}\; X_5^{1/(k_4-1)},$$

It's necessary to use expression for mass flow rate of the completely mixed stream

$$G_4 = 1333\sqrt{\left(\frac{k_4 m_4}{R T_{04}}\right)\left(\frac{2}{k_4+1}\right)^{\frac{k_4+1}{k_4-1}}}\; P_{04} F\, q_4(X_4)$$

for determination of stagnation pressure

$$P_{04} = G_4 \Big/ 1333\sqrt{\left(\frac{k_4 m_4}{R T_{04}}\right)\left(\frac{2}{k_4+1}\right)^{\frac{k_4+1}{k_4-1}}} \cdot F q_4(X_4) \qquad (18)$$

and static pressure of the supersonic stream

$$P_4 = P_{04}\, X_4^{k_4/(k_4-1)} \qquad (19)$$

Stagnation pressure subsonic stream after straight shock wave (Pitot pressure) may be found by similar method

$$P_{05} = G_4 \Big/ 1333\sqrt{\left(\frac{k_4 m_4}{R T_{04}}\right)\left(\frac{2}{k_4+1}\right)^{\frac{k_4+1}{k_4-1}}} \times F q_5(X_5) = P_{04}\, q_5(X_5)/q_4(X_4) \sim g_4(m_4 T_{04})^{0.5} \qquad (20)$$

Mach numbers M_i are connected with velocity coefficients λ_i with correlation:

$$M_{4,5} = \sqrt{\frac{2\lambda_{4,5}^2}{X_{4,5}(k_4+1)}} \qquad (21)$$

Formulas (0)÷(21) is solution of the given task and were used for calculation of the gasdynamic parameters for experimentally investigated nozzle bank.

Reaching of the highest recovery pressure requests the use heavy ejecting gases. It's necessary to use the gases with high specific hear ratio for obtaining the lower static temperatures.

These regularities may be received from the consideration of the expression for ejecting nitrogen momentum $M_N \sim G_1 A_1 \lambda_1 k_1/(k_1-1) = m_1 g_1 \sqrt{\frac{2R T_{01} k_1}{m_1(k_1+1)}}\; \lambda_1 k_1/(k_1-1) = g_1 \sqrt{m_1 T_{01}}\, f(k_1)\, \lambda_1$

where $f(k_1)$ is function depended on k_1 only.

It's easily to see that molar flow rate of the ejecting gas providing the same momentum M_N decreases with the raise of m_1, T_{01} ($g_1 \sim \frac{1}{\sqrt{m_1 T_{01}}}$).

Because it's possible to decrease considerably ejecting gas flow rate due to using very high stagnation pressure P_{01}, high stagnation temperature and keeping static pressure of the mixed streams. The same conclusion may be received from formula (20) also.

6. ? $_2$(?^{1}D) and iodine atoms production in the vortex discharge

Glow discharge was investigated as means to produce gaseous medium with high enough concentration of singlet delta oxygen and as a source of atomic iodine for oxygen-iodine laser.

As it is known, to achieve inversion in oxygen-iodine system, ? $_2$(?$^1\Delta$) content should exceed ~20% of O_2 molecules (at ~300 °K). Energy assessment shows that to achieve high singlet oxygen content in oxygen discharge plasma, power load in the discharge must be high – more than 1.5 kJ/g (~50 kJ/mol). This value is many times higher than typical for stationary glow discharge at high pressure.

Previous studies of vortex-stabilized dc discharge, performed in our group had shown its extreme stability [6.1]. With the help of the vortex flow, stable dc glow discharge existed up to 100 Torr pressure of oxygen, nitrogen and a number of gas mixtures and at high power load. The unique stability of this type of discharge stimulated the authors to investigate its applicability to produce singlet oxygen and atomic iodine using mixtures containing an iodine precursor.

Our previous experiments (before the beginning of the contract) had shown that dc glow discharge in vortex gas flow in oxygen remained stable at the pressure range 5-10 Torr and power load up to ~1.5 kJ/g [6.2, 6.3]. Measurements of ? $_2$(?$^1\Delta$) content were performed, detecting spontaneous emission at 1270 nm and calibrating the photodiod against black body radiation. They revealed that ? $_2$(?$^1\Delta$) concentration increased with increase of power load. The highest concentrations amounted to 2% and were achieved at the pressures 4 and 6 Torr and flow rates of 0.8 and 1.25 g/s accordingly. It was also found that ? $_2$(?$^1\Delta$) concentration could be increased up to 3 times if certain organic substances were added in the downstream afterglow or upstream of discharge.

In earlier experiments, the dependence of ? $_2$(?$^1\Delta$) concentration versus power load did not exhibit saturation up to the highest current possible ~300 mA, determined by capabilities of our experimental setup. Therefore, to make a discharge with higher power load was of interest, in order to determine the highest possible ? $_2$(?$^1\Delta$) concentration and to reveal the mechanisms of its limitation, so it was necessary to design more powerful discharge system.

According to work plan of the present contract, during the first quarter the modified discharge system was designed and manufactured. Experiments with discharge in oxygen were performed to measure ? $_2$(?$^1\Delta$) concentration and to optimize the system to obtain the highest ? $_2$(?$^1\Delta$) content at higher power load.

During the second quarter of the contract the experiments with oxygen mixtures as well as with pure oxygen were performed to obtain discharge products at higher pressures, which is favorable for systems with supersonic flow.

During the third quarter of the contract atomic iodine concentrations obtained with the help of the discharge products or discharge itself were measured and discharge system was optimized to produce iodine atoms at the highest possible carrier gas pressures.

*****

6.1. Modification of the existing discharge system considering previous experimental results with intention to further increase discharge power load.

Designing the discharge chamber the following goals were set to achieve long term discharge operation with current no less than 600 mA:

- the electrodes were insulated from the grounded parts of the chamber;
- parts of the gas flow channel where insulated separating discharge plasma from nearby conducting channel parts;
- electrode assemblies were designed water cooled providing effective heat removal.

To provide the possibility to change shape of the electrodes and distance between them, the working parts of the electrodes' assembly were made easily removable.The designed chamber is shown by the simplified drawing of in figure 6.1.1. The electrode assemblies are designed symmetrical about the discharge region, providing the possibility to change their polarity as related to gas flow direction.

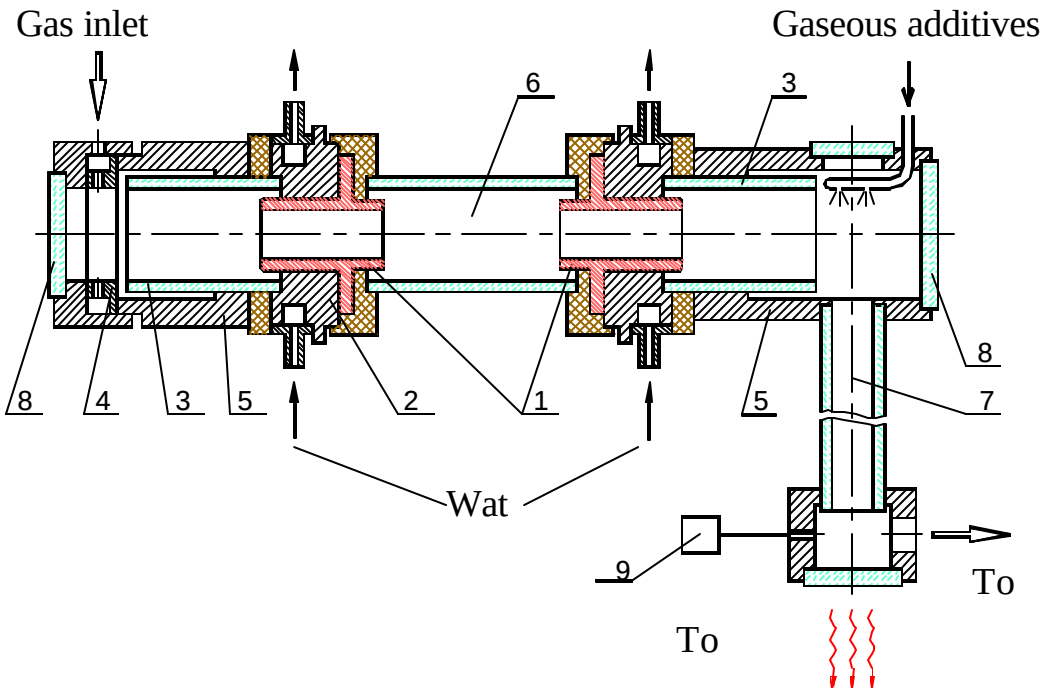

Fig. 6.1.1. Simplified drawing of the discharge chamber: 1 – electrodes, 2 – cooler, 3 – insulator, 4 – gas inlet nozzle, 5 – discharge chamber casing, 6 – discharge region, 7 – diagnostic arm, 8 – observation windows, 9 – pressure control.

The discharge chamber was manufactured in the workshop of Samara branch Lebedev Institute. Its overall view is presented in the photograph in figure 6.1.2. The discharge chamber was assembled, vacuum tested and installed in the experimental setup.

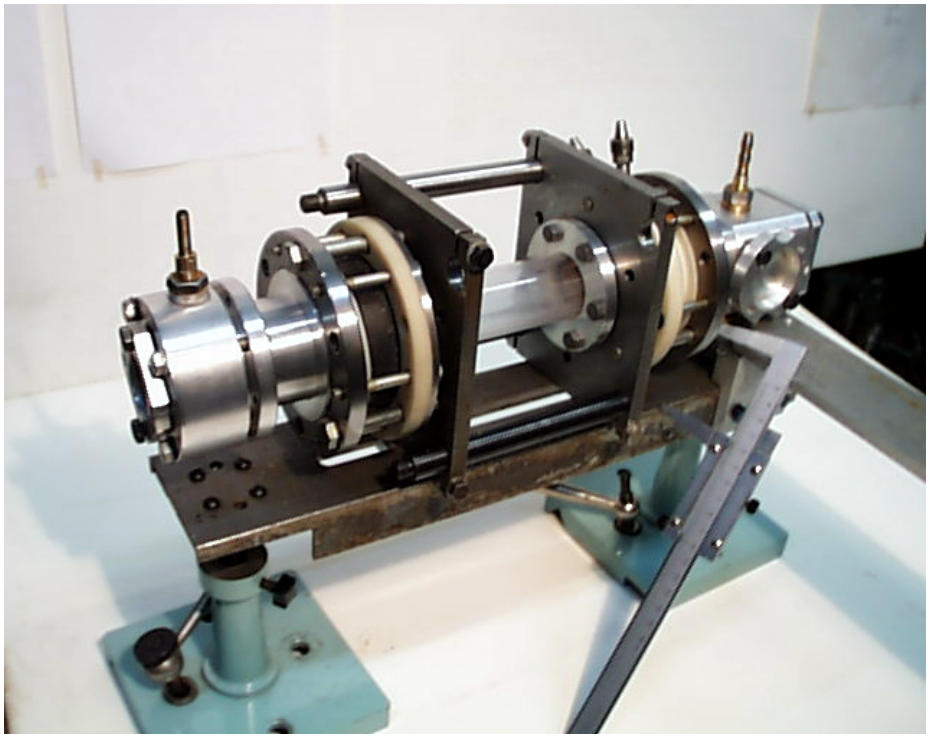

Fig. 6.1.2. Overall view of the discharge chamber.

Also, the necessary modifications of the discharge power supply were performed:

- new assemblies of diodes and ballast resistors were manufactured and installed, providing discharge current up to 1 A;
- the circuitry to measure discharge voltage and current in ground insulated high voltage circuits was manufactured and installed.

The tests of the new discharge chamber were performed. They proved the ability of the whole system to sustain long term normal operation of the discharge with current more than ~600 mA with power load into the discharge more than 600 W, which exceeds maximum values possible with the old chamber version 3-5 times.

6.2. Study of the vortex-stabilized discharge characteristics in pure oxygen and singlet delta oxygen content in the downstream afterglow region for power load up to 3 kJ/g.

Using the modified discharge system the experiments were performed with CW discharge in the pure oxygen flow in the pressure range from 4 to 8 Torr and gas flow rates from ~2 to ~6 mmol/s (0.07 – 0.2 g/s) respectively.

Voltage-current dependencies for a number of gas flow configurations were obtained: straight and vortex flow, flow direction from anode to cathode and vice versa. In these conditions the concentration of singlet delta oxygen (? $_2(^1\Delta)$) in the downstream afterglow (excited gas flowing out of the discharge region) was determined by means of emission spectroscopy measuring absolute intensity of spontaneous emission of the ? $_2(a^1\Delta) \rightarrow$? $_2(X^3\Sigma)$ band at 1270 nm. Absolute calibration was performed against black body radiation. The dependencies of ? $_2(a^1\Delta)$ concentrations on discharge current and power, discharge power load (J/g) were obtained for the above mentioned flow configurations.

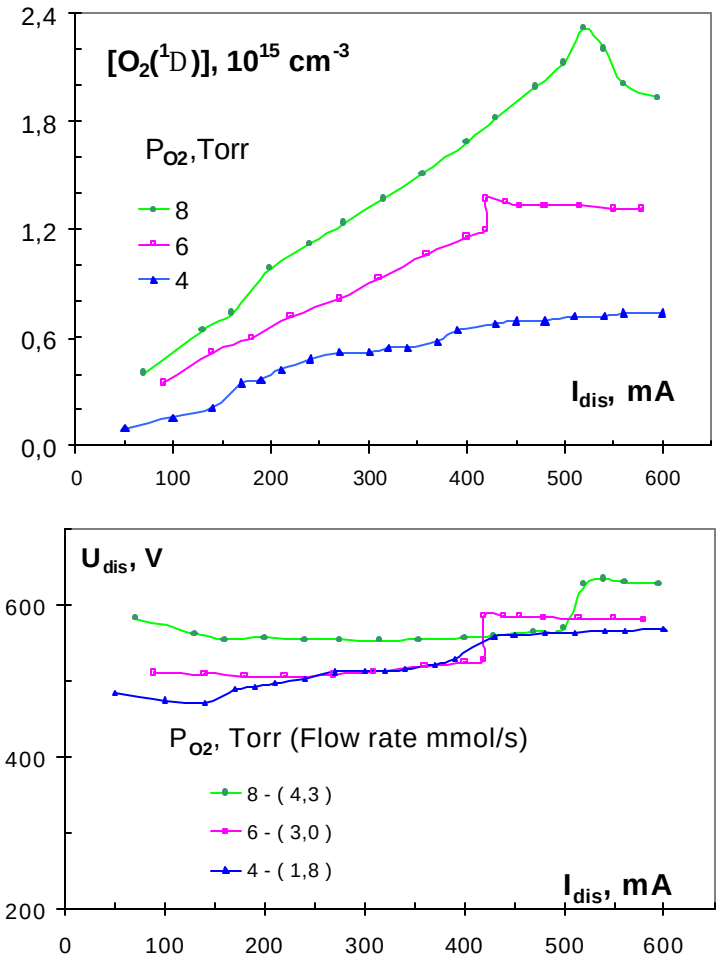

Fig.6.2.1. Voltage-current characteristics of the vortex flow dc discharge for pressure range 4-8 Torr (lower graphs) for gas flow direction from cathode to anode corresponding dependencies of ? $_2(?^1?)$ concentration. Interelectrode distance 46 mm.

A portion of the obtained data is represented in the figure 6.2.1.

It was found that in all cases voltage-current characteristics exhibit 'step' – sharp transition to higher discharge voltage when power load into positive column exceeds ~1 kJ/g (30 kJ/mol). In the analogous situation for the discharge without flow low voltage form was called T-form and high voltage – H-form. At that 'step' singlet oxygen concentration exhibited maximum and then deceased..

As far as authors know, the represented data is the first registration of those forms of discharge in the fast-flow discharge in oxygen, when the convective losses of the particles is substantial.

Our measurements revealed, that efficiency of ? $_2(^1\Delta)$ production was substantially higher in the T-form discharge for both straight and vortex flows. Moreover, ? $_2(^1\Delta)$ concentration increase with current in the T-form discharge and in the H-form – rapidly decrease.

To determine absolute ? $_2(a^1\Delta)$ concentrations we used the latest and it seems the most reliable value for Einstein A coefficient – $2.19 \cdot 10^{-4}$ s^{-1} [6.4].

The highest ? $_2(^1\Delta)$ concentration achieved in the experiments were obtained in the vortex-flow discharge for gas flow direction from cathode to anode for 8 Torr pressure and amounted to ~$2.4 \cdot 10^{15}$ cm^{-3}. Taking into account gas temperature it amounts to 2.5-3% of singlet oxygen content.

The experiments had shown substantial difference of the low and high voltage forms of the discharge for singlet oxygen production. Therefore, to increase ? $_2(?^1\Delta)$ concentration the conditions for existence of the low voltage form of the discharge in a wider range of currents should be found.

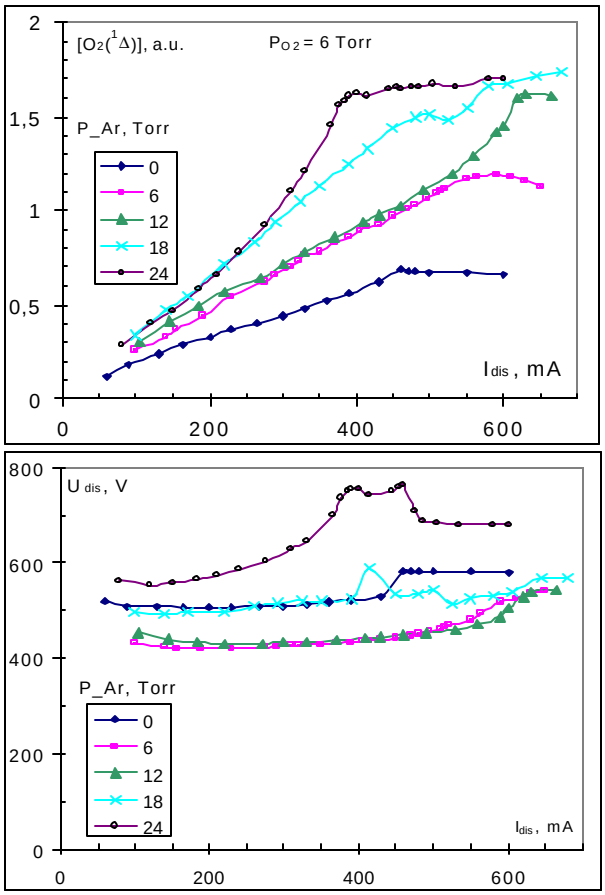

Fig.6.3.1. ? $_2$($a^1\Delta$) concentrations (arbitrary units) and discharge voltage with dependence on discharge current for oxygen-argon mixtures with 6 Torr oxygen. Argon pressure from 0 to 24 Torr. Vortex flow with the cathode upstream. Distance between electrodes is 46 mm. The largest ? $_2$($a^1\Delta$) concentration is $3.6 \cdot 10^{15}$ cm^{-3}.

6.3. Study of the singlet delta oxygen content in the downstream afterglow region using mixtures of oxygen with rare gases.

The intention of this second stage of the research was to determine the upper limits and optimal conditions of singlet oxygen ? $_2$($a^1\Delta$) production in glow discharge diluting oxygen by rare gases at increased pressure.

Higher pressure of discharged gas mixture is advantageous for further use in a supersonic flow system. At higher pressure wider range of supersonic flow regimes are possible, lower pump capacity is needed, mixing of the flows is improved. Developing the project, the authors assumed that it was possible to increase discharged gas pressure without decrease of the singlet oxygen fraction, diluting oxygen by rare gases. The experiments of the second stage of the contract were performed to determine: how much the oxygen could be diluted by the rare gas; what the discharge characteristics would be; the conditions most favorable for singlet oxygen production.

The highest ? $_2$($a^1\Delta$) concentrations for a number of mixtures with rare gases were determined experimentally. Experiments consisted of a series of measurements of singlet oxygen content with dependence on discharge current (power load) in the discharged oxygen mixtures with argon and helium. For the fixed oxygen flow rate, the flow rates of rare gases were varied.

The measurements were performed using the modified discharge system developed during the first stage of the contract. The discharge tube was 3 cm in diameter and distance between electrodes was 10 or 4.6 cm. Higher concentrations were observed for 4.6 cm interelectrode distance. Most of the experiments were performed for vortex gas flow, and several measurements were performed for straight flow as well.

? $_2$($^1\Delta$) concentration was determined by emission spectroscopy, measuring absolute intensity of the ? $_2$($a^1\Delta$) $\rightarrow$? $_2$($X^3\Sigma$) band in the 1270 ±12 nm wavelength region. Absolute calibration was performed against black body radiation.

The following data was obtained – current-voltage characteristics and the dependence of ? $_2$($^1\Delta$) concentration on discharge current for a number of oxygen pressures (flow rates) from 1 to 8Torr and a number of argon and helium pressures (flow rates) for each oxygen pressure. Rare gas flow rate amounted to 6 and more times of oxygen flow rate.

Besides, emission spectra in the region 1240 – 1300 nm were monitored to confirm the absence of stray spectral lines that might emerge from rare gases and interfere with ? $_2$($^1\Delta$) measurements. Those lines were indeed observed when old discharge system was used due to close proximity of the cathode glow.

The experiments showed that it is possible to increase gas pressure several times without any loss of singlet oxygen fraction using mixtures of oxygen with argon and helium.

Moreover, singlet oxygen content increases significantly, when oxygen is diluted by rare gases.

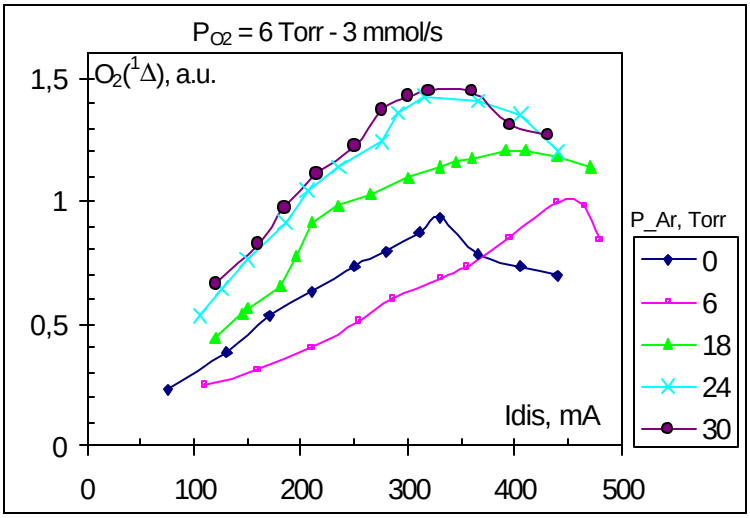

Fig.6.3.2. ? $_2(a^1\Delta)$ concentration (arbitrary units) with dependence on discharge current for oxygen-argon mixtures with 6 Torr oxygen. Ar pressure from 0 to 30 Torr (0-14 mmol/s). Vortex flow with the cathode upstream. Distance between electrodes 102 mm. The largest ? $_2(a^1\Delta)$ concentration is $2.5\cdot10^{15}$ cm^{-3}.

The results for oxygen pressure 6 Torr (in the diagnostics arm) and flow rate 3 mmol/s diluted by argon for two different interelectrode distances are shown in Fig.6.3.1-6.3.2. As it is seen, total pressure of the gas mixture was increased up to 36 Torr, i.e. 6 times. ? $_2(a^1\Delta)$ concentration increased with increase of Ar pressure. For the largest Ar pressure 30 Torr (14 mmol/s) used in experiments the highest ? $_2(a^1\Delta)$ concentrations were 1.6 times (for 102 mm distance between electrodes) and 2.5 times (for 46 mm) larger then in pure oxygen.

For the oxygen pressure 4 Torr (1.8 mmol/s) the largest dilution by argon in experiments was six times. ? $_2(a^1\Delta)$ concentration increased 3-3.5 times compared to pure oxygen.

Diluting oxygen with helium produced analogous effect on ? $_2(a^1\Delta)$ concentration. The highest concentrations in that case were a little larger then with argon. The results are shown in Fig.6.3.3 - 6.3.4 for different interelectrode distances.

For oxygen pressure 4 Torr (fig. 6.3.3) and 6 times dilution with He ? $_2(a^1\Delta)$ concentration increased 4 times. As shown in fig.6.3.4, for oxygen pressure 6 Torr the largest dilution was 4 times and total pressure amounted to 30 Torr. The highest ? $_2(a^1\Delta)$ concentration increased 2.5 times compared to pure oxygen.

Temperature measurements were not performed during these experiments and we can only estimate ? $_2(a^1\Delta)$ fraction from 2 to 4%. At present the reasons why ? $_2(a^1\Delta)$ concentration increases when oxygen is diluted by rare gases are not clear. They are determined by changes of discharge inner

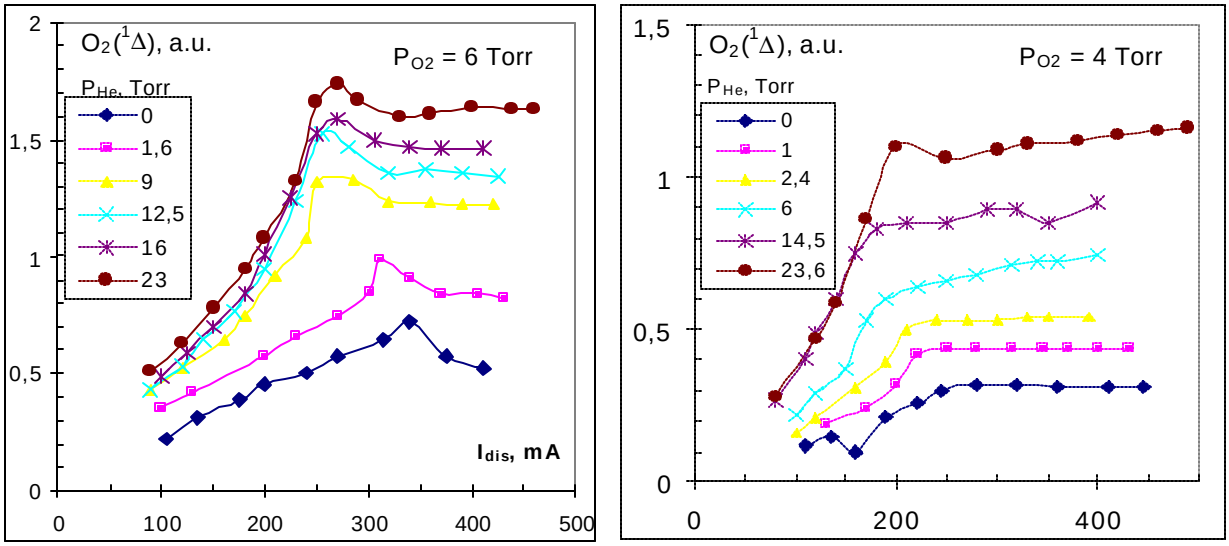

Fig.6.3.3 ? $_2(a^1\Delta)$ concentrations (arbitrary units) with dependence on discharge current for oxygen-helium mixtures with 6 and 4 Torr oxygen. Helium pressure from 0 to 24 Torr. Vortex flow with the cathode upstream. Distance between electrodes 102 mm. The largest ? $_2(a^1\Delta)$ concentrations are $3.7\cdot10^{15}$ cm^{-3} for 6 Torr and $2.5\cdot10^{15}$ cm^{-3} for 4 Torr.

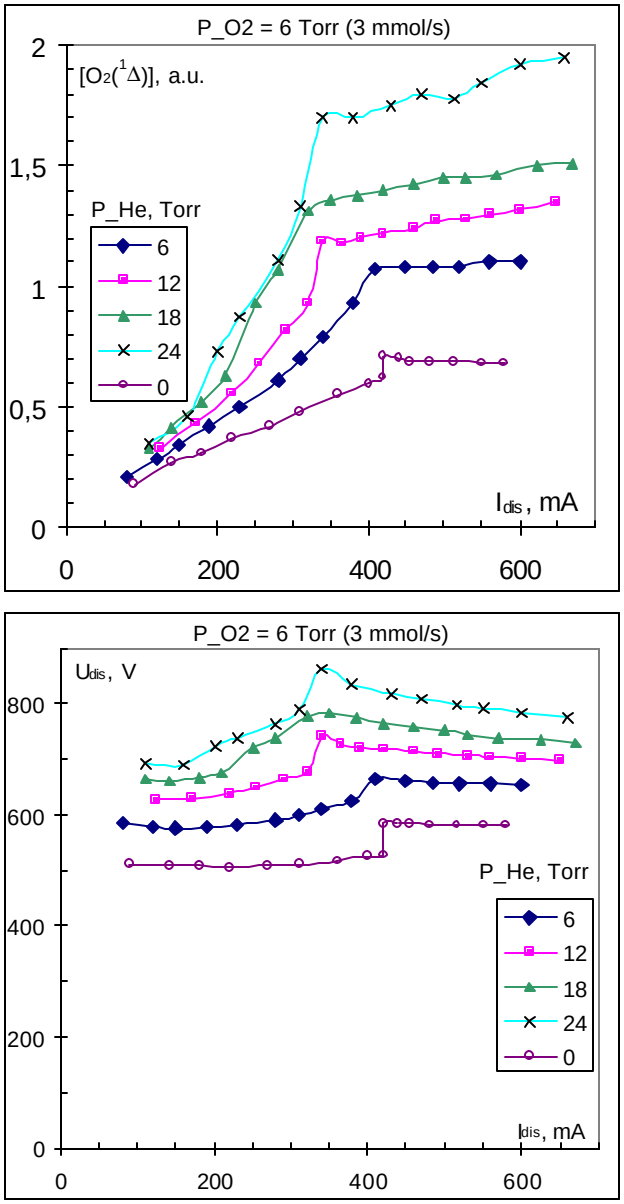

Fig.6.3.4. ? $_2(a^1\Delta)$ concentrations (arbitrary units) and discharge voltage with dependence on discharge current for oxygen-helium mixtures with 4 and 6 Torr oxygen. Helium pressure from 0 to 24 Torr. Vortex flow with the cathode upstream. Distance between electrodes 46 mm. The largest ? $_2(a^1\Delta)$ concentration is $4.1\cdot10^{15}$ cm^{-3}.

properties revealed by difference in appearance of current-voltage characteristics for pure oxygen and mixtures. With increase of rare gas fraction both the dip in current-voltage characteristic and the current when discharge transfers to high-voltage mode change. To reveal the physics of this phenomena more detailed investigations are needed. Therefore, experiments conducted during the second stage of the contract had shown that it is possible to increase pressure of the gas medium containing singlet oxygen produced by vortex-flow discharge using mixtures of oxygen with rare gases. The achieved pressures – 28 Torr for oxygen pressure of 4 Torr and 36 Torr for 6 Torr of oxygen are sufficient to conveniently organize supersonic flow. Moreover, in mixtures of oxygen with rare gases singlet oxygen content increased several times compared to pure oxygen.

6.4. Measurement of iodine atoms concentration when methyl iodide is mixed into the discharge or downstream afterglow regions.

Ground [I] and excited [I*] atomic iodine concentrations were measured for two different cases:

1) discharge was sustained in the pure oxygen or in the mixture of oxygen with argon, iodine precursor – methyl iodide was admixed in the downstream afterglow region;

2) discharge was sustained in argon, methyl iodide was admixed into discharge.

Ground state atomic iodine concentration [I] was measured via resonant absorption of laser radiation, using tunable semiconductor laser device temporary provided by Partner.

Excited atomic iodine concentration was measured using absolute intensity measurements of iodine emission at 1.315 μm. Calibration was performed against black body radiation. Besides, to interpret experimental results, a kinetic model that describes atomic iodine production in the reactions of methyl iodide with discharged oxygen was developed. There is a satisfactory qualitative and quantitative match of the results of numerical simulations and experiments.

6.4.1. Experimental setup and methods I.

The experiments were performed using an old version of discharge chamber. Schematic drawing of our experimental setup used for experiments with the discharge products is represented in the figure 6.4.1. DC glow discharge was sustained between water cooled copper electrodes in a tube of 17 mm inner diameter. Anode was shaped as a 12 mm cylinder and cathode – hollow cylinder of 10 mm inner diameter. Interelectrode distance in experiments with discharged oxygen products was 6 cm. Gas was injected near the wall in the cathode region normally to the tube axis forming the vortex and flowed

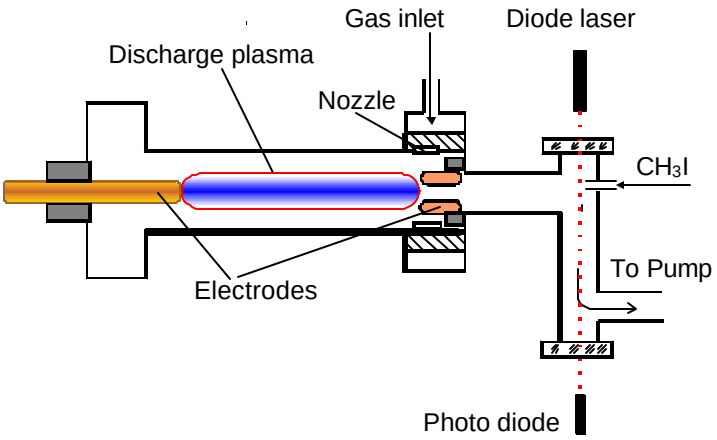

Fig.6.4.1. Experimental setup for atomic iodine production using discharge products.

through the cathode to the diagnostic region. Methyl iodide was admixed into the afterglow 2.5 cm downstream from the cathode. The flow retained its vortex motion there and mixing was efficient.

To determine atomic iodine concentration a tunable semiconductor laser system temporarily provided by Partner was used. Absorption line shape of iodine laser transition $^2P_{3/2}(F=4) \rightarrow {}^2P_{1/2}(F=3)$ was recorded for about half a minute than averaged and approximated by Voigt function. Atomic iodine concentration and temperature were deduced out of the line area and Voigt function parameters. We found that it was useful to couple Gauss and Lorenz parameters of the Voigt function through temperature to decrease error of approximation.

To estimate possible error due to the presence of iodine atoms at the upper laser level special measurements of their concentration were conducted detecting the overall signal at 1.315 μm from the diagnostic volume with the help of a monochromator and a photodiode. Calibration was performed against the black body radiation. The estimated concentration of the excited iodine atoms could amount up to 10% of atoms in the ground state, depending on experimental conditions, but that source of error was further neglected as it only effectively decreased measured iodine concentration somewhat.

Using the numerical model, described further, the atomic iodine recombination was assessed and found to be negligible in our experimental conditions partly due to rather high temperature (~ 400-600°K) and partly to initial absence of I_2. Wall recombination probability of atomic iodine is low (~10^{-3}-10^{-4}) and diffusion loss in the diagnostic arm was, therefore, neglected. Taking aforementioned in consideration, the measured iodine concentrations should be treated as integrated along the probe laser optical path and are lower than the highest achieved.

6.4.2. Experimental results I.

The typical dependence of atomic iodine concentration [I] for different methyl iodide flow rates on discharge current is shown in fig. 6.4.2. The curves exhibit saturation or weak maximum. Slow fall with current is presumably due to temperature rise. For the mixture O_2:Ar = 6:4 Torr the maximums were a little more profound and [I] values were 1.5 times higher then for the pure oxygen.

The dependencies of the highest [I] on CH_3I flow rate for different oxygen pressures and the same oxygen flow rate 4.2 mmol/s are shown in the fig. 6.4.3. Discharge current was not the same for these measured values and was in the range from 200 to 500 mA, and discharge voltage – from 600 to 800 V. As it is seen from fig. 6.4.3 for discharge in pure oxygen there is a linear dependence of [I] on CH_3I flow rate at small flow rates and than – saturation. No saturation was observed for O_2:Ar

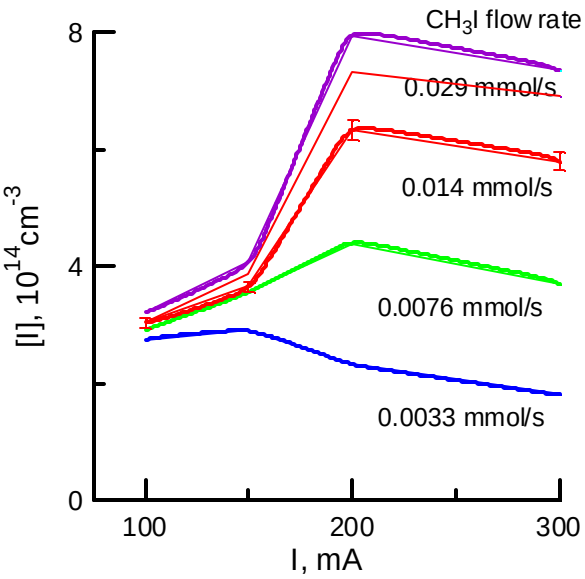

Fig.6.4.2. Dependence of [I] on current for various CH_3I flow rates. O_2 pressure 6 Torr. Oxygen flow rate – 4.2 mmol/s.

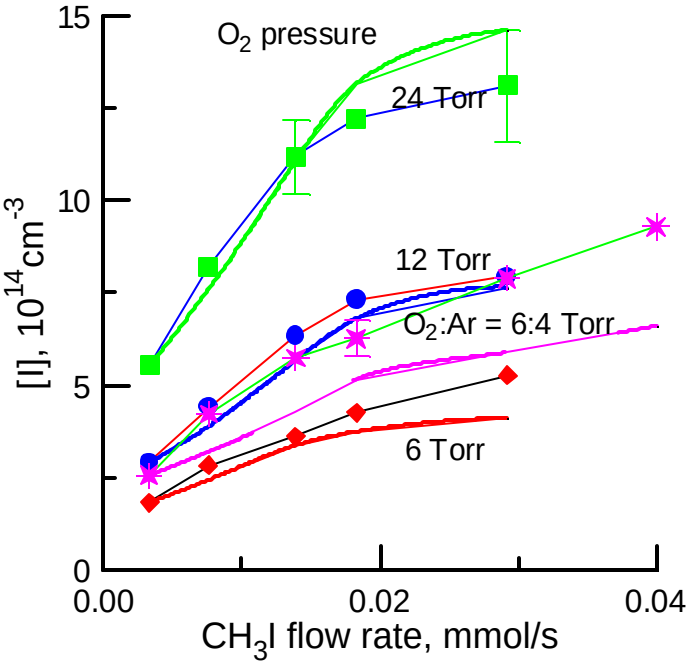

Fig.6.4.3. Dependence of [I] on CH_3I flow rate for various O_2 pressures and the same flow rate 4.2 mmol/s. Points – experiment, lines – modeling.

mixture for the range of CH_3I flow rates used in our experiments. The highest [I] concentrations were obtained for discharge in pure oxygen at 24 Torr pressure and amounted to $1.3 \cdot 10^{15} cm^{-3}$.

The fraction of atomic iodine produced out of methyl iodide – [I]/[CH_3I] was from 0.8 to 0.4 for the discharge in pure oxygen, and from 1 to 0.6 for O_2:Ar mixture decreasing with increase of CH_3I flow rate.

Part of iodine atoms in our experiments were in excited state. The measurements had shown that when methyl iodide was oxidized by discharged oxygen or oxygen-argon mixture up to ~ 10% of iodine atoms were in excited state. When methyl iodide was decomposed in discharge with argon – about 2-3% of iodine atoms were in excited state.

The measured excited iodine relative concentration and gas temperature permits to determine relative singlet oxygen concentration. For discharge current 200 mA at 6 Torr oxygen pressure the relative singlet oxygen concentration amounted to ~ 5% which is in good agreement with the measurements that used spontaneous emission at 1.27 μm.

6.4.3. Discussion I.

Earlier experiments revealed that in our experimental conditions there was 1-1.5% of atomic oxygen present in the downstream afterglow. Atomic oxygen $O(^3P)$ is the most active particle among the discharge products in the downstream afterglow. It rapidly oxidizes methyl iodide in the reaction $CH_3I + O$ forming IO, I, CH_3, OH and other products.

To estimate the contribution of various elementary processes into atomic iodine production a kinetic model was developed including 14 reactions represented in the table, without consideration of spatial distribution of the particles. As the initial concentrations of the main reagents were of the same order, only those processes were taken into account which rate constants in our experimental conditions differed no more than 2-3 orders of magnitude. The exception was three body iodine recombination, which proceeded slowly. No data could be found in the literature about rate constants of the reactions of CH_3I with $O_2(?^1\Delta)$ and $? _2(b^1\Sigma)$, except that methyl iodide does not react or reacts slowly with $O_2(?^1\Delta)$, and they were not taken into account.

[O] concentration for calculations was set according to our previous measurements. Temperature was set, according to measured, from the iodine line Doppler width. Modeling results are represented in the fig. 6.4.3 as lines. For comparison with the model only the highest [I] concentrations were considered. As it is seen from the fig. 6.4.3 good qualitative and quantitative match is observed.

Computations had shown that for small [CH_3I] concentrations, less than 0.5[O], first four reactions had the highest rates – of the same order of magnitude. Next two reactions are more than an order of magnitude slower and contribution of others is negligible.

Methyl iodide is oxidized by atomic oxygen forming IO and a small amount of I. Mostly, atomic iodine is produced through further oxidation: $IO + O \rightarrow I+O_2$. Due to its high rate [IO] concentration is always 1-2 orders of magnitude lower than [O]. Rival processes, where O atoms are wasted are the reactions $?H_3+O$ and OH+O. Computations has shown that in our experimental conditions [I] had almost reached steady state in $\sim 2.5 \cdot 10^{-4}$s, after that the main reaction rates had become two orders of magnitude lower.

Reaction (channel fraction)	Rate constant, cm^{-3}/s, cm^{-6}/s	Source
$CH_3I+O \rightarrow IO+CH_3$ (0.44) $\rightarrow I+H+CH_2O$ (0.07) $\rightarrow OH+CH_2I$ (0.16)	$1\cdot10^{-11}\cdot\exp(160/T)$	[5]
$IO + O \rightarrow I + O_2$	$1.2\cdot10^{-10}$	[6]
$CH_3 + O \rightarrow$ products	$1.2\cdot10^{-10}$	[7]
$OH + O \rightarrow H + O_2$	$2.3\cdot10^{-11}\cdot\exp(110/T)$	[8]
$IO + IO \rightarrow I + I + O_2$	$8\cdot10^{-11}$	[6]
$CH_3 + CH_3 \rightarrow C_2H_6$	$4\cdot10^{-11}$	[7]
$I_2 + O \rightarrow IO + I$	$1.4\cdot10^{-10}$	[6]
$CH_3 + O_2 + O_2 \rightarrow CH_3O_2 + O_2$	$1\cdot10^{-30}\cdot T^{-3.3}$	[7]
$CH_3 + H + O_2 \rightarrow CH_4 + O_2$	$2.2\cdot10^{-21}\cdot T^{-3}$	[7]
$OH + OH \rightarrow H_2O + O$	$7.9\cdot10^{-14}\cdot(T/298)^{2.6}\cdot\exp(945/T)$	[8]
$OH + OH+O_2 \rightarrow H_2O_2 + O_2$	$6.9\cdot10^{-31}\cdot(T/300)^{-0.8}$	[8]
$OH + H + O_2 \rightarrow H_2O + O_2$	$6.9\cdot10^{-25}\cdot T^{-2}$	[7]
$I + I + O_2 \rightarrow I_2 + O_2$	$1.9\cdot10^{-32}$	[9]
$I_2 + OH \rightarrow HOI + I$	$2.1\cdot10^{-10}$	[10]

Modeling has shown, that the highest possible [I] concentration, with enough initial [CH_3I] for all atomic oxygen to react, equals to about one third of initial atomic oxygen concentration. With further increase of initial [CH_3I] ([CH_3I] > 0.5·[O]), [I] increased noticeably slower. In that case the contribution of the reaction $IO+IO \rightarrow 2I+O_2$ to atomic iodine production became larger and became comparable to $IO+O \rightarrow I+O_2$ reaction when [CH_3I] ≈ [O]. In experiments with pure oxygen the saturation of [I] was observed with increase of CH_3I flow rate at 0.02-0.03 mmol/s. Atomic oxygen flow rate at that moment amounted to ~0.04mmol/s.

Computations produced somewhat lower results than measured [I]. Besides model imperfection possible reason of this discrepancy could be presence of I_2 vapor in the reaction zone with concentration about $10^{14}cm^{-3}$. Iodine molecules could be present in CH_3I as a result of its partial decomposition, or emerged from the walls of discharge chamber. For computations initial I_2 concentration was set to match the experimental points at the lowest CH3I flow rate (as seen in the fig.6.4.3). For different O_2 pressures these concentrations also differed and amounted to one third or one half of CH_3I concentrations at the lowest flow rate. If initial molecular iodine concentrations were taken into account, better agreement between computed and measured results was achieved for experiments with pure oxygen. Qualitative results remain the same if molecular iodine is taken into account.

For the mixture of oxygen with argon modeling gave 1.5 times lower [I] concentrations than measured in experiment, indicating unknown channels of atomic iodine production in that case.

The dependence of [I] on current is not described by this model at low currents, possibly because of unknown temperature dependence of the main reaction rates.

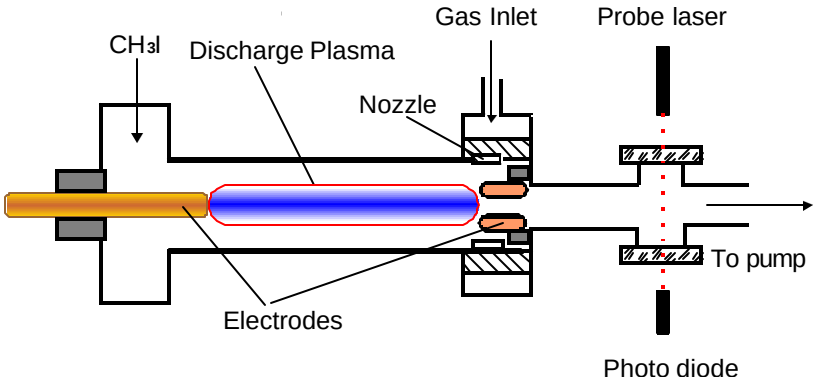

Fig.6.4.4. Experimental setup used for atomic iodine production in discharge.

It should be noted that CF_3I could also be a good iodine precursor. IO production amounts to 85% in this case, contrary to 44% for CH_3I. Rate coefficient of $CF_3I + O$ reaction is twice lower than in the case of methyl iodide, but still it is quick enough.

6.4.4. Experimental setup and methods II.

Schematic drawing of our experimental setup is represented in the figure 6.4.4. It was the same as used in the aforementioned experiments, except CH_3I was admixed into the discharge region from anode side of the tube and transverse flow was organized in the diagnostic region.

To estimate possible error due to the presence of iodine atoms at the upper laser level special measurements of their concentration were conducted detecting the overall signal at 1.315 μm from the diagnostic volume with the help of a monochromator and a photodiode. Calibration was performed against the blackbody radiation. The estimated concentration of the excited iodine atoms amounted to 2% of atoms in the ground state and that source of error was further neglected.

No observable recombination of atomic iodine was detected in our experiments along the flow 1.5 cm apart in the diagnostic region, corresponding to time delay about 10^{-4}s. However the measurements that were performed across the flow revealed about 10% decrease of atomic iodine concentration at the diagnostic window boundaries indicating inhomogeneous distribution of iodine atoms across the flow. Therefore, the measured iodine concentrations should be treated as integrated along the probe laser optical path and are lower than the highest achieved.

6.4.5. Experimental results II.

Usually, discharge plasma was localized near the center of the tube occupying about one fifth of its diameter. Argon, helium, oxygen, nitrogen and air were tried as carrier gases. The largest atomic iodine concentrations were obtained with argon. In helium and oxygen the concentrations were twice lower and in nitrogen and air – an order of magnitude lower. In oxygen and, especially, in nitrogen and air the electrodes and walls of the discharge tube became contaminated after several minutes of work, deteriorating the discharge performance. In argon and helium wall contamination proceeded slower. In our opinion, this problem could be solved if some other iodine precursor is used. It seems that hydrogen iodide is promising for that purpose, because it does not contain carbon and does not deteriorate active medium.

There is a dependence of atomic iodine concentration on current as it is shown in the figure 6.4.5 for different initial methyl iodide flow rates. Argon pressure in this experiment was 6 Torr, flow rate 3 mmol/s and electrode spacing 6 cm. Note, that there is a maximum on current and then – a decrease that is

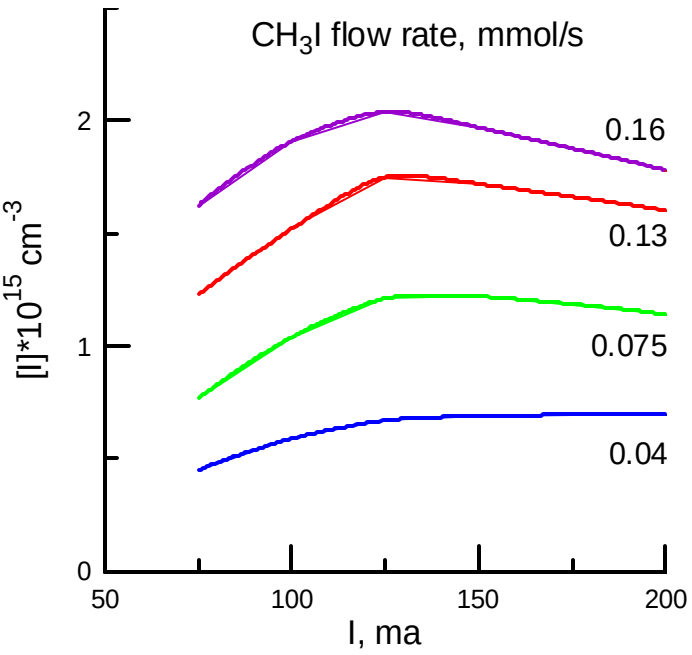

Fig.6.4.5. Dependence of [I] on current for various CH3I flow rates. Ar flow rate 3 mmol/s at 6 Torr pressure.

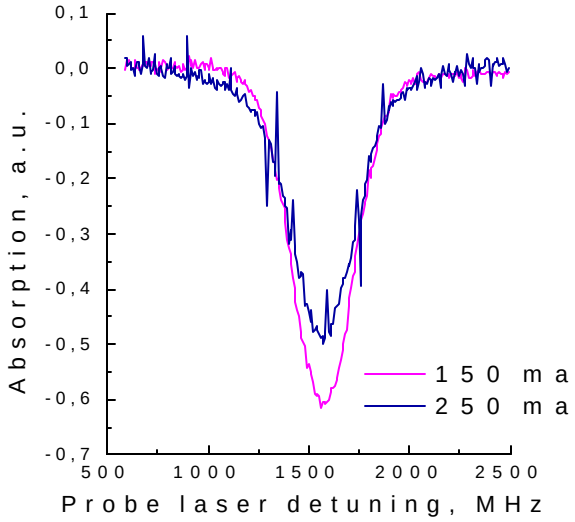

Fig.6.4.6. Detected line shape at two different discharge currents illustrates discharge instability.

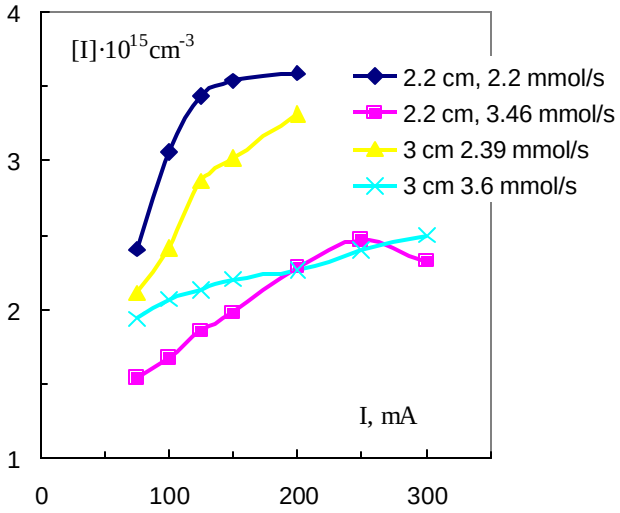

Fig.6.4.7. The dependence of atomic iodine concentration upon discharge current for two different values of electrode spacing and different flow

supposed to be due to temperature rise, same as in fig.6.4.2. With increase of methyl iodide flow from 0.04 up to 0.16 mmol/s atomic iodine concentration increased and in maximums amounted to 40% of initial concentration of methyl iodide. When methyl iodide flow increased from its lowest to highest value discharge voltage increased from 500 to 850 volts, indicating high electronegativity of the mixture.

With increase of discharge current atomic iodine concentration exhibited maximum or saturation and then sharply decreased as the discharge became unstable. The detected signal remarkably changed at that moment as illustrated in the figure 6.4.6. At first the detected line had Voigt shape, and when the discharge current exceeded certain value the line became noisy and its area decreased.

Making electrode spacing smaller, down to 2.2 cm we managed to sustain stable discharge in argon up to 20 Torr pressure and obtained atomic iodine concentration $2 \cdot 10^{15} cm^{-3}$.

The dependence of atomic iodine concentration upon discharge current for two different values of electrode spacing and different flow rates is shown in the figure 6.4.7. Note that concentration is quite sensitive to the flow and discharge configuration parameters, indicating that discharge instability is present.

The largest atomic iodine concentration achieved in our experiments amounted to $3.6 \cdot 10^{15} cm^{-3}$. It was obtained for 15 Torr of argon pressure and 2 mmol/s flow rate. Distance between electrodes was 2.2 cm in that case. In these experiments atomic iodine concentration was about 20% of methyl iodide initial concentration. Gas temperature determined from line shape approximation by the Voigt function amounted to 570 degrees Kelvin.

6.4.6. Discussion II.

Estimating the discharge parameters achieved in our experiments, mean electron energy in argon should be ~10 eV and electron density $\sim 10^{12} cm^{-3}$. The following reactions between electrons and methyl iodide could be imagined:

- $CH_3I + e \rightarrow CH_3 + I^-$ – dissociative attachment with subsequent iodine ion recombination;
- $CH_3I + e \rightarrow CH_3 + I + e$ – electron impact dissociation;
- $CH_3I^+ + e \rightarrow CH_3 + I$, $CH_3I^+ + I^- \rightarrow CH_3 + 2I$ – dissociative recombination.

All those processes are very quick with rate constants of $\sim 10^{-7}$-$10^{-9} cm^3/s$. The reverse reaction between methyl radical and iodine atom was found to be negligible, compared to mutual recombination of these radicals during the studies of the photo dissociative iodine laser.

Therefore, by estimations, methyl iodide dissociation should be completed during less then 1 ms, for the largest. Gas mixture in our experiments had flown between electrodes 2-3 ms or even more, but

we observed only 20-40% dissociation. Two possible reasons could be imagined: first – as the discharge plasma was localized near the axis of the discharge tube not all the parts of the gas flow had enough time to interact with electrons; second – atomic iodine concentration had maximum at the center of the flow and the optical path length of the probe laser was smaller then we considered and the real concentrations, therefore, higher.

Lifetime of iodine atoms is also important for the laser system. For our experimental conditions three body recombination on undissociated methyl iodide molecules determine this lifetime. We estimated atomic iodine lifetime with the help of the kinetic model including the following reactions and rate constants for Ar pressure 15 Torr and temperature 500 °K:

$I + I + M \rightarrow 2I + M$, where M:

I_2 $k = 3 \cdot 10^{-31}$ cm^6/s [11];
CH_3I $k = 8 \cdot 10^{-32}$ cm^6/s [12];
Ar $k = 3 \cdot 10^{-33}$ cm^6/s [13];

For the measured iodine atoms concentration and gas temperature, taking into account that in the worst case only 20% methyl iodide molecules had dissociated we obtained that after one millisecond 1% of atomic iodine is lost through recombination and after five milliseconds – about 5%. Therefore, in our experimental conditions there is enough time to deliver iodine atoms to the mixing zone with oxygen.

6.4.7. Summary and conclusions.

The main results are as follows:

For the first case:

- The experiments had shown, that using oxygen atoms in the discharge products of the discharged oxygen or discharged mixture of oxygen with argon, iodine atoms may be produced in large enough quantities for further use in active medium of oxygen-iodine laser.
- Using discharge products of the dc vortex-flow glow discharge in oxygen and methyl iodide as the precursor, atomic iodine concentrations up to $1.3 \cdot 10^{15} cm^{-3}$ – usual for oxygen-iodine laser active medium were obtained.
- On the basis of the developed model we conclude that the main mechanism of atomic iodine production out of methyl iodide has two stages. At the first stage IO molecules are produced through methyl iodide oxidation. At the second stage iodine atoms are produced either through further oxidation by O atoms or through the reaction of these molecules with each other.

For the second case:

- Atomic iodine concentration up to ~ $4 \cdot 10^{15} cm^{-3}$ was obtained – enough to operate oxygen-iodine laser.
- Use of the vortex gas flow allowed to sustain the dc glow discharge in a highly electronegative halogen containing gas mixture of argon with methyl iodide at pressures up to ~ 15-20 Torr. These pressures are enough to inject iodine atoms into the active medium of supersonic oxygen-iodine laser.

References.

6.1. S.F. Adyasov, A.I. Voronov, V.A. Katulin, P.A. Mikheyev, A.L. Petrov, A.A. Shepelenko. “A vortex-gas-flow electric-discharge CO_2 laser”. Kvantovaya Electronica (Moscow) 537-543, (1989).

6.2. Mikheyev P.A., Shepelenko A.A., Kupryayev N.V., Voronov A.I. Exited oxygen in glow discharge afterglow. *Proc. SPIE*, 1999, v.3612, pp. 85-87.

6.3. A.A. Shepelenko, P.A. Mikheyev, A.I. Voronov, N.V. Kupryayev. Oxygen metastables excitation in vortex-flow discharge. Izvestiya Academii Nauk, 2000, v.64, #7 pp. 1259-1265 (2000).

6.4. S. M. Newman, I. C. Lane, A. J. Orr-Ewing at al. J.Chem.Phys. V.110 (22) pp.10749-10757, (1999).

6.5. M.K.Gilles, A. A. Turnipseed, R. K. Talukdar et.al. Reactions of $O(^3P)$ with Alkyl Iodides: Rate Coefficients and Reaction Products. // J. Phys. Chem. 1996. V. 100. ? 33. P. 14005.

6.6.B. Laszlo, M. J. Kurylo, R. E. Huie. Absorption Cross Sections, Kinetics of Formation, and Self-Reaction of the IO Radical Produced via the Laser Photolysis of $N_2O/I_2/N_2$ Mixtures. // J. Phys. Chem. 1995. V. 99.? 30. P. 11701.
6.7. Combustion chemistry, Edited by W.C.Gardiner, Jr. Springer-Verlag, 1984.
6.8. R. Atkinson, D. L. Baluch, R. A. Cox, et. al. Evaluated Kinetic and Photochemical Data for Atmospheric Chemistry. //J. Phys. Chem. Ref. Data. 1997. V. 26. ? 6. P.1329.
6.9. G. A. Fisk, G. N. Hays. Kinetic rates in the oxygen-iodine system. // J. Chem. Phys. V. 77. ? 10. 1982. P.4965.
6.10. Atkinson, D. L., Baluch, R. A. Cox, et. al. Evaluated Kinetic and Photochemical Data for Atmospheric Chemistry. //J. Phys. Chem. Ref. Data. 2000. V. 29. ? 1. P.167.
6.11. Bunker D.L., Davidson N., J.Am.Chem.Soc., 1958, 80, p.5085.
6.12. Engelman R., Jr., Davidson N.R., J.Am.Chem.Soc., 1960, 82, p.4770.
6.13. J.K.K. Ip, G. Burns. J.Chem.Phys., 1972, 56(6), p.3155.

7. SUMMARY OF PROJECT TECHNICAL REPORT

During this project period 8 different ejector COIL nozzle banks were designed, manufactured and tested. Detail "cold" gasdynamic tests of these nozzle banks were made. The gas flow performances in the mixing chamber was compared for these banks. The next parameters have been measured during experiments: oxygen plenum pressure, static wall pressure at the distance 64 mm from the nozzle bank, Pitot pressure at the distance 90 mm from the nozzle bank in the center of the mixing chamber, Mach number of the gas flow. The experiments were made for 500 mmole/s of primary nitrogen (ejecting flow), 39.2 mmole/s of air (ejected flow) through oxygen nozzles and 11 mmole/s of secondary nitrogen (carrier of iodine). The typical values of the static and Pitot pressures were about 10 torr and 100 torr, correspondingly. Measurements of the Pitot pressure distributions in the cross section indicate that the gas jets' mixing is not finished completely on the distance to 90mm. The LIF experiments showed that iodine flow is totally mixed with flow from oxygen nozzles but is not completely mixed with ejecting nitrogen flow. The choking of the oxygen flow was found at increasing ejecting nitrogen flow rate more 250mmole/s which resulted in the raise of JSOG pressure and decreasing singlet oxygen yield. It's necessary to use additional methods for intensification of the mixing process and to continue the search suitable nozzle bank design which should be scaleable to powerful lasers.

The LIF experiments and aerodynamic experiments showed that gas mixing is better in the nozzle bank NB-1 and NB-2 with small scale nozzles. The small signal gain (SSG) of the order of $5x10^{-3}cm^{-1}$ is achieved in NB-1 and NB-2 for primary nitrogen molar flow rate 500 mmole/s and 39.2 mmole/s of chlorine flow rate. Simultaneously the gas velocity 620 m/s, temperature 180K and the Pitot pressure (88÷110) torr in "hot" experiments with NB-1 have been achieved. The active medium generated by NB-1 is more cold than active medium generated by NB-2. At lower ejecting nitrogen flow rate small signal gain was higher and reached value of $7x10^{-3}cm^{-1}$ for NB-1. The COIL lasing experiments showed also that NB-1 is more preferable. Pre-dilution chlorine with helium (up to 1:1) improved laser performance and allows to reach chemical efficiency of 25% at 250 mmole/s and 23% at 500 mmole/s of ejecting nitrogen though the static temperature was lower in the second case. Pitot pressures were 60 torr and 100 torr correspondingly in these experiments.

The nozzle bank NB-6 with wider oxygen slots (3.5mm instead of 2.5mm) and conical nozzles for ejecting gas has been developed specially for up to twice higher chlorine flow rates with weakened "choke" effect. But mixing efficiency of the gas jets was much worse than in the cases of the nozzle banks NB-1 and NB-2. Upgrade of this nozzle bank due to using of induced intensification of the mixing allowed to improve COIL operation and reach chemical efficiency 18.8% at 56mmole/s of chlorine flow rate and 500mmole/s of the ejecting gas flow rate.

High resolution diode laser spectroscopy was used for diagnostics of the active medium formed by the ejector nozzle banks of the supersonic COIL. The ejector nozzle bank produces the active medium with high total pressure and high small signal gain. Static temperature due to gas-dynamic cooling reached ~160K° at which threshold singlet oxygen yield equal to ~0.05. The initial tangential breaks in values of gases' parameters lead to producing of the turbulence which provides very high mixing rate. The thermal velocity of the very heavy iodine atoms is closed to ~100 m/s at low gas temperature ~150 K°. The estimations of the characteristic initial transverse pulsating velocity give value of ~(20÷30) m/s (or ~ (20÷30)% of thermal velocity of iodine atoms) at absolute gas velocity ~600 m/s. The neglect of the spectral broadening due to transverse pulsation velocity leads to overestimation of the static temperature on (10÷20)K°. The last circumstance is very important because the measured static temperatures are used for comparisons with three dimension gas dynamic calculations. On the base of these comparisons one makes conclusion about correctness of the rate constants values which computer simulations are used. Concentration of the iodine atoms in the investigated stream region (taking in to account possible its' losses due to attachment to ice particles) correspondents (50÷60)% of the initial iodine molecules only. Analysis of small signal gain spectrum for the off-normal incidence of probe beam allowed to determine the main parameters of the active

medium including average gas velocity. Estimation of the static pressure in the flow core from spectroscopic data is very close to static pressure in the boundary layer measured by pressure gauge.

The method of high resolution diode spectroscopy was used to measure the temperature dependence of pressure broadening of the atomic iodine line $^2?_{1/2}$-$^2?_{3/2}$ in the range T=220°? ÷340°? . For oxygen-nitrogen mixture the FWHM depends on temperature like $(300/T)^{\gamma}$, where γ=0.87±0.13. This dependence correlates with Van-der-Vaalce potential $V \sim R^{-6}$ of interaction that course pressure broadening.Given investigations allowed us to understand how to design scaleable ejector nozzle bank for powerful industrial lasers.DC glow discharge was investigated as means to produce gaseous medium with high concentration of singlet delta oxygen and as a source of atomic iodine for oxygen-iodine laser.

Previous studies of vortex-stabilized dc discharge, performed in our group had shown its extreme stability. With the help of the vortex flow, stable dc glow discharge existed up to 100 Torr pressure of oxygen, nitrogen and a number of gas mixtures and at high power load. The unique stability of this type of discharge stimulated the authors to investigate its applicability to produce singlet oxygen and atomic iodine out of discharged iodine precursor containing mixtures.

According to work plan of the present contract, during the first quarter the modified discharge system was designed and manufactured (Task 9). Experiments with discharge in oxygen were performed to measure $?_2(?^1\Delta)$ concentration and to optimize the system to obtain the highest $?_2(?^1\Delta)$ content at higher power load (Task 10).

During the second quarter of the contract the experiments with oxygen mixtures as well as with pure oxygen were performed (Task 11) to obtain discharge products at higher pressures, which is favorable for systems with supersonic flow.

During the third quarter of the contract atomic iodine concentrations obtained with the help of the discharge products or discharge itself were measured (Task 12) and discharge system was optimized to produce iodine atoms at the highest possible carrier gas pressures.

*****

Designing the discharge chamber the goal was set to achieve long term dc discharge operation with current no less than 600 mA. For that matter both electrodes were designed water cooled. To provide the possibility to change shape of the electrodes and distance between them, the working parts of the electrodes' assembly are made easily removable. The electrode assemblies are designed symmetrical about the discharge region, providing the possibility to change their polarity as related to gas flow direction.

The chamber was designed, manufactured and its tests were performed. They proved the ability of the system to sustain long term normal operation of the dc discharge with current more than ~600 mA with power load into the discharge positive column up to 3 kJ/g (100 kJ/mol) at 8 Torr. Using the modified discharge system the experiments were performed with CW discharge in the pure oxygen flow in the pressure range from 4 to 8 Torr and gas flow rates from ~2 to ~6 mmol/s (0.07 – 0.2 g/s) respectively. In these conditions the concentration of singlet delta oxygen ($?_2(^1\Delta)$) in the downstream afterglow (excited gas flowing out of the discharge region) was determined by means of emission spectroscopy measuring absolute intensity of spontaneous emission from the $?_2(a^1\Delta) \rightarrow ?_2(X^3\Sigma)$ band at 1270 nm. Absolute calibration was performed against black body radiation.

Voltage-current dependencies for a number of gas flow configurations were obtained: straight and vortex flow, flow direction from anode to cathode and vice versa, the flow with the highest possible and lowest flow rates. The dependencies of $?_2(a^1\Delta)$ concentrations on discharge current and power, discharge power load (J/g) were obtained for the above mentioned flow configurations.

It was found that voltage-current characteristics exhibit 'step' – sharp transition to higher discharge voltage when power load into positive column exceeds ~1 kJ/g (30 kJ/mol). At that 'step' singlet oxygen concentration exhibited maximum and then deceased. The highest concentration achieved in experiments with pure oxygen amounted to $2.4 \cdot 10^{15} cm^{-3}$ at 8 Torr pressure. Taking into account gas temperature it amounts to 2.5-3% of singlet oxygen content.

The experiments had shown substantial difference of the low and high voltage forms of the discharge for singlet oxygen production. Therefore, to increase $?_2(?^1\Delta)$ concentration the conditions for existence of the low voltage form of the discharge in a wider range of currents should be found.

Singlet delta oxygen content in the downstream afterglow region using mixtures of oxygen with rare gases was measured with intention to determine the upper limits and optimal conditions of $?_2(a^1\Delta)$ production in glow discharge diluting oxygen by rare gases at increased pressure.

Emission spectra in the region of 1240 – 1300 nm in the downstream afterglow were monitored to confirm the absence of any stray spectral lines that might emerge from rare gases and interfere with $?_2(a^1\Delta)$ measurements.

The experiments showed that it had been possible to increase gas pressure several times without any loss of singlet oxygen fraction using mixtures of oxygen with argon and helium. Moreover, singlet oxygen content increased significantly, when oxygen was diluted by rare gases.

In experiments, using Ar and He total pressure of the gas mixture was increased up to 36 Torr. The largest $?_2(a^1\Delta)$ concentration amounted to $4\cdot10^{15}cm^{-3}$ and estimated singlet oxygen fraction was up to 4%. Ground [I] and excited [I*] atomic iodine concentrations were measured for two different cases:

1) discharge was sustained in the pure oxygen or in the mixture of oxygen with argon, iodine precursor – methyl iodide was admixed in the downstream afterglow region;
2) discharge was sustained in argon, methyl iodide was admixed into discharge.

Ground state atomic iodine concentration [I] was measured via resonant absorption of laser radiation, using tunable semiconductor laser device temporary provided by Partner.

Excited atomic iodine concentration was measured using absolute intensity measurements of iodine emission at 1.315 μm. Calibration was performed against black body radiation.

Besides, to interpret experimental results, a kinetic model that describes atomic iodine production in the reactions of methyl iodide with discharged oxygen was developed. There is a satisfactory qualitative and quantitative match of the results of numerical simulations and experiments.

The main results of the experiments with iodine atoms are as follows:

For the first case:

- The experiments had shown, that using oxygen atoms in the discharge products of the discharged oxygen or discharged mixture of oxygen with argon, iodine atoms may be produced in large enough quantities for further use in active medium of oxygen-iodine laser.
- Using discharge products of the dc vortex-flow glow discharge in oxygen and methyl iodide as the precursor, atomic iodine concentrations up to $1.3\cdot10^{15}cm^{-3}$ – usual for oxygen-iodine laser active medium were obtained.
- On the basis of the developed model we conclude that the main mechanism of atomic iodine production out of methyl iodide has two stages. At the first stage IO molecules are produced through methyl iodide oxidation. At the second stage iodine atoms are produced either through further oxidation by O atoms or through the reaction of these molecules with each other.

For the second case:

- Atomic iodine concentration up to ~ $4\cdot10^{15}cm^{-3}$ was obtained – enough to operate oxygen-iodine laser.
- Use of the vortex gas flow allowed to sustain the dc glow discharge in a highly electronegative halogen containing gas mixture of argon with methyl iodide at pressures up to ~ 15-20 Torr. These pressures are enough to inject iodine atoms into the active medium of supersonic oxygen-iodine laser.

Part of iodine atoms in our experiments were in excited state. The measurements had shown that when methyl iodide was oxidized by discharged oxygen or oxygen-argon mixture up to ~ 11% of iodine atoms were in excited state. When methyl iodide was decomposed in discharge with argon – about 2-3% of iodine atoms were in excited state.

The measured excited iodine relative concentration and gas temperature permits to determine relative singlet oxygen concentration. For discharge current 200 mA at 6 Torr oxygen pressure the relative singlet oxygen concentration amounted to ~ 5% which is in good agreement with the measurements that used spontaneous emission at 1.27 μm.

Therefore, the experiments had shown applicability and prospects of the vortex-flow discharge to further improve oxygen-iodine laser system.

7.1. Presentation of the project results

1. G.D. Hager, V.D. Nikolaev, M.V. Zagidullin, M.I.Svistun, " The diagnostic of active medium of supersonic COIL with advanced nozzle bank", LASERS'2000.-25-28 December 2000.-Albuquerque.

   The advanced nozzle bank of the supersonic COIL consists of slit nozzles for energizing gas $O_2(^1\Delta)$, cylindrical nozzles for N_2 buffer gas with high stagnation pressure and nozzles for I_2+N_2 gas mixture. These three streams are mixed under supersonic conditions in the chamber 50×15 mm^2 without tunnels for mirrors. The walls of chamber have 2° angle relative to the gas flow. The beam of the probe laser is directed under angle 27.5° to the normal of the gas flow. The atomic iodine gain line for the probe laser splits onto two Foight peaks as result of Doppler effect. The analysis of the gain line allows to estimate the peak gain, the gas flow velocity, the pressure broadening WL and Doppler broadening WG line widths. These three parameters allowed to calculate the gas temperature, Mach number and pressure in mixing chamber. The experiments have been performed in a wide range of the gas flow parameters and nozzle bank configuration. For particular gas flow conditions and geometry of the mixing chamber the next parameters were obtained: the gas flow velocity 570 m/s, gas temperature 200K, Mach number near 2, the static pressure 7.7 torr. For these flow conditions the peak gain was equal to 0.7%/cm.
2. Hager G. D., Madden T.J., Khvatov N.A., Nikolaev V.D., Zagidullin M.V., Svistun M.I., "An efficient chemical oxygen- iodine laser with the high total pressure in the active medium", Quantum Electronics, vol. **31,** No. 1, pp. 30-34, (2001)

   The new nozzle concept was suggested and tested for chemical oxygen-iodine laser (COIL). The nozzle bank consists of the array of cylindrical nozzles for pure N_2 flow, slit nozzles for $O_2(^1\Delta)$ flow. The N_2+I_2 jets are injected into turbulent wakes between oxygen and N_2 streams through small cylindrical orifices. The LIF was used for the visualization of the iodine mixing efficiency in the mixing chamber. It was found practically uniform distribution of iodine molecules in the supersonic flow on the distance about 60 mm downstream nozzle bank. The COIL experiments were performed with this nozzle bank and at 5 cm gain length COIL cavity. The output power 700 W or chemical efficiency 19.7% have been achieved for the chlorine molar flow rate 39.2 mmole/s. Simultaneously the static pressure 10.9 torr in laser cavity and pressure 100 torr in Pitot tube have been achieved. The estimated Mach number of the flow was equaled to 2.6 and total pressure in the laser cavity was equaled to 218 torr. High dilution of the oxygen by nitrogen 1:11 results in small growth of the stagnation temperature of the gas flow and creates good conditions for the pressure recovery in the diffuser.
3. Khvatov N.A., Nikolaev V.D., Zagidullin M.V., Svistun M.I., "The temperature dependence of the collisional broadenning of $^2?_{1/2}$-$^2?_{3/2}$ line of atomic iodine", Quantum Electronics, vol. **31,** No. 4, pp.373-376, (2001)

   The FWHM of pressure broadening of atomic iodine line $^2?_{1/2}$-$^2?_{3/2}$ depends on temperature like W_L~~$(300/T)^{0.75\pm0.05}$ in the temperature range T=220°?÷340°? of chemical oxygen-iodine laser active medium. This dependence correlates with Van-der-Vaalce potential V~R^{-6} of interaction that course pressure broadening.
4. Hager G. D., Nikolaev V.D., Zagidullin M.V., Svistun M.I., " The diagnostic of active medium of supersonic COIL with advanced nozzle bank", Quantum Electronics, vol. **31,** No. 7 , (2001)

The high resolution diode laser spectroscopy was used to measure the gain, the temperature and the absolute gas velocity of the supersonic oxygen-iodine laser active medium generated by the ejector nozzle bank. The formation of the gain occurs at the distances less than 44 mm from the nozzle bank for the absolute stream velocity ~600 m/s. The gain value 7×10^{-3} cm^{-1} , gas temperature 200°?, absolute gas velocity 580 m/s and Pitot pressure 58 torr were achieved for 1:6,9 dilution of oxygen by primary nitrogen. The increase of dilution up to 1:13,5 resulted in gain value 4.5×10^{-3} cm^{-1}, gas temperature 180°?, absolute gas velocity 615 m/s and Pitot pressure 88 torr. The increase of the water vapor fraction in the oxygen flow resulted in the growth of the temperature of the active medium and decreasing of gain.

5. Nikolaev V.D., Zagidullin M.V., "Calculation of the mixing chamber of the ejector chemical oxygen – iodine laser", Quantum Electronics, vol. **31,** No. 6, pp.30-34, (2001)

Calculation of the gas parameters at the exit plane of the mixing chamber of the ejector chemical oxygen – iodine laser (ECOIL) is presented. The nozzle bank consisting of three types of the nozzles provides formation of the active medium with the full pressure much more higher than pressure in the singlet oxygen generator. Such method of the formation of the ECOIL active medium allows to simplify the exhaust of gas into atmosphere using a diffuser and one step water sealed vacuum pump.

6. Khvatov N.A., Nikolaev V.D., Svistun M.I., Zagidullin M.V., "New Experimental Results of the Ejector COIL Power Extraction", COIL R&D Workshop, Prague 2001,28-29 May

Ejector COIL provides lasing with high chemical efficiency.

Chemical efficiency decreases with the raise of the ejecting nitrogen flow rate due to "choke" effect for oxygen jets. Using mixture Cl_2+He improves conductivity oxygen channels, decrease JSOG oxygen partial pressure and leads to increasing chemical efficiency. Estimated $O_2(^1\Delta)$ losses during gain formation from SSG experiments are overestimated due to incompleteness of the mixing process on the distances up to 90mm from nozzle bank. Increasing the width of the oxygen slots from 2.5 mm to 3.5mm results in deterioration of the jets' mixing and decreasing chemical efficiency although "choke" effect was weaker in this case. It's necessary to develop the scaleable ejector nozzle bank for real industrial COIL with small mixing space scale and to weaken "choke" effect.

7. Khvatov N.A., Nikolaev V.D., Svistun M.I., Zagidullin M.V., "Gain and Gas-dynamic Parameters of COIL Active Medium Generated by Ejector Nozzle Bank", COIL R&D Workshop, Prague 2001, 28-29 May

Ejector nozzle bank generates low temperature, high gain, high Mach number active medium. Gain is generated at distances <50 mm from nozzle bank for absolute gas velocity 600 m/s. The nature of fast drop of the gain along the flow is not understood finally. Observed $O_2(^1\Delta)$ losses ΔY during gain formation more than 20%. The temperature dependence of pressure broadening was measured.

8. Mikheyev P.A., Shepelenko A.A., Kupryayev N.V., Voronov A.I., "Atomic Iodine Production in Vortex-Flow Glow Discharge", COIL R&D Workshop, Prague 2001, 28-29 May

Atomic iodine concentration enough to operate oxygen-iodine laser with carrier gas pressure high enough to provide injection into singlet oxygen flow, was obtained externally using the vortex-stabilized dc glow discharge. We had found that atomic iodine concentration depended on the sort of the carrier gas used. When methyl iodide is used as atomic iodine precursor its incomplete dissociation does not lead to substantial concentration of molecular iodine contrary to the case when molecular iodine is dissociated. Transport time of atomic iodine for concentrations and temperatures obtained in our experiments may amount to several milliseconds. In our opinion, the problem of discharge setup contamination could be solved if hydrogen iodide is used as a precursor.